EVOLUTION OF MECHANICAL PROPERTIES OF M50 BEARING STEEL DUE TO ROLLING CONTACT FATIGUE

By

BRYAN D. ALLISON

A DISSERTATION PRESENTED TO THE GRADUATE SCHOOL
OF THE UNIVERSITY OF FLORIDA IN PARTIAL FULFILLMENT
OF THE REQUIREMENTS FOR THE DEGREE OF
DOCTOR OF PHILOSOPHY

UNIVERSITY OF FLORIDA

2013

ACKNOWLEDGMENTS

Special thanks to my advisor, Professor Ghatu Subhash, for his support and encouragement. His enthusiasm for research serves as a representation of how we should all pursue our goals. Another special thanks to Professor Nagaraj Arakere for his knowledge and guidance.

Thanks to my committee members, Professor Peter Ifju and Professor Michelle Manuel, for reviewing my research and their advice along the way. I would also like to thank my lab mates and friends, whom have assisted in countless ways. Thanks to Ericka Garcia for editing this dissertation (twice) and for reminding me that there is more to life than work.

This research was partially sponsored by National Science Foundation Award CMMI-0927849 under program officer Dr. Clark V. Cooper, in addition to a contract with David Haluck, Bill Ogden, and Herb Chin at Pratt and Whitney, East Hartford, CT. Sincere thanks to Bryan McCoy and Don Anthony of SKF, Falconer, NY and Nelson Foster of Air Force Research Lab, Dayton, OH for supply of materials for this research.

Finally, thanks to my family for their support during my time as a graduate student. This process would have been much more difficult without them.

TABLE OF CONTENTS

page

LIST OF TABLES

LIST OF FIGURES

LIST OF ABBREVIATIONS

DER	Dark Etching Region
FE	Finite Element
FEA	Finite Element Analysis
LER	Light Etching Region
MP	Mechanically Processed
RCF	Rolling Contact Fatigue
S	Spall
XRD	X-ray Diffraction

Abstract of Dissertation Presented to the Graduate School
of the University of Florida in Partial Fulfillment of the
Requirements for the Degree of Doctor of Philosophy

EVOLUTION OF MECHANICAL PROPERTIES OF M50 BEARING STEEL DUE TO ROLLING CONTACT FATIGUE

By

Bryan D. Allison

December 2013

Chair: Ghatu Subhash
Cochair: Nagaraj Arakere
Major: Mechanical Engineering

Current bearing life models significantly under predict the life of bearings made of modern ultra-clean steels. New life models that include the constitutive response of the material are needed. However, the constitutive response of bearing steel is known to change during bearing operation. In the current study, the evolution of the mechanical properties of M50 bearing steel due to rolling contact fatigue (RCF) was investigated. A combination of M50 balls and rods were subjected to RCF testing under various conditions (e.g. number of RCF cycles, applied Hertzian stress, and interacting material). Additionally, some of the balls tested went through a proprietary mechanical process to induce compressive residual stresses over the first several hundred microns into the depth of the ball prior to RCF testing.

After RCF testing, the specimens were subjected to a number of tests. First, the residual stresses within the subsurface RCF affected region were measured via x-ray diffraction. The residual stresses within the mechanically processed (MP) balls were found to not significantly change due to RCF, while a linear relationship was found between the maximum residual stress with the RCF affected zone and the Hertzian

stress for the unprocessed balls. Then, the specimens were sectioned, polished, and chemically etched to study the evolution of the microstructure due to RCF. A similar relationship was found between the size of the dark etching region (DER) and the Hertzian stress. Formation of a light etching region (LER) is demonstrated to not correlate with a decrease in material strength and hardness, but it does serve as a predictor for failure due to spall. Micro-indentation was performed within subsurface to estimate the local yield stress. Micro-indentation is not able to provide information about the stress-strain response, only the yield strength. Hence, a novel method to extract and test miniature compression specimens from within the RCF affected regions of balls after RCF was developed. Using this method, it is possible to determine the full stress-strain response of material after material that has undergone RCF. The micro-hardness of the material within the RCF affected region was found to increase by nearly 10% and yield strength increased 13% when high contact stress levels were employed in fatigue experiments. It was demonstrated that the number of cycles does contribute to hardness increase, but the applied Hertzian stress is the dominant factor. Mechanical processing was found to significantly retard the rate of mechanical property evolution, implying that it would also significantly improve the life. Similarly, it was observed that the rate of hardening is slower when silicon nitride is used to interact with the M50 specimen than another M50 component. This supports the idea that hybrid bearings last longer than more traditional all-steel bearings. Finally, an empirical model of the evolution of the constitutive response of the bearing material within the RCF affected region was developed based on the results of these analyses. This model can be used to predict the constitutive response of the material within the RCF affected

region of an M50 steel ball, given the initial hardness, number of RCF cycles, and applied Hertzian stress. Further, it is now possible to solve the local yield strength as a function of depth within the RCF affected region given these same parameters.

CHAPTER 1
INTRODUCTION

Bearing Application

Jet Engine Performance

Jet engines provide the thrust for an aircraft. Jet engines have three main sections, as outlined in Fig. 1-1. Air enters the engine into the compressor; here the pressure of the air is reduced. In the next section, the combustor, the air is mixed with fuel and ignited, increasing the amount of energy in the air. Finally, as the exhaust gas from the combustor passes into the turbine, the gas turns the turbine blades, thereby powering the compressor. The air is then released out of the back of the engine resulting in the thrust force.

Engine performance and reliability are crucial to the performance of a jet aircraft. Engine failure can lead to the loss of a multimillion dollar aircraft, as well as compromise the safety of the pilot and all passengers. Thrust loaded ball bearings along the main engine shaft are critical components, which limit the reliability of jet engines. Therefore, these are the focus of this paper.

Bearing Design and Performance

Bearings reduce friction during rotation of concentric shafts or a shaft and the main engine housing. Ball bearings consist of a set of balls, an inner and outer raceway which define the path for the balls to travel, and a cage that maintains a set distance between the balls, see Fig. 1-2. Ball bearings have a smaller contact area and thus higher contact stress than roller bearings. Some ball bearings can carry an axial load, in addition to the radial loads, in so called thrust bearings.

Bearing geometry has a direct effect on the distribution of the contact stresses between the balls and the two raceways (frequently called “contact patches”). An elliptical contact patch is formed in ball bearings due to the conformal geometry of the ball and raceway, see Fig. 1-3. Calculations to determine the contact patch size based on loading and bearing geometry can be found in literature [1,2]. Large contact patches generate excessive heat and friction which reduce the speed and performance, while smaller contact patches induce high stresses, leading to local plasticity and premature failure. The design goal is to transmit the greatest allowable thrust load through the bearing, while simultaneously maximizing life.

Bearing Fatigue Failure

A well lubricated bearing operated under proper conditions is expected to eventually fail due to fatigue caused by subsurface initiated spall [2, 3]. This failure mode is caused by microplastic deformation, typically at microstructural discontinuities such as inclusions and carbide clusters which act to increase the local stress [3-7]. This will cause damage which begins as a subsurface crack where the cyclic shear stresses are greatest and propagate to the surface which forms a spall. The bearing industry is currently working to increase the life of ball bearings by several orders of magnitude. New ultra-clean steels have been created to accomplish this. However, the current life models are still largely based on the classical Lundberg-Palmgren model developed in 1947 [8, 9]. These models are empirical in nature, and do not directly consider the constitutive behavior of the materials under contact loading. These models significantly underestimate the life of these modern bearing steels.

Bearing fatigue life is defined as the time or number of stress cycles required for a small surface spall to develop. If the spall is allowed to continue to propogate it can

lead to engine failure. Estimation of bearing fatigue life has been an active area of study for many years [8-16]. Most modern probabilistic models for the fatigue life of ball bearings are extensions of the earlier work of Lundberg and Palmgren [8, 9]. They assumed that failure initiate due to a crack nucleating at the intersection of a weak point in the material and the maximum orthogonal shear stress. Similarly, the weak points discussed were assumed to be distributed evenly throughout the material. A Weibull distribution was applied to the strength of the material within the stressed volume to determine a probability of survival. The Lundberg-Palmgren model states that a bearing has a probability of survival, S, that can be found by the equation:

$$ln\frac{1}{S} = A\frac{N^e \tau_0^c V}{z_0^h}. \quad (1\text{-}1)$$

where, N is the number of cycles, τ_0 is the maximum orthogonal stress, z_0 is the depth of the maximum orthogonal stress, and V is the volume of stressed material. A, e, c, and h are all material parameters, which must be determined experimentally. The main problem with this method is that it assumes stress follows pure Hertzian contact, which ignores any thrust load or lubrication effects. Another concern with this model is that it assumes perfect contact surfaces, whereas real surfaces contain roughness, scratches, and dents. The current ISO standard [17] is based on a modification of the Lundberg-Palmgren model.

Several different methods have been proposed to estimate bearing life based on plastic strain accumulation in strain hardening materials. Most of these only consider the crack initiation life, but a few are used to estimate the crack propagation life either in addition to the initiation life or exclusively. Crack initiation is generally considered to occur due to plastic deformation in the material near the location of maximum stress in

the ball. Jiang and Sehitoglu developed a semi-analytical plasticity model accounting for ratcheting in pearlitic rail steel [18]. Maitournam et al. developed a fatigue life model for multiaxial out-of-phase loading where the material is elastic or undergoing elastic shakedown on a global scale, but undergoing plastic shakedown or ratcheting on a mesoscopic (grain) scale [3,4].

More recently, the idea that failure is initiated near inclusions has lead to a number of researchers to explore mesoscopic computational models [3-7, 21-23]. Melander [5] studied the effect of four different common inclusions in bearing steels (pores, manganese sulfide, titanium nitride, and alumina). First, the thermal cycles used for heat treatment were simulated to determine which inclusions would debond from the matrix, as well as inducing residual stresses. Then several cycles of a rolling contact load were applied and the crack energy release rate, G, was tracked throughout the process. In this way, it was possible to compare the relative significance of each of these inclusions. It was shown that the cracked alumina particle was the most critical inclusion, while the uncracked was the least critical. Kabo and Ekberg [3, 5-7] developed a series of models for railways. They used a pore to approximate the response of a manganese sulfide inclusion, since the pore should be more detrimental. They demonstrated that larger defects as well as clusters of defects together tend to be the most detrimental to fatigue life.

Bearing Materials

Due to the high performance required from aerospace bearings, materials have been developed specifically for this application. The most common bearing materials are hardened bearing steels. The chemical composition of several of the most common bearing steels are given in Table 1-1. A VIM-VAR (vacuum induction melting, vacuum

arc remelting) casting method is used to produce these materials, which results in a homogenous microstructure with consistent chemical composition and ultra-high cleanliness.

Through-hardened bearing steels are the simplest and most common materials used in aerospace bearing applications. These have all of the alloying elements to be used introduced during initial casting and thus have a uniform chemical composition throughout. AISI 52100 steel is currently the most common bearing material. It has high carbon content for increased hardness, but lacks a number of the other alloying elements used for corrosion resistance, aid in carburization, control carbide formation, etc. 52100 steel traditionally only undergoes a single tempering cycle, and therefore contains a significant proportion of retained austenite [6]. This retained austenite will transform during RCF into martensite, inducing tensile residual stresses which may lead to premature failure. M50 is another common through-hardened bearing steel. It contains a number of additional alloying elements compared to 52100 that help to form fine precipitated carbides that will improve the mechanical properties. A representative M50 micrograph is given in Fig. 1-4. The material is composed of a martensite matrix with grains varying from 10 to 15 microns. M50 has both large primary carbides (5-10 microns) and smaller carbides (<5 microns) nearly uniformly distributed through the entire material with approximately 12 vol% total (Fig. 1-5) [7,8]. The larger carbides form during casting due to the high initial carbon content. These large carbides tend to become oriented in bands during the rolling/forging processes, see the inset in Fig. 1-5. The smaller, secondary carbides precipitate during tempering and are randomly oriented. The most common form for the carbides to form are $M_{23}C_6$ and M_7C_3, where M

represents a metal and C represents carbon [9]. The most common forms are iron and chromium carbides, although some molybdenum and vanadium carbides also exist. Finally, initially there is a small amount (<1%) austenite, which transforms due to rolling contact fatigue (RCF).

A common method to improve bearing performance, which has been adopted within the aerospace community, is case hardening. M50NiL is an M50 variant with a much lower initial carbon content during casting and a high nickel content to aid in carburization. After the part is formed but prior to tempering, certain critical faces are case carburized to a carbon content, and thus hardness, which is comparable to M50 at the surface. Due to the carburizing procedure being diffusion controlled, there exists a gradient in the distribution of the carbides from case layer to core, with the case layer having a large volume fraction of carbides, which decreases gradually with depth. Due to the lower initial carbon content during casting, carburized steels lack the large primary carbides observed in the through-hardened steels discussed previously containing mainly smaller carbides which only form during subsequent tempering cycles. These carbides are on the order of 1 to 3 μm in size, and well distributed, see Fig. 1-6. P675 is a similar case carburized steel with the main difference being the high chromium content for corrosion resistance. Research is currently being performed on so-called duplex hardened steels. These materials are first case carburized to a depth of approximately 2 mm, and then case nitrided to a much shallower depth of approximately 0.1 mm. These materials are expected to have similar properties to case carburized materials, but with even better hardness and scratch and wear resistance at the surface due to the additional nitriding.

In addition to the gradient in carbide volume fraction, a residual compressive stress develops in the outer case layer of the carburized materials. This is due to the volumetric expansion from the martensitic transformation that occurs when the samples are quenched following carburization [10]. Due to the gradient in carbon content, the expansion of the outer case layers is greater than the inner material. However, given that the outer material is constrained by the core, a residual compressive stress develops. A portion of this residual compressive stress is relieved during the subsequent tempering cycles [11]. The direction of this residual compressive stress is parallel to the surface; while relatively little residual stress exists normal to the surface. This stress state has been shown to increase the performance of carburized materials by decreasing the effective mean tensile stress induced during rolling contact loading. Conversely, the through hardened materials do not develop notable residual compressive stresses during heat treatment, due to the lack of gradation in carbon distribution [11]. A new proprietary method for mechanical processing has been developed which can induce compressive residual stresses in a material that follow a similar distribution to the distribution of residual stress seen in case hardened materials i.e. the maximum residual stress occurs at the surface and then gradually reduce to a near constant value within the core region.

The most recent advancement in bearing materials is the use of hybrid bearings. These bearings consist of steel raceways and silicon nitride balls. The main advantage of using silicon nitride balls is the reduction of centrifugal forces on the outer raceway due to the balls' lower density [12,13]. Silicon nitride also has higher corrosion resistance, higher hardness, higher elastic modulus, and lower friction coefficient than

steel [12,13,14]. The silicon nitride balls are formed through hot isostatic pressing (HIP), through which it is possible to achieve near theoretical density [15]. The low void content and high strength of the silicon nitride leads to the steel raceway often being the limiting factor in the life of the bearing. Research has shown that hybrid bearings have a longer life and less variability in life than all steel bearings [16,17,18].

Current Study

Bearing manufacturers are currently working to increase the life of ball bearings by several orders of magnitude. New ultra-clean steels have been created to accomplish this goal. However, the current life models are still largely based on the classical Lundberg-Palmgren model developed in 1947 [19,20]. These models are empirical in nature, and do not directly consider the constitutive behavior of the materials under contact loading, hence significantly underestimating the life of these modern bearing steels. This manuscript is part of an effort towards an improved life model that will more accurately predict the fatigue life of modern ball bearings. Finite element programs are increasingly being used in the engineering community due to the relative ease and cost. Unfortunately, the constitutive response is a necessary input for this type of study. The problem that will be undertaken in this dissertation is to create a model for the constitutive response of the material within the RCF affected region in bearing steel due to rolling contact fatigue.

M50 bearing steel was chosen for this study due to its common application in aerospace applications, availability, and the through-hardened nature should make evaluation simpler for a first iteration. Six of the balls used in this study had initial residual stresses that were induced though a proprietary mechanical process (denoted as MP). Mechanical processing creates compressive residual stress in the hoop

direction, which reduces with depth up to a final depth of approximately 700 μm, where the residual stress is the same as the residual stress in a virgin (unprocessed) ball. The residual stresses are nearly uniformly distributed at a given depth below the surface. It is expected that these residual stresses will inhibit plasticity due to RCF and thus reduce the amount of change observed in the constitutive response of M50 bearing steel due to RCF.

The purpose of this research project is to investigate the evolution of the mechanical properties of M50 bearing steel due to rolling contact fatigue. The chapters of this thesis are organized according to the various experiments and analyses performed. Chapter 2 describes the two test methods that were used to perform the RCF tests on the specimens. The specimens tested were balls and rods made out of M50 steel. Chapters 3-6 go into detail about the various experiments performed on the balls after RCF testing. Only a selection of balls was used for each of the tests (Table 1-2) due to the destructive nature of several of the methods. The residual stress within the subsurface of the balls was measured using X-ray diffraction (XRD), as discussed in Chapter 3. Next, micro-indentation was used to measure the local hardness within the subsurface RCF affected region (Chapter 4). The indentation hardness can be used to estimate the yield strength, but cannot give insight into the full constitutive response. Hence, miniature compression specimens were extracted from within the RCF affected region to determine the full constitutive response (Chapter 5). The evolution of the microstructure due to RCF is discussed (Chapter 6). A subset of the same experiments were performed on the rods tested using the ball-rod RCF method (Chapter 7). The microstructural evolution of these was not studied and the residual stresses were

measured for a selection (Table 1-3). Miniature compression testing was not performed on these specimens because the RCF affected region is too small for the current method. The rod experiments made it possible to study the effects of a wider range of cycles and different materials. Finally, an empirical model for the evolution of the constitutive response of balls made out of M50 bearing steel due to RCF is derived in Chapter 8. Using this model, it is possible to estimate the stress-strain response of the material within the RCF affected region given the initial hardness or yield strength, the number of RCF cycles, and the Hertzian stress.

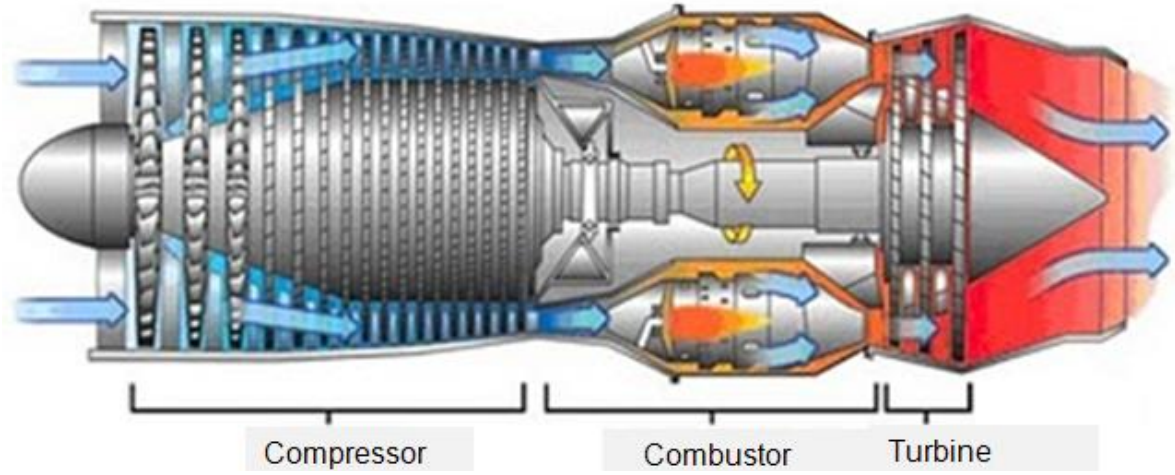

Figure 1-1. Schematic of a jet engine with the primary sections identified [21].

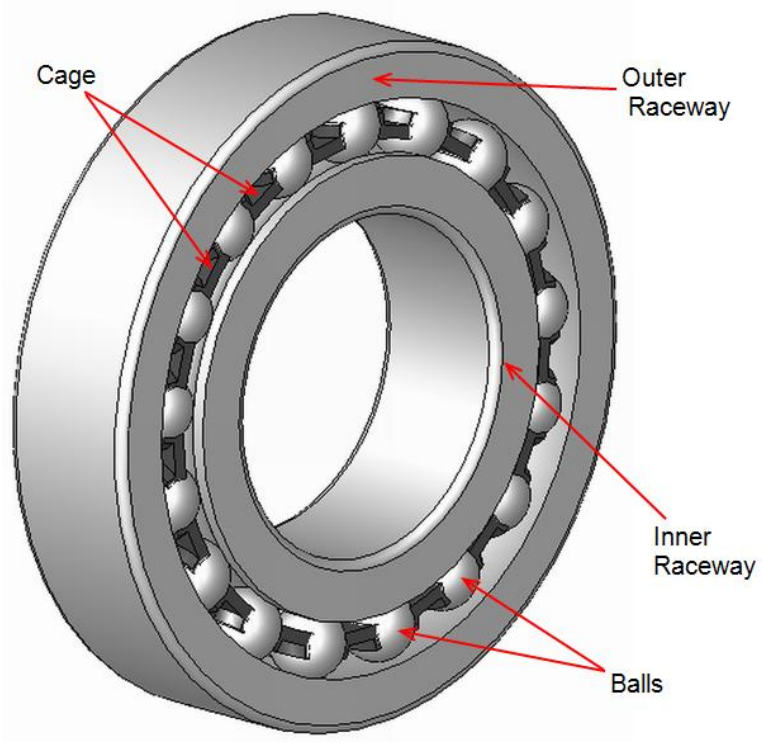

Figure 1-2. Ball bearing with the components identified [22].

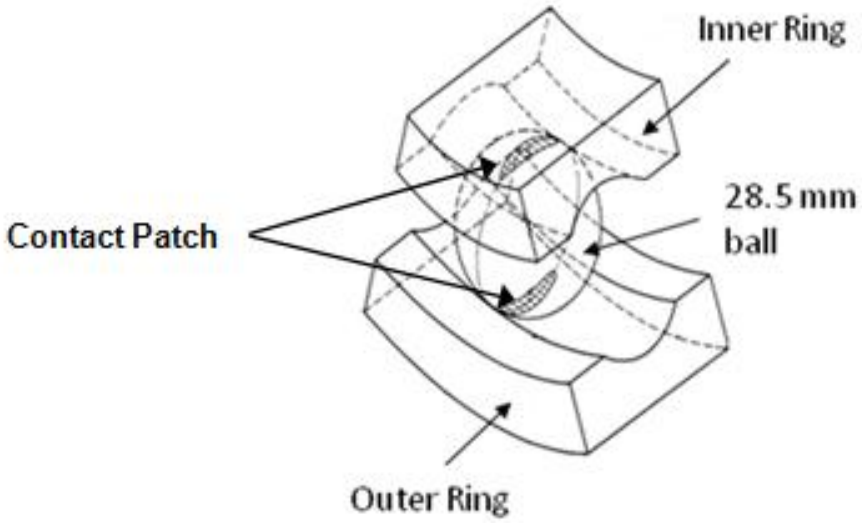

Figure 1-3. Schematic of a section of the ball bearing showing the contact patch formed between the ball and rings [23].

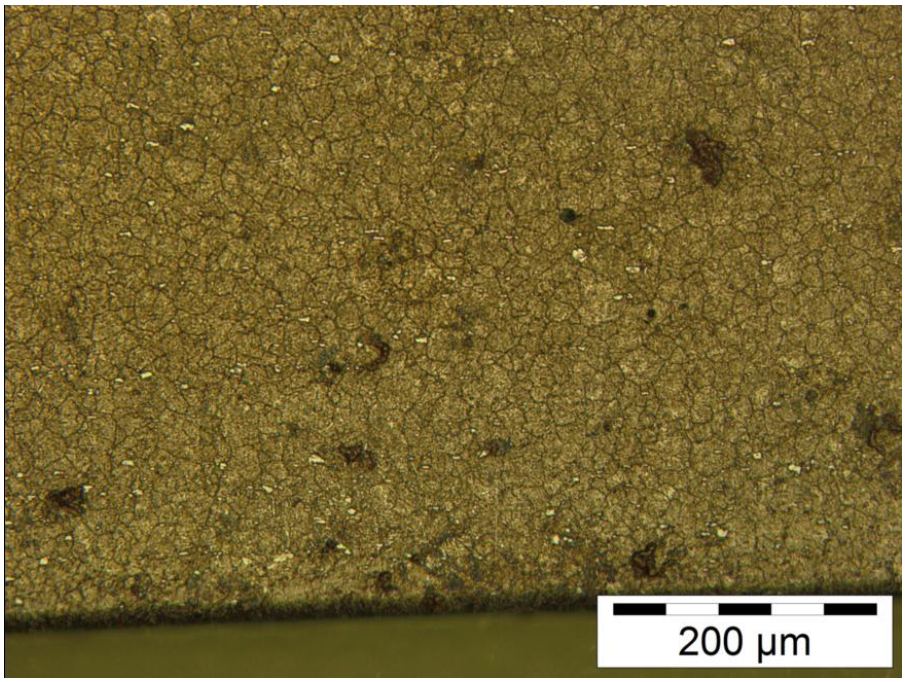

Figure 1-4. Micrograph of virgin M50. It is formed of a martensite matrix with grains between 10 and 20 microns.

Figure 1-5. Distribution and size of carbides in M50 bearing steel.

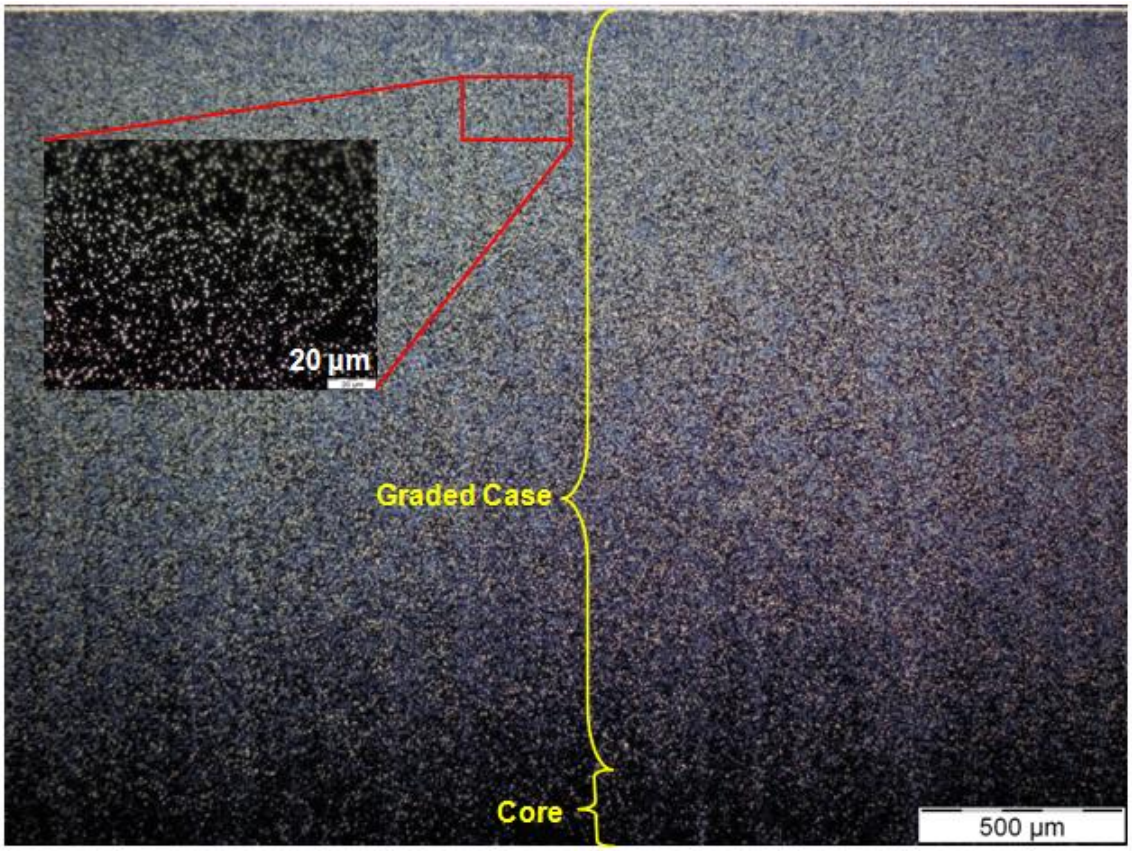

Figure 1-6. Distribution and size of carbides in the case layer of M50NiL bearing steel.

Table 1-1. Chemical constituents of several common bearing steels. The values are given in weight %. M50NiL and P675 are later case carburized significantly increasing the amount of carbon near the surface beyond those listed here.

	C	Mn	Cr	Mo	V	Co	Ni
52100	1.0	0.25	1.3	--	--	--	--
M50	0.88	0.35	4.0	4.25	1.0	--	--
M50NiL	0.13	0.2	4.1	4.3	1.3	--	3.4
P675	0.07	0.65	13	1.8	0.60	5.4	2.6

Table 1-2. RCF conditions and tests performed on each ball.

Ball ID #	Peak Hertzian Stress (MPa)	Run Time (M of cycles)	Residual Stress	Microstructure	Micro indentation	Miniature Compression
1	2330	36	✓	✓	✓	
2	2330	360	✓	✓		✓
3	2330	360	✓	✓	✓	
4	2740	36	✓	✓	✓	
5	2740	108		✓	✓	
6	2740	180		✓	✓	
7	2740	180	✓	✓	✓	✓
8	3360	36	✓	✓	✓	
9	3360	(S)52		✓	✓	
10	3360	(S)103		✓	✓	✓
11	3360	108		✓	✓	
12	3360	(S)122	✓	✓	✓	
13	2325	360		✓	✓	
14	2380	360		✓	✓	
15	2430	360		✓	✓	
MP1	2170	360	✓			✓
MP2	2430	360		✓	✓	✓
MP3	2535	360		✓	✓	✓
MP4	2790	360		✓	✓	✓
MP5	2920	360		✓	✓	
MP6	2950	360	✓	✓	✓	

Table 1-3. RCF conditions and tests performed on each rod track.

Track ID #	Ball material	Max Hertzian stress (MPa)	Run time (M of cycles)	Micro-indentation	Residual Stress	
1	Si_3N_4	6200	0.98	✓		
2	Si_3N_4	6200	9.98	✓		
3	Si_3N_4	6200	25.00	✓		
4	Si_3N_4	6200	49.95	✓		
5	Si_3N_4	6200	100.10	✓		
6	Si_3N_4	7240	0.01	✓		
7	Si_3N_4	7240	0.08	✓		
8	Si_3N_4	7240	0.13	✓		
9	Si_3N_4	7240	0.57	✓		
10	Si_3N_4	7240	0.98	✓		
11	Si_3N_4	7240	10.60	✓		
12	Si_3N_4	7240	26.4(S)	✓		
13	Si_3N_4	7240	53.87(S)	✓		
14	Si_3N_4	8270	2.21(S)	✓		
15	Si_3N_4	8270	19.92(S)	✓		
16	Si_3N_4	8270	25.18(S)	✓		
17	Si_3N_4	8270	49.4(S)	✓		
18	52100	7240	1.00	✓		
19	52100	7240	5.16	✓		
20	52100	7240	7.84(S)	✓		
21	52100	7240	8.75(S)	✓		
22	M50	7240	0.67	✓		
23	M50	7240	2.27	✓		
24	M50	7240	2.43	✓		✓
25	M50	7240	5.16	✓		✓
26	M50	7240	7.74	✓		✓
27	M50	7240	10.30	✓		✓
28	M50	7240	15.48	✓		✓
29	M50	7240	18.06	✓		✓
30	M50	7240	20.64	✓		✓
31	M50	7240	62.07	✓		
32	M50	7240	68.90	✓		

CHAPTER 2
ROLLING CONTACT FATIGUE TEST METHODS

Background

The time and cost required for full-scale bearing testing has lead to the development of various accelerated methods to test the effects of RCF on bearing materials. Each of these methods allows for the control the RCF conditions i.e. temperature, number of cycles, and applied stress. The reason that such a large number of test methods have been developed is the competing nature of the cost, difficulty, and time required for testing as well as the similarity between the conditions experienced during testing and the conditions experienced by the bearing during actual application. NASA developed and extensively used a five-ball RCF tester [24,25,26,27,28,29]. The bottom of this tester is composed of four balls that are placed inside of a cage and outer raceway. A fifth ball is placed above the lower balls and centered between them. This top ball is then pushed down with the appropriate load and spun at a prescribed speed, which in turn spins and loads the lower balls. This method is expected to subject the lower balls to similar conditions to a thrust loaded ball in normal engine application. Hampshire et al. [30] developed a flat washer experiment that is simple and effective for relative comparison of different materials. For this method, the test specimen is a flat washer with prescribed inner and outer diameters. One washer is placed on a vertical shaft. A set of balls in a cage, followed by a second washer, are then placed over it. The top washer is then loaded vertically and spun. After testing, the lower washer is inspected for the amount of damage, type of damage, etc. The loading experienced is quite different from that experienced in a bearing, but the cost and simplicity of testing make it valuable for relative effectiveness of new

materials. Bamberger and Clark [31] developed a method that uses a cylindrical rod as a test specimen, which is tested between two large drums. The lower drum is free to spin, while the top drum is free to spin driven about its center axis and along the vertical axis. The rod is held between the two drums and allowed to spin about its axis as the top drum is loaded and spun, thus subjecting the rod to RCF. The rod can then be advanced to a new axial position and another test performed. Similar to the previous method, the loading experienced by the specimen is different than that of a full bearing, but the simplicity and cost makes it useful for comparison purposes. Many more RCF methods have been developed, but this list serves to show an overview of the various approaches and the competing nature of the criterion desired for an accelerated test. Two methods were employed in this study: a single ball test and a three ball-rod test.

Experimental Methods

The purpose of this study is to determine the effect of RCF on the mechanical behavior of bearing steels. A key step towards this goal is subjecting the material to RCF. Two accelerated rolling contact experiments were used for this study i.e. a single ball test and a three ball-rod test. Both of these methods were utilized as each has pros and cons. The single ball tests were performed by SKF Aerospace in Falconer, NY through a contract with Pratt & Whitney in East Hartford, CT. The single ball test method uses actual balls from an aerospace engine bearing and subjects the balls to a similar stress condition to that experienced in an actual bearing and the balls accumulate approximately 60000 RCF cycles per minute. However, this method is prohibitively slow and expensive limiting the number of tests that can be performed. Hence, a second RCF test was used; the three ball-rod RCF method. Some of the three ball-rod tests were performed at the Air Force Research Lab in Dayton, OH, and

the rest were performed in-house. In this method, the test specimen is a cylindrical rod similar to the one used by Bamberger and Clark [31], but instead of two drums with flat circumferences, the rod is contacted by three balls. This difference means that the rod will experience a stress distribution that is closer to that used in a true bearing. The details of each of these methods is described below.

Single Ball Fatigue Test

A single ball tester, as shown in Fig. 2-1 was used to perform accelerated fatigue tests with RCF conditions similar to those experienced under normal operation. The specimens used were 28.575 mm and 41.275 mm balls made out of M50 bearing steel. A total of 21 balls were tested out of which six were subjected to proprietary mechanical processing (MP) to induce residual stress. These balls are identified as MP1-MP6. The balls were RCF tested with the applied Hertzian stress and number of cycles given in Table 1-2 at nominal engine operating temperatures. It is of note that three balls (#9, #10, and #12) have an “S” next to their run time, which indicates that the testing was stopped prematurely due to spall. Flats were cut on the sides of the ball, so that the same section was overrolled during each rotation of the ball. This allowed both for quicker testing as well as a known number of cycles. The basis of the test rig is two 160.8 mm drums. The outside circumference of each of these drums is conformed to the ball, such that only one large RCF affected zone will develop. The ball bearing was placed between the two rings and a vertical force was applied to the top drum via a hydraulic press. A plastic box was used to hold the ball in place. The inner ring was then rotated at 10000 rpm, resulting in the ball experiencing 60000 load cycles/min. A drip system is used to maintain ball lubrication during the test. An accelerometer was attached to the top drum, and was used to detect spall. When a preset vibration limit

was exceeded, indicating the presence of a surface crack or fatigue spall, the motor spinning the lower drum was automatically stopped. The test was continued until the desired number of cycles had been experienced or either the raceway or ball spalled. The number of RCF cycles, Hertzian stress, and initial residual stresses were each varied between trials, so that the effect of each of these could be determined. All of the RCF tests were performed at normal engine operating temperatures.

Since the outside circumference of the two drums is conformed to the ball, one large wear track is formed in the ball (Fig. 2-2). After RCF testing, the ball is sectioned parallel to the wear track (Fig. 2-3B). This section named the equatorial section has two elliptical RCF affected region, one on either end of the section. The section perpendicular to this (meridial section) has a ring of RCF affected material around the perimeter of the section (Fig. 2-3A).

Ball-Rod Fatigue Test

Accelerated rolling contact experiments were performed using a ball-rod bench tester similar to the one described by Glover [32], see Fig. 2-4. In this method, the specimen is a 9.52 mm diameter x 76 mm length rod made of M50 bearing steel (Fig. 2-5A). The rod is held vertical and three 12.7 mm diameter balls are used to apply a radial load to the rod (Fig. 2-5B). Balls made out of 3 different materials (i.e. 52100 steel, M50 steel, and silicon nitride) were used in various tests to study the effect of ball material. Springs are used to apply a load to the balls through tapered cups, which in turn creates the radial load applied to the rod. These three balls are each held 120 degrees away from each other using a retainer which is allowed to rotate concentric to the rod, see Fig. 2-4C. The rod is spun at 3600 rpm by an electric motor resulting in any given point along this cross section of the rod experiencing 2.389 RCF contacts per

revolution, or 8600 contacts/minute. This is less than three balls times 3600 rpm due to sliding as discussed by Glover [32]. A drip system is used to lubricate the rod at a rate of 10 drops/min during the experiment. The lubricant used was MIL-PRF-7808L. All of the tests were performed at room temperature to reduce the effect of this confounding variable. An accelerometer is used to monitor vibration (Fig. 2-4B). When a preset vibration limit was exceeded, indicating the presence of a surface crack or fatigue spall, the motor spinning the rod is automatically stopped. The test was ended either at the initiation of spall or after a prescribed amount of time. The test duration is measured by an electrical timer connected to the motor. Up to 20 experiments were performed on a single rod to minimize the effect of initial material properties on the test results (Fig. 2-4C). This was accomplished by advancing the rod axially each experiment.

Conclusions

Two methods were used to perform RCF tests i.e. a single ball method and a three ball-rod method. The single ball method uses actual balls used in bearings and subjects them to RCF conditions similar to those seen in field application. Three different stress levels were used on the unprocessed balls and the number of cycles was varied between 36 and 360 million cycles. The MP balls were tested for 360 million cycles over a range of stresses similar to those used for the unprocessed balls. The ball-rod method was used to supplement the number of tests performed due to the limited number of single ball tests performed. Three stress levels were also used for the rod tests, but the applied stresses are much higher than those used for the single ball tests to further accelerate testing. Three ball materials (i.e. 52100 steel, M50 steel, and silicon nitride) were used to test the rods, to investigate the effects of material properties and the potential utility of hybrid bearings.

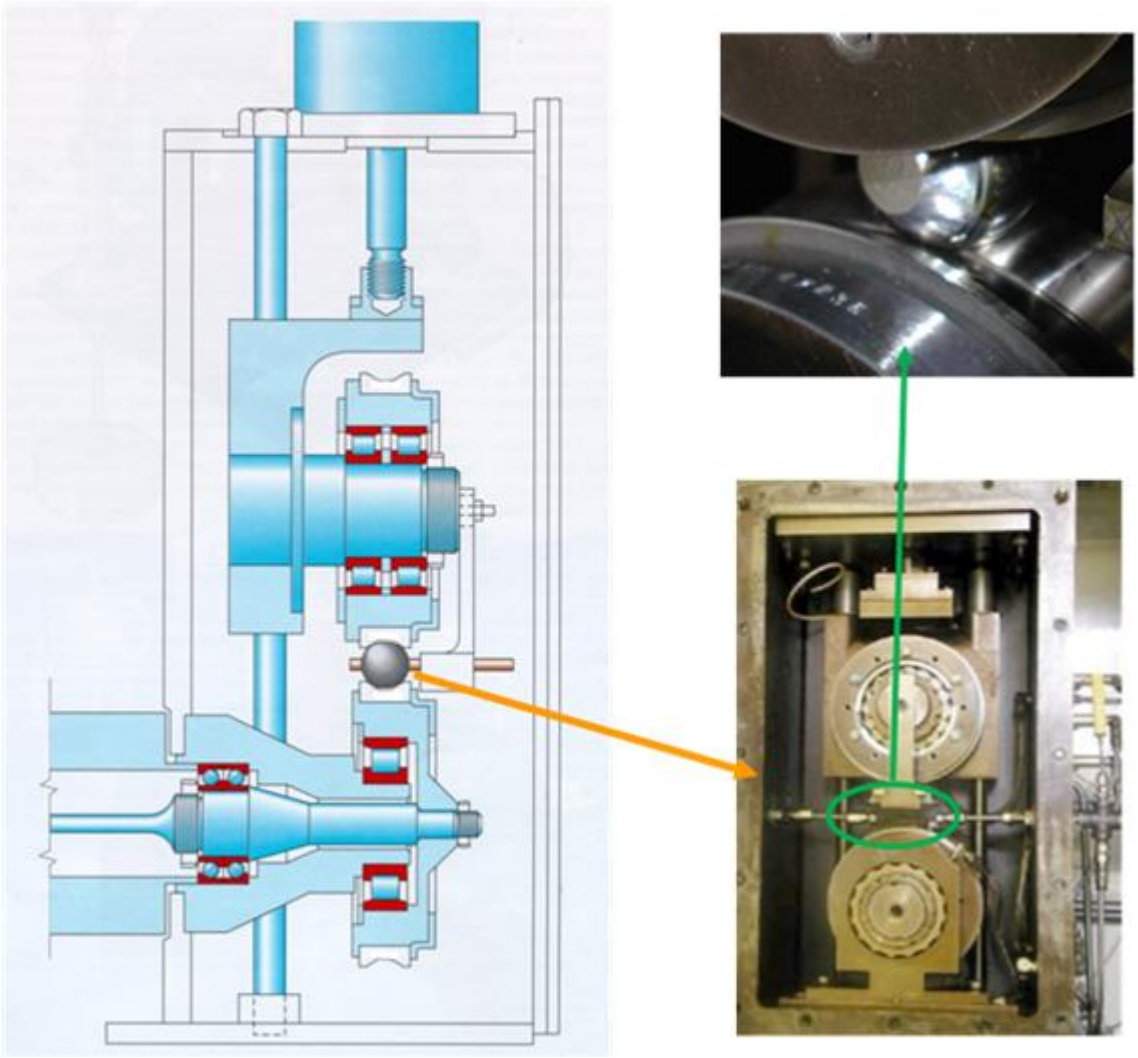

Figure 2-1. Schematic of the single ball fatigue apparatus. (Photos courtesy of Pratt & Whitney, East Hartford, CT)

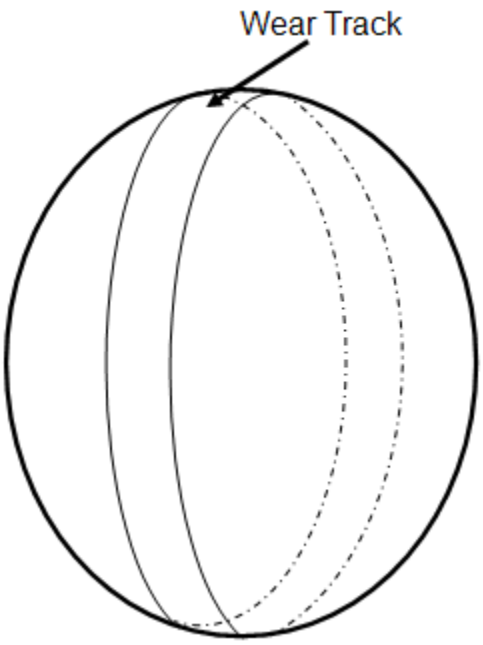

Figure 2-2. Schematic of the ball showing the single wear track that is formed.

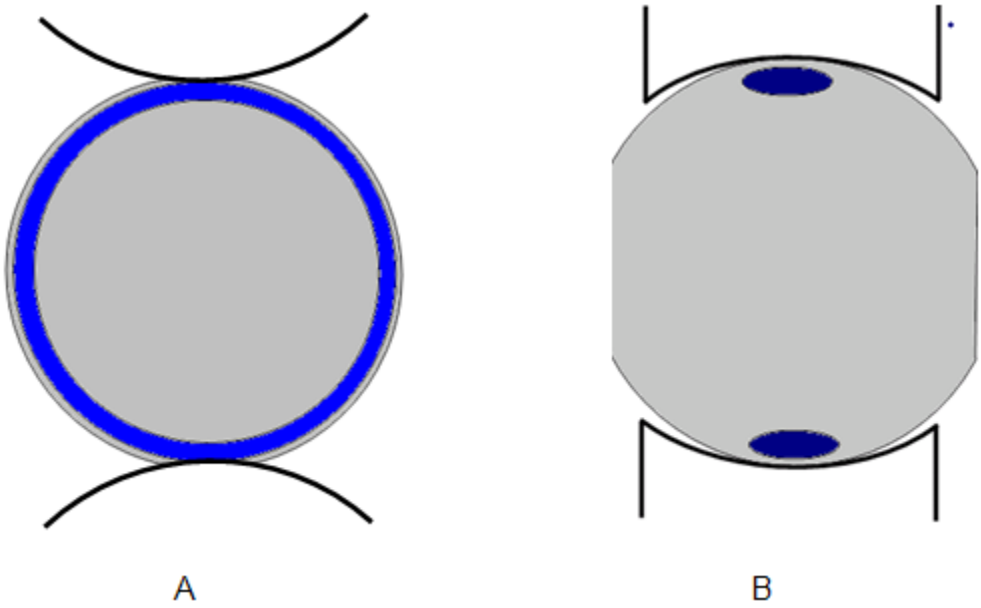

Figure 2-3. Schematic of the ball after sectioning. A) parallel to the wear track (meridial section) and B) perpendicular to the wear track (equatorial section).

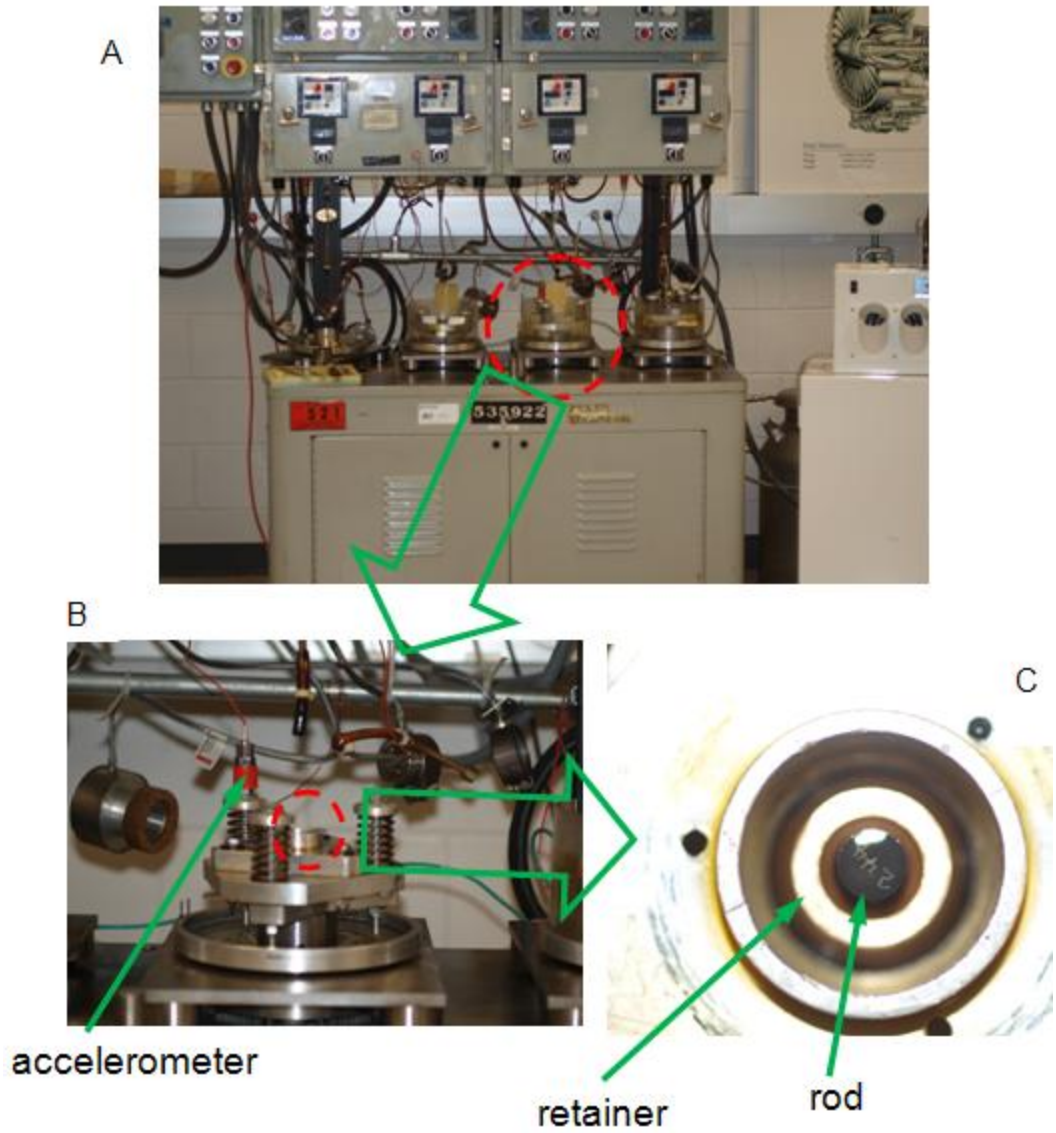

Figure 2-4. Setup used to perform three ball rod tests. A) Full setup showing the four stands and the control panel above. B) Single test stand C) Overhead view showing the rod and the retainer, which holds the balls at the proper angle. (Photos courtesy of Bryan Allison)

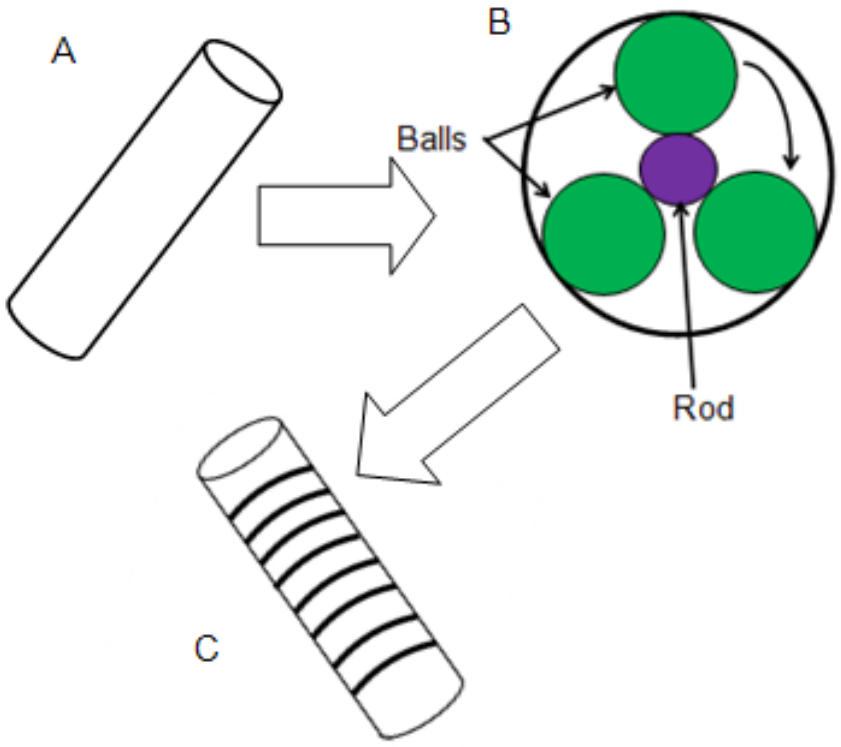

Figure 2-5. Schematic of the ball-rod RCF test A) Virgin rod. B) Balls loaded radially against the rod during testing. C) Rod with wear tracks after testing.

CHAPTER 3
RESIDUAL STRESS

Background

The effect of residual stress on rolling contact fatigue (RCF) life of a bearing is an area of immense interest among the bearing community. There is a general consensus that inducing compressive residual stress on the surface, and subsurface regions, in bearing raceways and rolling elements prior to operation substantially increases their RCF life [33,34,35,36,37,38,39,40,41,42], although some researchers have concluded otherwise [43,44]. Compressive residual stress is one of the benefits of using case carburized materials [45], however case carburizing is a difficult process [46]. Hence, several manufacturing processes are used to induce residual stresses in through-hardened materials including shot peening, overloading, turning, and grinding. Xiao et al. [33] performed RCF experiments on steel balls, which had been shot peened, and demonstrated that compressive residual stresses increase RCF life by as much as 40%. Cretu and Popinceanu [47] performed RCF experiments on roller and ball elements, which had been prestressed by overloading the specimen for the first few cycles. They demonstrated the fatigue life of prestressed specimens to be over twice the life of specimens that had not been prestressed. Guo et al. [37,38,48] compared the magnitude and distribution of residual stresses introduced through grinding and turning, and studied how these residual stresses will affect the propagation of fatigue damage due to RCF using a combination of experiments and numerical analysis. Warhadpande et al. [34] simulated a rolling element using an elastic-plastic finite element model to study the effect of residual stresses on the hardening. It was found that the initial residual stress leads to the material experiencing a reduced von Mises stress, but the

local yield stress is also decreased. This leads to a theoretically optimum preload, which is dependent on the service load.

It is also known that residual stresses increase over the operational life of a bearing [39,43,49,50,51]. This increase in residual stress has been reported to be as high as 28% of the applied stress [39]. It is evaluated by measuring the residual stress within the specimens before and after RCF testing using XRD. Ishida and Abe [51] performed rail-wheel experiments considering the effects of lubricant, radial load, and tangential load on the formation of residual stresses and RCF life. They showed that increased tangential force lead to increased residual stresses, and thus shorter RCF life. This is due to residual shear stress causing shell type cracks near the surface of the material. Rivero and Ruud [50] performed experiments on 52100 steel balls and concluded that the increase in residual stresses is due to a combination of phase transformation of the retained austenite and strain hardening. Voskamp [49] mapped the residual stresses as a function of depth within the RCF affected region. The maximum residual stresses were found to occur at the same depth as where micro-plasticity is expected supporting the theory that the increase in residual stresses is due to strain hardening. Matsumoto and Uehara [43] discovered that the evolution of residual stresses is highly dependent on the applied Hertzian stress and initial surface roughness, but not the number of cycles since the residual stress becomes nearly constant after a few thousand cycles. This is true even when the surface roughness continued to change with the number of cycles.

Several methods have been proposed on how to account for residual stresses in RCF life prediction models [34,41,48,52,53]. This usually involves modifying a popular

RCF or multiaxial fatigue model to account for residual stresses. Warhadpande [34] et al. used an elastic-plastic finite element model to determine the changes in the Von Mises stress during rolling and then modified the Lundberg Palmgren model to reflect the change in stress. Bernasconi et al. [41] superimposed the residual stresses with the applied stresses and then used the Dang Van failure criterion. Guo et al. [48] modified a multiaxial fatigue parameter initially fatigue parameter initial derived by Socie [54], which predicts whether K_I or K_{II} crack growth will dominate. Choi and Liu [52,53] developed a model for the RCF life based on crack formation and propagation. A crack initiation life was developed, which is based on the Basquin equation. A crack propagation life model was then developed by modifying the Paris law to account for local variation in hardness. The superposition of the two of these defines the fatigue life. This model was then used to predict the life of specimens, and it was shown to predict lives much closer than the more common Lundberg-Palmgren model.

Experimental Methods

The circumferential residual stresses induced due to manufacturing in several of the balls (both MP and unprocessed) were measured using XRD before and after RCF testing. This work was performed by Pratt & Whitney in East Hartford, CT. First, the residual stress was measured at the surface of the ball using XRD. Electropolishing was then used to remove material from the surface to a specified depth (up to 250 microns in each step), and the residual stresses were remeasured at this depth. This process was repeated at various depths below the surface of the ball to determine the distribution of residual stresses as a function of depth. Next, the balls were subjected to RCF in a single ball tester as discussed previously in Chapter 2. Finally, the

measurement of residual stresses was repeated after RCF testing, for some of the balls as shown in Table 1-2, to examine the evolution of residual stresses due to RCF.

Results and Discussion

The residual stress profile parallel to the rolling direction for a representative set of MP balls as well as for an as-manufactured virgin ball are provided in Fig. 3-1. The maximum residual stress for the unprocessed (virgin) ball is around 400 MPa at the surface, which quickly drops to 160 MPa over the first 2 μm, and then to a value of around 40 MPa in the subsurface at a depth of 300 μm. On the other hand, the residual stress in the MP balls (no RCF) ranges between 200 and 400 MPa near the surface and then gradually decreases into the core of the ball. Even at a depth of 500 μm, the compressive residual stress remains at a relatively large value of 200 MPa. It is expected that the residual stress in the MP balls beyond the depth of processing would be equivalent to the unprocessed ball, but measurements were not taken at a sufficient depth to validate this statement. After 360 million RCF cycles at the given stresses, the residual stress distribution remains relatively the same as the virgin MP balls at 250 μm, but decreases by almost half the value at a depth of 500 μm compared to virgin MP balls.

The residual stress measurements parallel to the rolling direction before and after RCF for the unprocessed balls are given in Fig. 3-2. Again, the residual stresses are compressive in nature. In contrast to MP balls, the maximum residual stress is at a significant depth below the surface. All the balls have moderate to high compressive residual stresses (150 – 550 MPa) near the surface which may have been generated during the manufacturing process and are not affected by the RCF. The residual stresses at the surface vary widely between balls and reduce dramatically over the first

25 microns depth. For the unprocessed balls, the depth of maximum residual stress increases with an increase in peak Hertzian stress used in the RCF test. The residual stresses continue to increase with increased RCF cycles, but the increase in compressive residual stress is a stronger function of peak Hertzian stress as will be shown in Fig. 3-3. At relatively low applied Hertzian stress (2320 MPa), the residual stress increases by only 40 MPa from 36 million cycles (ball #1, Fig. 3-2A) to 360 million cycles (ball #2 and #3, Fig. 3-2B), whereas at higher Hertzian stress (3360 MPa) the residual stress increases by 140 MPa from 35 million (ball #8) to 122 million cycles (ball #12). Figure 3-3 summarizes the results from Fig. 3-1 and 3-2 and reveals the relationship between the maximum residual stress developed in each ball after RCF cycling and the applied peak Hertzian stress during RCF. The residual stresses for the MP balls do not significantly change with variations in the Hertzian stress, but it appears to change linearly for the untreated balls when the number of RCF cycles varied from 36 million to 360 million. It is known that RCF induces a complex triaxial state of residual stress that is superposed on the existing residual stress state [34]. The net result of RCF testing on MP balls is that the residual stresses are virtually unchanged due to RCF. This result is in contrast to the unprocessed balls, which showed significant increase in compressive residual stress relative to the virgin ball, see Fig. 3-1.

Summary

The residual stresses parallel to the rolling direction were measured as a function of depth for a selection of the balls tested before and after RCF. It was shown that the highest residual stresses are found at the surface for the MP balls, but at some depth below the surface for the unprocessed balls. Further, it was found that the residual stress within the MP balls either does not change, or slightly decreases, during RCF,

while the residual stress in the unprocessed balls clearly increases during RCF. A linear relationship was found to exist between the maximum residual stresses after RCF for the unprocessed balls independent of the number of RCF cycles.

The evolution of residual stresses due to RCF is generally attributed to strain hardening and/or the transformation of retained austenite [49,55,56,57]. In Chapter 4, micro-indentation is performed within the subsurface of the balls to investigate amount of hardening within the RCF affected zone. In Chapter 6, the subsurface is chemically etched to study the evolution of the microstructure. The combination of these two may provide more insight into the cause of the evolution of residual stresses during RCF (or lack thereof for the MP balls).

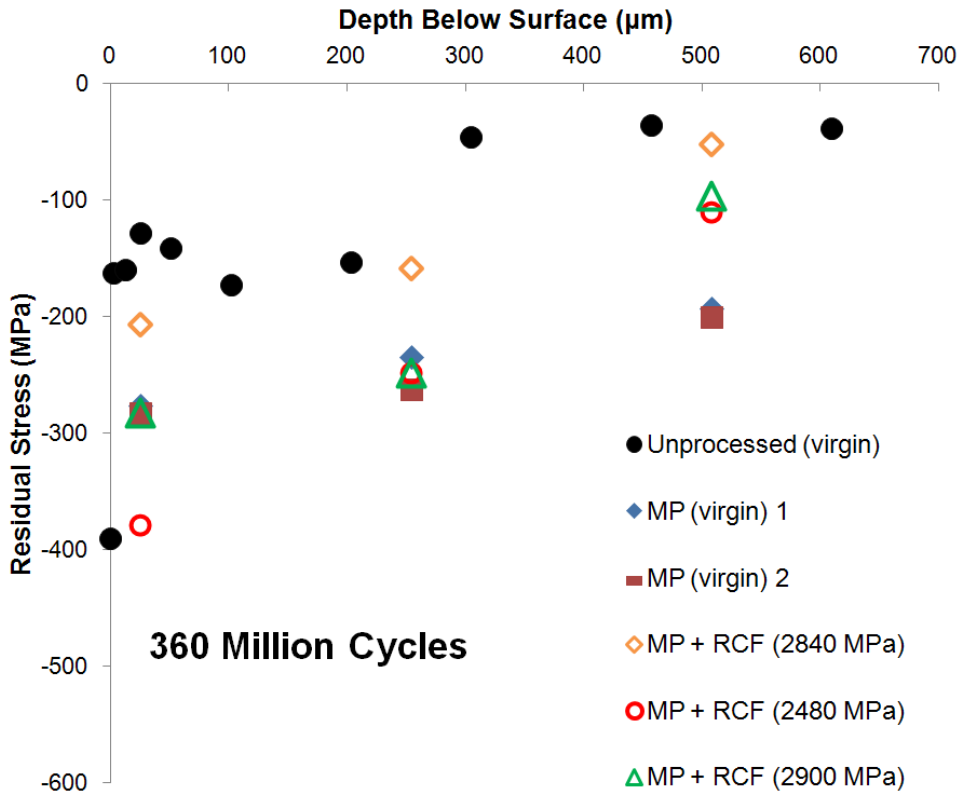

Figure 3-1. Residual stress distribution parallel to the rolling direction in unprocessed (virgin) balls, MP balls, and MP+RCF balls.

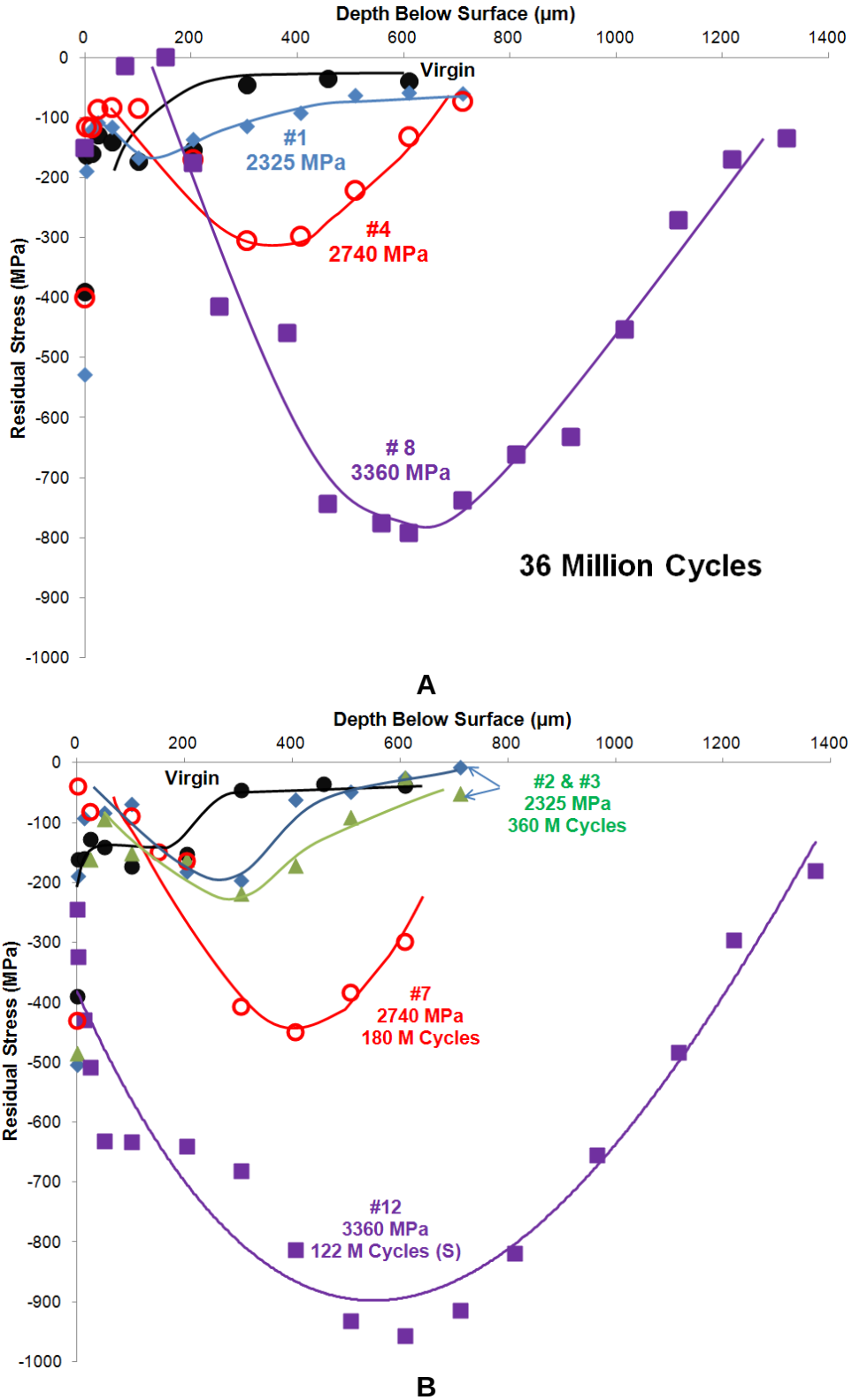

Figure 3-2. Residual stress distribution parallel to the rolling direction in unprocessed balls after RCF after: A) 36 million RCF cycles. B) The maximum number of RCF cycles tested.

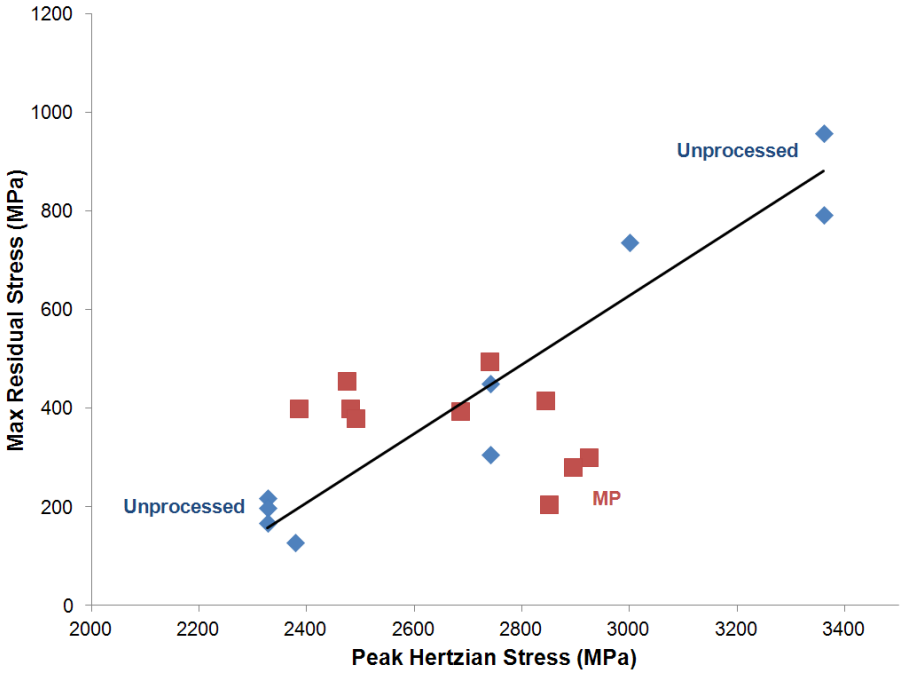

Figure 3-3. Relationship between peak residual stress and peak Hertzian stress.

CHAPTER 4
MICRO-INDENTATION

Background

Indentation is a popular method for studying the distribution of mechanical properties within a material. Branch et al. used micro-indentation within the subsurface beneath a macro-indent, in conjunction with finite element modeling to determine the constitutive response of case hardened bearing steels [58,59,60]. Klecka [61] then extended this work such that the constitutive response as a function of depth could be determined with only a series of surface indents. Ahlstrom and Karlsson [62] used micro-indents to map the hardness of rail steel after manufacturing to determine the variation in flow stress over the cross section and identified the weakest section. Xiao et al. [33] introduced residual stresses in ball bearings using shot peening and mapped micro-hardness as a function of depth, before and after shot peening, to determine the increase in hardness of the material due to this surface treatment. The balls were then RCF tested to demonstrate that the shot peened balls have a longer fatigue life, but no additional micro-indentation testing was performed after RCF testing.

Indentation has been previously used to study the evolution of the mechanical properties of RCF affected material. Eden et al. [63] compared the microstructure and hardness of newly manufactured rail steel and one that had been taken out of service due to RCF cracks. They performed micro-indentation and nano-indentation within the subsurface of each and found significant hardening within the RCF affected steel to a depth of 5 mm. This hardness was seen for both of the microstructural constituents in the material, pearlite and ferrite. Arakere and Subhash [64] performed micro-indentation within the subsurface of case hardened M50NiL steel rods after RCF testing

at 5.5 GPa. A 12% increase in the hardness was found after 13.5×10^6 cycles. They reported that the hardness increases for the first several million cycles and then remains constant thereafter. Rivero and Ruud [65] performed surface indents on 52100 balls after RCF and demonstrated a significant loss of hardness. Reichard et al. [66] performed indents as a function of depth within the RCF affected region and found a similar decrease. Recently, Bhattacharyya et al. [67] used micro-indentation to map the subsurface after RCF of case hardened steel rods. They reported softening in the regions surrounding the strain hardened region. This softened region may be a prime candidate for failure initiation.

Micro-indentation was performed within the subsurface of the balls tested in this thesis. Micro-indentation provides qualitative information about the local mechanical properties. The distribution of micro-hardness illustrates the distribution of the strain hardening of the material within the RCF affected region that may provide some further insight into how the residual stresses discussed previously form. The size of the plastic region and the magnitude of hardness increase, relative to the virgin material, are compared for balls which were tested subjected to RCF under varying conditions. Micro-hardness can also be used to estimate the local yield strength through the Tabor's relationship, $H = C\sigma$, where σ is the flow stress at 8% strain, C is the constraint factor (taken to be approximately 3 for most metals), and H is the indentation hardness [68,69].

Experimental Methods

Micro-indentation was performed within the RCF affected zone of the balls tested. First, the balls were sectioned perpendicular to the rolling direction. On this

cross section, the RCF zone is an ellipse at either end of the specimen, as shown in 4-1. This section was polished following standard metallurgical practices to a final polish of 6 μm. Micro-Vickers indentation was performed on 21 of the 22 balls tested (Table 1-2) using a Wilson Tukon 2100B. A 200 gram load was selected because it is the smallest indent that can be reliably measured with an optical microscope. This resulted in an average indent diagonal length of approximately 20 μm. Indents were spaced 75 μm apart as well as from the edge as per ASTM E384 [70]. Indentations were performed as a function of depth into the ball within the RCF affected zone, see Fig. 4-1. Five parallel rows of indents were made at each depth to give an average hardness. The stress experienced will vary between each of these rows, but the distance between them was small enough compared to the width of the RCF affected zone that it was assumed all of the rows would experience the same stress. Several indents were also made within the core of each ball, where the material is unaffected by the RCF, to compare the hardness evolution relative to the virgin material. Indentation was performed to a depth of at least 1000 μm, whereas mechanical processing only influences the first approximately 700 μm below the surface and the maximum stress due to RCF occurs at a depth of approximately 300-400 μm. Mechanical processing should not affect the results of the hardness measurements since indentation with a sharp indenter is not expected to be affected by residual stresses [45,71,72]. This was verified further by performing micro-indentation within the MP region of one ball (M3) and it was found that the indentation hardness within this region was nearly identical to the hardness of the core of this ball, see Fig. 4-2.

Results and Discussion

Micro-indentation was performed on 21 of the 22 balls used in this investigation. The summary of these results is provided in Table 4-1. The virgin hardness of each ball along with the maximum hardness within the RCF affected zone is shown. The balls came from three separate batches: balls #1- #12 came from batch 1, #13 - #15 came from batch 2, and the MP balls came from batch 3. There is a significant variation (at 95% confidence) between the virgin hardness of each of the three lots (Fig. 4-3). Hence, the hardness increase (the difference between the maximum hardness within the RCF affected zone and the virgin hardness of the same ball) is used for comparison, rather than comparing the maximum hardness of each ball after RCF. In general, it is noted that for unprocessed balls there is an increase of up to 10% in measured hardness in the RCF affected zone (ball #12) whereas the increase was less than 2% for MP balls. Also, there is a consistent increase in hardness of well above 6% in balls subjected to the highest Hertzian stress of 3360 MPa (#8 – #12) even after only 36 million RCF cycles.

The maximum shear stress calculated using Hertzian stress theory [73] and the measured hardness as a function of depth within the RCF affected region for a representative ball (ball #8) are shown in Fig. 4-4. The measured hardness near the surface (at 75 μm depth) is slightly more than that of the virgin core material and then it increases to a maximum value at a depth of approximately 400 μm below the surface and then gradually decreases until it reaches the core hardness at a depth of approximately 900 μm. No softening was observed. The calculated maximum shear stress is seen to follow a similar trend.

The hardness increase as a function of the number of RCF cycles for various balls is given in Fig. 4-5. Notice the grouping of the MP balls in the lower right corner which highlights that mechanical processing prevents hardening. All of the unprocessed balls that were tested for 360 million RCF cycles hardened significantly more than the MP balls (at 95% confidence), even though they were tested with lower Hertzian stress. The balls that were tested at 3360 MPa peak Hertzian stress (the group on the top left of Fig. 4-5) exhibited an increase in hardness of nearly 500 MPa over the first 50 million cycles (balls #8 and 9), and then an additional increase of another 100-150 MPa over the next 60 million cycles (balls #10, #11, and #12) at which point the balls spalled and hence the test was terminated. The balls that were subjected to 2740 MPa (group at the bottom left of Fig. 4-5) only hardened by 120 MPa over the first 30 million cycles (ball #5) and then hardened nearly linearly up to 200 MPa after 180 million cycles (ball #6). It is generally found that the microstructure and mechanical properties of bearing material undergoing RCF will evolve at a slow linear rate after an initial shakedown [56,74,75,76,77]. Therefore, if the increase in hardness is approximated as linear from the first measured ball at each stress level, then it is seen that the rate of hardening is much higher for the balls that were subjected to higher stresses as shown by the linear trends for each group of data. The balls tested at the lowest stress level (2330 MPa) show virtually no additional hardening after the first 36 million cycles (balls #1, #3, #13, and #14), whereas the balls tested with 3360 MPa (#8-#12) failed as early as 50 million cycles. This illustrates that Hertzian stress has a more dominant effect on the hardening and eventual spall than the number of RCF cycles. Also, the MP balls show no significant hardening (at 95% confidence), even with

significantly higher stress than the stress on the unprocessed balls after the same number of RCF cycles.

Summary

Micro-indentation was performed on 20 of the 22 balls tested. A significant variability (at 95% confidence) in virgin hardness was found between lots, so the hardness increase was used for all analysis rather than the hardness after RCF. Mechanical processing was shown to not affect the indentation hardness of the balls. The hardness increase was shown to follow a similar trend to the max shear stress, τ_{xz}. Hardening of the unprocessed balls was shown to be primarily dependent on the applied Hertzian stress, while the number of RCF cycles plays a minor role. Over a 9% increase in hardness was seen for the balls tested at the highest Hertzian stress. A linear relationship between the hardness increase and the number of cycles seems to fit reasonably well for the balls tested at each Hertzian stress level. The testing of three of the five balls that were tested at the highest Hertzian stress (3360 MPa) was stopped prematurely due to spall. No significant hardness increase (at 95% confidence) was found to occur within the MP balls even when tested with high Hertzian stress for a high number of cycles.

While the above technique of micro-hardness measurement provides the local changes such as hardness or yield strength of the RCF affected regions, it cannot provide information about the full constitutive response of the material, which is of value in understanding and modeling the RCF life of a bearing material. A technique has been successfully developed by the authors to study the evolution of yield strength and work hardening rate as a function of the RCF parameters (contact stress and number of

RCF cycles) [78]. This method is used to determine the constitutive response of RCF affected material in the following chapter.

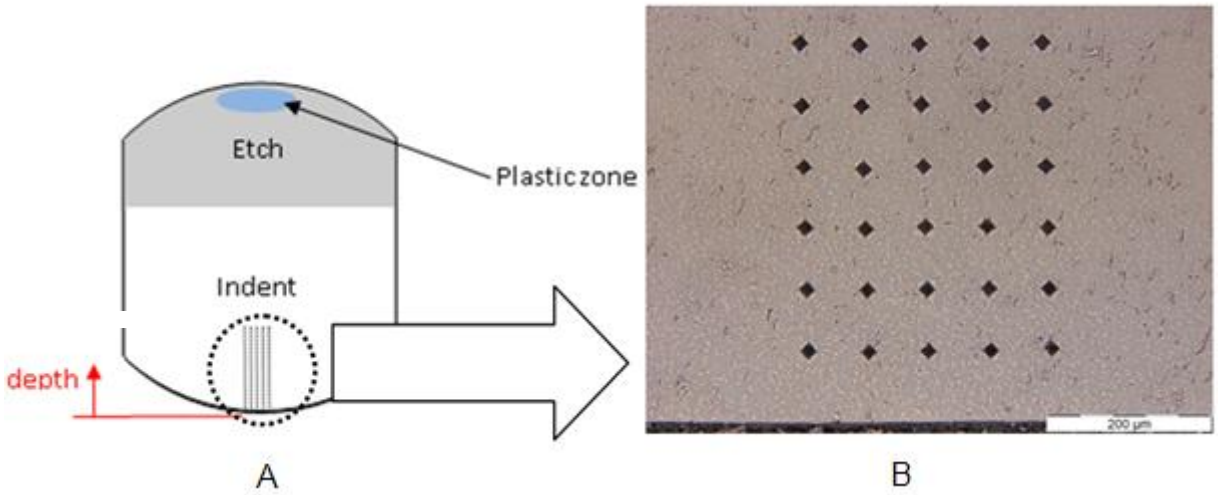

Figure 4-1. Location of the micro-indents made on the ball cross section. A) Schematic of the ball section showing the etched region, plastic zone, and indent field. B) Micrograph of the indent field in the subsurface RCF affected region.

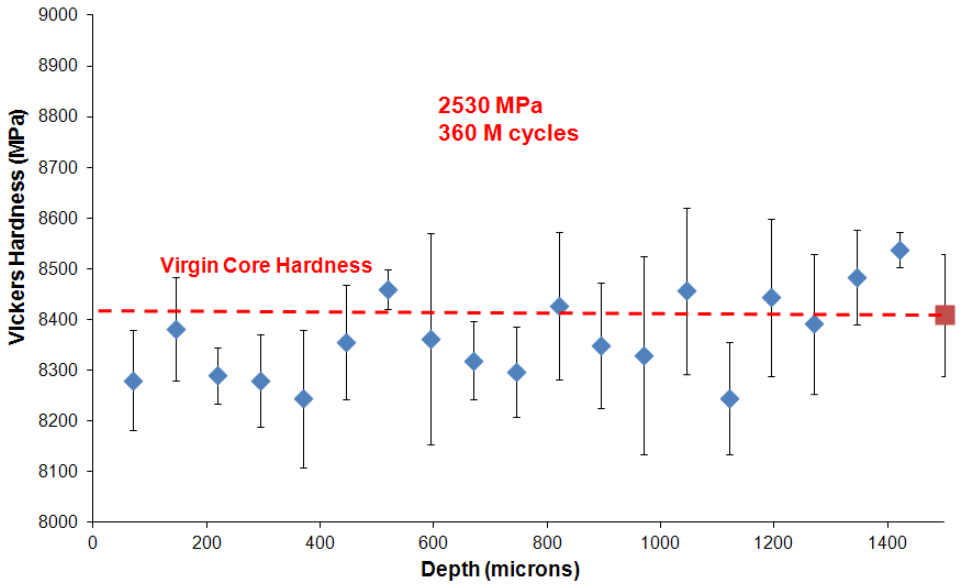

Figure 4-2. Representative indent map of one of the MP balls (MP3) prior to RCF.

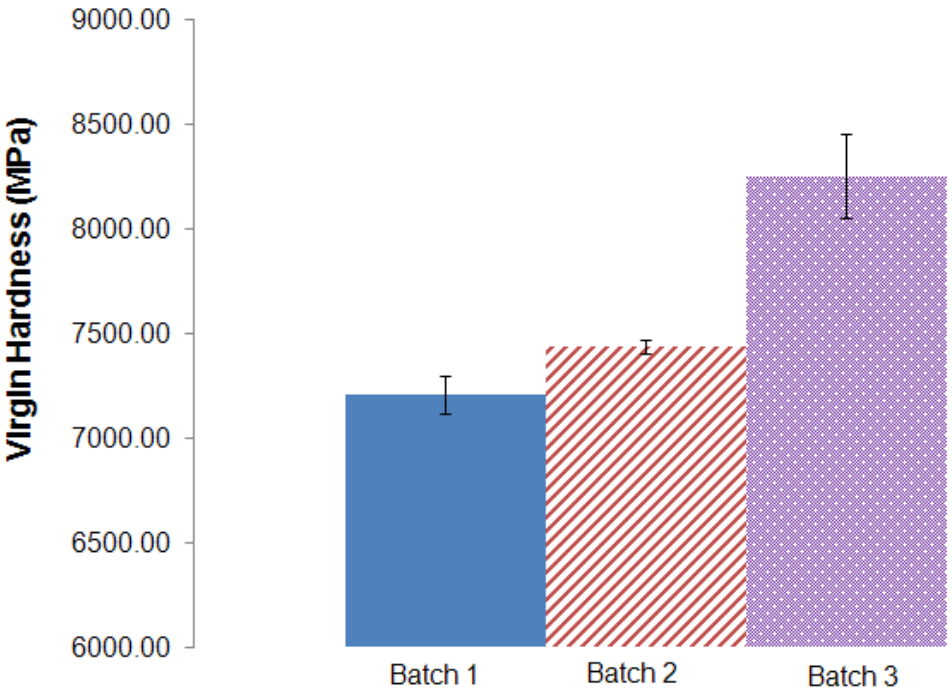

Figure 4-3. Virgin hardness of the balls tested.

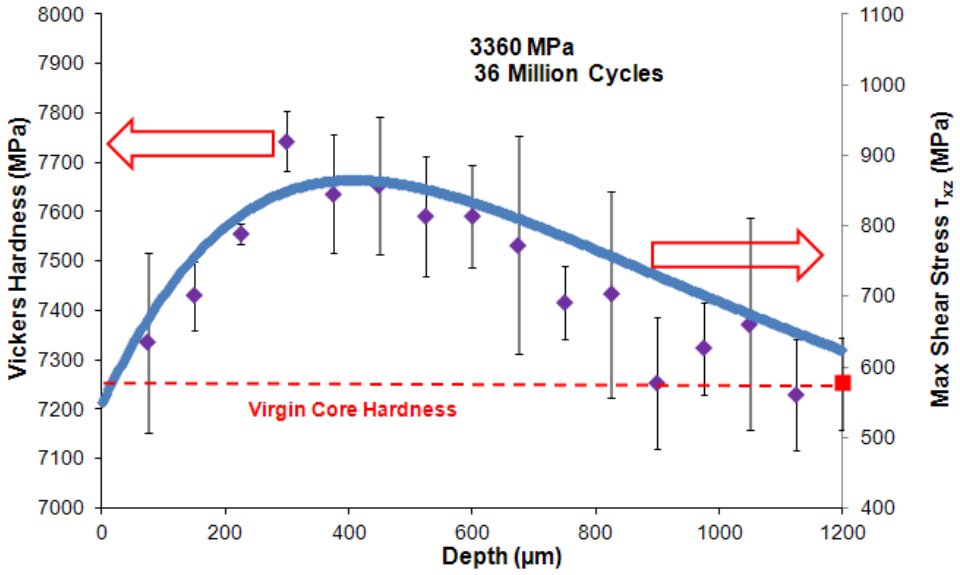

Figure 4-4. The trends in measured hardness (symbols) and calculated max shear stress (solid line) as a function of depth for a representative ball (ball #8). The two follow a similar trend within the depth of the material.

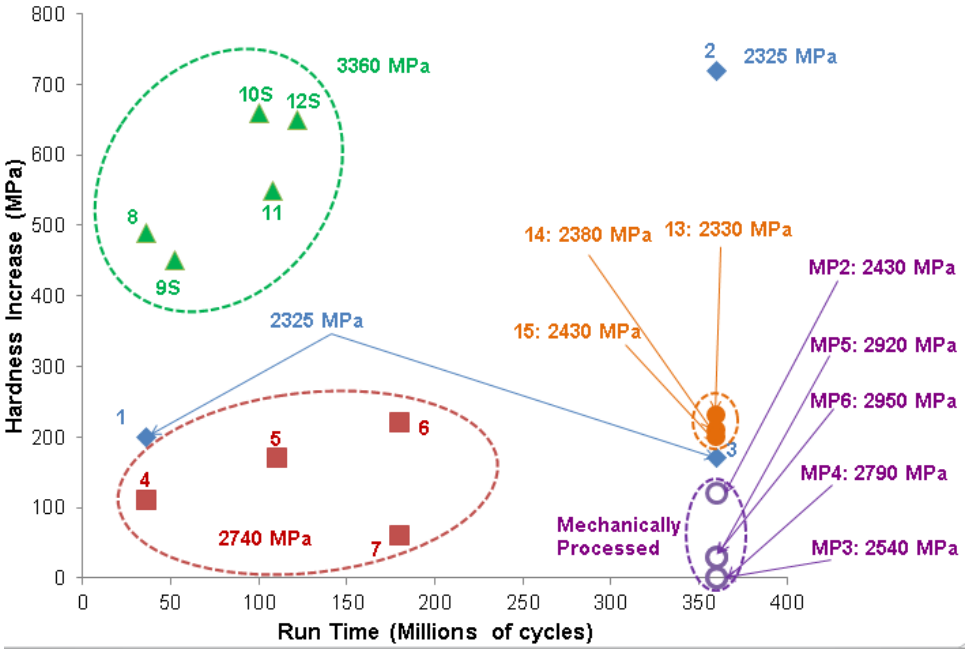

Figure 4-5. Hardness increase for various balls as a function of RCF cycles. The MP balls are denoted by MP, while the balls that were stopped prematurely due to spall are denoted by an S.

Table 4-1. RCF test conditions for balls and the measured hardness before and after testing.

Ball ID #	Peak hertzian stress (MPa)	Run time (M of cycles)	Virgin hardness (MPa)	Max hardness (MPa)	Hardness increase (MPa)	% Hardness increase (MPa)
1	2325	36	7060±110	7260±50	200±50	2.8±0.77
3	2325	360	7180±100	7350±40	170±30	2.4±0.40
4	2740	36	7280±70	7390±90	110±40	1.5±0.59
5	2740	110	7200±60	7370±60	170±30	2.4±0.42
6	2740	180	7320±60	7540±160	220±70	3.0±0.99
7	2740	180	7240±40	7300±40	60±20	0.8±0.28
8	3360	36	7250±90	7740±60	490±30	6.8±0.47
9	3360	52 (S)	7170±110	7620±120	450±60	6.3±0.83
10	3360	100(S)	7370±50	8030±110	660±50	9.0±0.69
11	3360	108	7160±90	7710±80	550±40	7.7±0.58
12	3360	122 (S)	7090±70	7740±120	650±50	9.2±0.79
13	2325	360	7470±200	7700±140	230±80	3.1±1.0
14	2380	360	7430±210	7640±60	210±50	2.8±0.73
15	2430	360	7410±120	7610±140	200±70	2.7±0.92
MP2	2430	360	8390±130	8510±170	120±80	1.4±0.97
MP3	2535	360	8430±170	8420±200	0±100	0.0±1.1
MP4	2790	360	8370±140	8360±120	0±60	0.0±0.74
MP5	2920	360	8010±190	8040±210	30±100	0.4±1.3
MP6	2950	360	8070±140	8100±130	30±70	0.4±0.82

CHAPTER 5
MINIATURE COMPRESSION

Background

Due to the simplicity of specimen geometry and ease of interpretation of test results, uniaxial compression testing has become one of the most common experimental methods to obtain the constitutive response of materials. Traditional compression tests are generally performed on specimens with diameters of 1 cm or larger as per ASTM standard E9 [79]. When the specimen size is reduced to 1 mm or smaller, sample geometry and alignment tolerances become much more challenging. Furthermore, small samples tend to have proportionally smaller magnitude of deformation (change in length) and therefore, the deformation due to machine compliance is often comparable to, or even larger than, the specimen deformation, and must be appropriately accounted for in the stress-strain response.

In recent years, there has been significant research interest in the field of micro-compression testing of specimens of a few hundred micrometers in size. The most common test method is to use a commercial nano-indenter and a modified Berkovich tip to perform compression tests on samples that are on the order of a few hundred microns or smaller in diameter [80,81,82,83,84,85,86]. A focused ion beam (FIB) is used to cut small cylinders (as small as 200 nm in diameter) from a thin film, while the specimens are left connected to a base layer of the material [81,82,83,84,87,88]. These small specimens are then compressed with a nano-indenter. This type of testing largely focuses on single crystals and nanograined polycrystalline materials. A number of issues must be carefully considered while interpreting these micro-compression tests. One of the most studied is the size effect; specimens smaller than 50 microns in

diameter show increased strength with a decrease in diameter [81,82,83,84,87,88]. This size dependence is observed in materials which exhibit both single slip as well as multiple slip systems. Another common criticism of the above micro-compression technique is that the specimen stays connected to the bulk of the base material and therefore, there is additional deformation from the bulk of the sample which cannot be easily corrected for in analysis. Other known problems with the micro-compression testing of samples cut by FIB include the potential for impinging ions to be embedded into the sample surface thus altering its composition and properties, the lack of any lubrication during testing, and a nonuniform diameter of the specimen over their length (the FIB process generally results in samples with increasing diameter along their length). Zhang et al., [89] performed a series of finite element analyses to consider the effect of friction, aspect ratio, misalignment, and taper. They concluded that the lack of friction is acceptable for aspect ratios (length/diameter) smaller than 5 and that tapering leads to overestimated elastic modulus as well as increased apparent yield stress. Moser et al., [90] proposed a new method that involves in situ testing within a SEM. By recording the deformation of the specimen and using digital image correlation, the strain is calculated over the entire sample.

Despite numerous studies on micro-compression testing, the authors are unaware of any common method and/or guidelines for testing samples in the range of 0.5-2 mm diameter and similar length. This range of specimen dimensions would be useful in obtaining macroscopic mechanical properties of a small volume of bulk material which has been stressed, and the changes in the properties of the stressed volume are to be determined. One such classic example is ball and roller bearing

elements where a small volume of material on the order of a few cubic millimeters is stressed due to rolling contact fatigue (RCF) loading [64]. The RCF affected bearing subsurface material experiences cyclic micro-plastic loading over hundreds of millions of cycles leading to microstructural evolution, material degradation, and eventually fatigue spallation [56,74,75,76,77,91].

Both micro-indentation and miniature compression were used since they each have different advantages and limitations. Micro-indentation allows probing of a smaller volume of material such that the material properties can be examined on a local scale. The method also requires minimal material preparation and can be used to determine the local flow stress. However, its limitation is that the constitutive response of the material cannot be obtained using this method. On the other hand, miniature compression testing allows average material response to be determined over a small region affected by the RCF [78]. Thus, miniature compression can be used to determine the entire constitutive response of the material at selected intervals during the RCF process rather than just the yield strength. However, sample preparation for miniature compression testing is much more time consuming and expensive than for micro-indentation.

In this manuscript, the influence of various geometric imperfections on the compression stress-strain response of a miniature cylindrical specimen using finite element analysis (FEA) is investigated and limits on tolerances for a valid compression test are established. Electric discharge machining (EDM) was used to cut miniature cylindrical specimens from virgin and RCF affected regions of bearing steels and measure the flatness and parallelism of the loading surfaces as well as the

perpendicularity of the cylindrical axis to the loading surfaces. A specimen preparation method is developed which ensures tolerance limits to be achieved on these small specimens. Finally, compression testing is performed on these miniature specimens extracted from the virgin material of a ball bearing and the results are verified. The results are then compared to the response of the material from the RCF affected regions and the behavior is analyzed.

Experimental Methods

Finite Element Analysis

Geometric imperfections are an important consideration for compression testing. ASTM E9 [79] suggests parallelism, perpendicularity, and flatness within 0.0001 mm/mm. The smallest size that is suggested in this test standard is 13 mm in diameter and 25 mm in length, although it is not uncommon to test even smaller specimens using this standard. These dimensions are an order of magnitude larger than the specimens being considered here. Manufacturing to these tolerances (0.0001 mm/mm) becomes increasingly difficult, and prohibitively expensive, with decreasing sample size. To understand the influence of these tolerances on the stress-strain response, a series of finite element (FE) models and established criterion for allowable tolerances on a specimen for compression testing were developed. The FE software ABAQUS (ver. 6.9) was used to perform the analyses. The effect of edge retention was studied rather than local flatness since the polishing technique used results in surface flatness well below that recommended by ASTM E9 [79].

A 1.5 mm dia. x 1.5 mm height cylindrical specimen similar to that used in the experiments was modeled in the finite element analysis (FEA) and assigned the material properties of M50 bearing steel. The entire specimen assembly, consisting of

the specimen held between two rigid tungsten carbide (WC) platens (similar to the geometry used in the experiments to be discussed later) was considered. The specimen was modeled as a deformable body with a power-law hardening elastic-plastic response. Using a conventional compression specimen size of 5 mm dia. X 10 mm height, the stress-strain curve for this material was experimentally determined previously by Klecka et al., [45]. An elastic modulus of 219 GPA and a power-law curve fit of $\sigma=3.83\varepsilon 0.053$ (GPA) were found to accurately capture the constitutive response and were input into the FEA model as an ideal response. The lower platen was constrained for vertical motion (Fig. 5-1) and rotation about the two horizontal axes. The upper platen was brought down at a constant velocity of 1.5x10-3 mm/s, which resulted in a strain rate of 0.001/s in the specimen, similar to the experiments to be discussed in the next section. The displacement of the upper platen and the corresponding force were recorded to construct the stress-strain response of the specimen. This procedure mimics the experimental setup where a load cell and a deflectometer were used to record similar data. A frictionless contact was assumed between the specimen and the platens. Although not included, a separate study on the effects of different friction coefficients was also conducted, but no significant differences in the results were observed.

The FEA was conducted to evaluate the limits on tolerances for flatness, parallelism of the loading surfaces, and perpendicularity of the axis with the loading surfaces. Using standard metallurgical polishing methods, it is easy to obtain the surface flatness suggested by ASTM E9 [79], except that the specimen edges tend to fillet. Therefore, the amount of edge retention was modeled instead of flatness, see Fig.

5-1A. In practice, the edge retention will be very nearly axisymmetric since the main cause of loss of edge retention is the nap of the polishing pads, which results in curvature of the edge. A 2-D axisymmetric model was used to model edge retention to reduce computation time. Full 3-D models were used to model parallelism and perpendicularity since these are inherently not axisymetric.

Edge Retention

The influence of edge retention on compression response was studied. The edge retention was defined as the fraction of the specimen radius that is in the plane of contact during the initial loading as shown in Fig. 5-1A. Three-node linear triangular (CAX3) elements were used in this model, and the edge retention was modeled as a fillet around the entire circular loading edge of the cylindrical sample. This fillet was modeled on the top edge only; the bottom of the sample was not filleted. The fraction of the radius (r/R) that is initially in the plane of loading (i.e., initially in contact with the WC platen) was varied to determine the minimum contact radius required to give the same flow curve as an ideal (100% contact) sample. The contact ratio (r/R) was varied from 100% (ideal sample) to 80%. The resulting stress-strain responses are shown in Fig. 5-2. It is seen that when at least 90% of the radius is initially in contact with the platen, the resulting stress-strain curve is similar to the ideal material response. For 90% contact, the difference in flow stress at 0.02% strain offset was less than 0.75%.

Perpendicularity

A 3-D FE model was used to determine the effects of perpendicularity. Four-node linear tetrahedral (C3D4) elements were used to mesh the specimen geometry. The measure of perpendicularity was defined as the angular deviation, ‘Θ,’ of the cylindrical axis to the vertical as shown in Fig. 5-1B. For these tests, both loading

surfaces were kept perfectly parallel, but the axis connecting the centers of the two circular surfaces was inclined to the vertical by an angle 'Θ' which was varied up to 10 degrees, and the resulting flow curves are shown in Fig. 5-3. While a 1 degree deviation from the vertical resulted in virtually no change, an inclination of 2.7 degrees resulted in a decrease in both the elastic modulus and yield strength by approximately 0.5%. Further increase in angle causes a further decrease in these properties, but the hardening response remains nearly identical to the ideal specimen.

Parallelism

A 3-D FE model similar to the one previously described for the investigation of perpendicularity was used to determine the effects of non-parallelism between the two loading surfaces. The parallelism was defined as the maximum difference in height (Δh) of the sample on opposing edges of the loading surfaces as shown in Fig. 5-1c. Four-node linear tetrahedral (C3D4) elements were used to mesh the specimen geometry. In this model, the bottom surface was perpendicular to the axis of the cylinder, while the inclination of the top surface with respect to the horizontal was varied. The maximum height of the specimen on one edge was kept constant at 1.5 mm, while the height of the opposite edge was decreased to create the non-parallelism. The resulting flow curves are shown in Fig. 5-4. Even a 5 micron height difference (Δh) will result in a heel in the early stages of the stress-strain response, which implies loss of stiffness at the beginning of loading. However, this effect can be accounted for by translating the stress-strain curve to the left until the line representing the modulus (slope of the linear phase of the response) intersects at (0, 0). Once this heel has been corrected for, the curves are nearly the same up to a 10 micron height difference (Δh). There is a slight decrease in yield strength as well as modulus after a 20 microns height

difference (Δh), but the plastic response (tangent modulus) remain unaltered. Beyond this limit, the initial heel is very large, and the modulus decreases to nearly half of its original value. One can extrapolate these results to the case of lack of local flatness which can be interpreted as having sharp peaks and valleys. The tallest peak will be the first one to be in contact with the loading surface and hence gives an extremely low value of nominal (average) stress but large deformation. The result is similar to the situation in Fig. 5-1C, which causes a severe loss of early stiffness such as the one shown in Fig. 5-4.

Test Specimen Geometry

The results of the aforementioned FE analyses provide guidance on tolerances for the above geometric features of miniature compression specimens. While the effect of each geometric feature was considered separately in the previous FEA, in reality, they may co-exist on any given specimen with the potential for confounding effects. Therefore, the chosen limits on the experimental specimens were somewhat tighter than those determined as acceptable in the finite element analysis. Accordingly, the parallelism limit was set at 4 microns, the perpendicularity at 2 degrees, and the edge retention at 90%. These are not necessarily the least stringent tolerances that would yield reliable results, but these tolerances could readily be attained on the specimen through metallographic polishing, so no further analysis was performed to find the maximum allowable tolerances. To accommodate the possibility of all three tolerance limits co-existing on the same specimen, one final model was analyzed with all the proposed limiting geometries simultaneously, see Fig. 5-1D. The resulting constitutive response can be seen in Fig. 5-5. The elastic modulus of the imperfect specimen was

only 0.1% below the ideal specimen, and the yield strength was off by only 1.3%. This deviation is negligible compared to the typical scatter expected in experimental data.

Specimen Extraction

Miniature compression testing was performed on specimens extracted from a selection of the balls tested, see Table 1-2. To locate and reveal the subsurface regions affected by the RCF, these balls were cut in half, perpendicular to the rolling direction, using EDM. This plane, which is perpendicular to the rolling direction, is called the equatorial plane, and the rolling plane is called the meridial plane, see Fig. 5-6A. The EDM cut surfaces were polished using the standard metallurgical practices and then a final polishing step was performed using chemical-mechanical polishing (CMP) with a mixture of 0.05 micron colloidal silica and alumina with a pH of 8.5. This procedure slowly removes the steel matrix and exposes the hard carbide phase. To further enhance the contrast under an optical microscope, the ball surfaces were etched with a 3% nital solution. The RCF affected zone appears as a bright elliptical region on the equatorial surface (Figs. 5-6A and C) and as a circumferential ring on the meridial surface (Figs. 5-6A, B, and D). The size of this region varies depending on the RCF conditions, but the typical size of the major and minor axes of the elliptical region were 3500 μm and 600 μm, respectively.

To extract compression test specimens from the small RCF affected zone, a 2 mm thick disc containing the RCF zone was EDM cut along two sections parallel to the meridial plane, see Fig. 5-6D. Specimens were then extracted from the RCF affected zone of this disc. In Figs. 5-6A and B, the dotted circles represent the specimens that are to be extracted, while an actual meridial section is shown in Fig. 5-6D. Specimens were also extracted from the regions away from the RCF affected zone, which are

composed of virgin material. The resulting specimens have EDM damage and also do not meet the previously set requirements for flatness, parallelism, and perpendicularity for a valid compression test. Therefore, these specimens must be further prepared.

First, the specimens were manually polished to remove EDM damage from the cylindrical surface. Then, the specimens were finely polished on the loading surfaces to meet the final specifications for flatness and parallelism using a novel approach where gauge blocks and WC tabs were used as shown in Fig. 5-7. The current length of the specimen was subtracted from the length of the WC and a gauge block with a height slightly smaller than this difference was chosen. The specimen was then held on the gauge block, and the entire assembly was cast in acrylic as shown in Fig. 5-7. This assembly was then polished using standard metallurgical practices down to a 1 micron final polish. Since WC is much harder than the bearing steel, the length of the WC tabs will not change significantly while the steel specimen surface is polished away and simultaneously becomes flat and parallel to the attached gauge block surface. After this surface has been polished sufficiently, the acrylic mount was broken, and the specimen was remounted for polishing of the other surface. The entire process usually takes around 6 hours and results in a specimen with both ends flat and parallel to each other. The perpendicularity is less controlled as it is influenced by manual polishing only. If any of the geometric tolerances were not met, then the specimen was re-polished and re-measured.

The flatness and parallelism of the two end surfaces of the specimens and the perpendicularity of these surfaces to the cylindrical axis were then evaluated in a Zygo NewViewTM 7300 optical profilometer. A silicon wafer, which was flat to within 100 nm,

was used as a reference flat for these measurements. First, the wafer was placed on the working surface of the profilometer, and the polished specimen was placed on top of the wafer with its axis vertical. The microscope was focused on the top surface of the specimen and the working surface was rotated until the top surface of the specimen was perpendicular to the measurement. The top surface was then scanned, which gives information about the flatness of the surface as shown in Fig. 5-8. The specimen was then flipped over and the flatness of the opposite surface was measured. To measure the parallelism, the specimen was flipped, and the focus re-adjusted, but the working surface was not rotated. A third scan was then performed. This process provides a combined measure of the parallelism of the two surfaces as well as the flatness of the sample. Therefore, if the measurement is within the parallelism tolerance defined previously in the FE analysis, then the specimen's parallelism must be within the tolerance. Finally, the specimen is laid on its side and scanned along the cylindrical edge and the loading surfaces, see Fig. 5-9. This provides a projected view of the specimen from which one can measure the angle between the cylindrical side and the top/bottom surfaces, i.e., the perpendicularity of the surfaces to the cylinder axis. This measurement is repeated at least 5 times with the sample rotated on its cylindrical surface to different orientations. Finally, the cross sectional area and any taper (change in diameter along the length) of the specimen can be determined from these images.

Miniature Compression Experimental Details

A tabletop universal test machine (Test Resources Inc, Shakopee, MN) was used to perform the compression experiments with a 10 kN load cell. The specimen deflection was measured using an Epsilon model 3540 deflectometer. The specimen was placed between two tungsten carbide inserts (12.7 mm dia. X 6.35 mm length), and

this assembly was placed inside a subpress as shown in Fig. 5-10. The loading ends of the WC platens as well as the subpress were verified to be flat and parallel within 0.0002 mm/mm as per ASTM E9 [79]. The subpress helps evenly distribute the load on the loading surface and align the specimen. This is important because small specimens tend to misalign and are prone to uneven loading resulting in an invalid stress-strain response, so care must be exercised to align the specimen. WC is significantly stiffer and stronger than the steel being tested, therefore it prevents the specimen from indenting into the subpress, which may result in inaccurate deflection measurements as well as damage the test setup.

A small amount of lubricant (combination of petroleum jelly and graphite) was applied between the loading surface and the specimen. This assembly was then placed in the center of the bottom platen of the test machine. The top platen was lowered until it was very nearly touching the top of the subpress (within approximately 0.1 mm), and then the deflectometer was put into place. The tip of the deflectometer must be in contact with the top platen while the body of the deflectometer is kept horizontal. At this point, the load and deflection were each zeroed and the test program was started. The specimens were compressed at a rate of approximately 0.1 mm/min, which results in a strain rate of approximately $1x10^{-3}$/s. After initial yielding of the specimen, a series of unloads were performed to determine the elastic modulus, see Fig. 5-11. This method is less sensitive to initial discrepancies in flatness, parallelism, and alignment than the measurement of elastic modulus during the initial loading phase.

Data Analysis

Due to the small size of the specimens, the deformation of the test frame was on the same order of magnitude as the deformation of the test specimen. Therefore, the

compliance of the test machine must be accounted for in post-test data analysis. To accomplish this task, the same test procedure as described above was repeated without the specimen, and the load-displacement curve of the setup was recorded. For a given force, the deflection of the test setup without a specimen was subtracted from the recorded deflection with a specimen in the machine to obtain the deflection of the specimen only. To measure the elastic modulus of each specimen, the specimen was unloaded twice after the yield point. This unloading procedure allows for any minor misalignment of the specimen in the test fixture during the early loading stage, as well as any imperfections in the specimen geometry to be corrected. Because unloading response is always elastic, unloading after the initial yield provides an accurate measure of elastic modulus. The average of the two unloading steps was taken as the measured modulus. From the force-deflection measurements, the true stress-true strain curve of the specimen is obtained. Typical stress-strain curves are shown in Fig. 5-11. For clarity, the unloading phase is shown only for one of the curves. For all the specimens, the yield strength was measured at a 0.2% offset.

Results and Discussion

Verification using Virgin Specimens

M50 bearing steel specimens extracted far from the RCF regions (Fig. 5-6A) were tested to verify the validity of the miniature compression test method described above. From the stress-strain curves provided in Fig. 5-11, it is noted that the flow curves for the two virgin specimens extracted from two different balls are almost identical. The average measured unloading modulus on each curve was 204.5 GPa, whereas the modulus for M50 reported in literature is 203 GPa [92,93,94]. Similarly, the measured yield strength for virgin M50 was 2610 MPa, whereas the yield strength

reported in literature is 2620 MPa [92,94]. Both of these values are within 0.5% of the literature values (and 1 standard deviation), leading to the conclusion that the procedure followed for specimen extraction and preparation is a valid method for miniature compression testing.

Comparison of Virgin and RCF Specimen Response

After verifying the method by testing the virgin M50 material, specimens extracted from the RCF affected zone (Fig. 5-6) were tested. Balls #2, #3, #7 and #10 were used to obtain the constitutive response of the RCF affected material. The test conditions for each of the ball are illustrated in Table 5-1. Stress-strain curves from one representative specimen from each ball are plotted in Fig. 5-11. It is clear that all of the specimens extracted from RCF affected zones have hardened relative to the virgin material i.e., both the yield strength and the work hardening exponent (n) in the power-law model have increased compared to the virgin material. The ball (#10) that was subjected to RCF with the highest Hertzian stress shows the highest increase in yield strength, even though it experienced fewer RCF cycles. Therefore, it appears that the imposed Hertzian stress has more influence on the yield stress than the number of RCF cycles. The work hardening exponent (n) is not significantly different (at 95% confidence) between balls for the unprocessed RCF balls despite the differences in Hertzian stress and number of RCF cycles. In balls #2 and #7, the increase in yield strength was around 5.75% and in Ball #3 the increase was around12%. Similarly, the work hardening exponent (n) increased by around 5% in the RCF affected region compared to the virgin material, which is a significant increase (at 95% confidence).

Comparison with Mechanically Processed

Balls MP1, MP2, MP3, and MP4 were used to obtain the constitutive response of the MP + RCF affected material. Figure 5-12 shows a comparison of the average yield strength before and after RCF testing for each of the balls tested in compression. Virgin specimens were not extracted from some of these balls (balls #2, #3, and MP4). The hardness and constraint factor discussed below were used to estimate the virgin yield strength of these balls. It is demonstrated that mechanical processing significantly reduces the rate of hardening during RCF. The MP balls were RCF tested for a similar time and at higher stress than ball #2 and #3, but show significantly less hardening. Another important result is that all of the balls have continued to harden for the number of RCF cycles tested.

Figure 5-13 shows the increase in yield strength (difference in yield strength of RCF material and virgin core material) as a function of number of RCF cycles. It is clear that the Hertzian stress is a dominant factor compared to the number of RCF cycles on the amount of hardening during RCF. Ball #10 had over twice as much hardening as balls #2 and #3 with less than 1/3 of the number of cycles. This behavior can only be attributed to the high Hertzian stress during RCF testing.

Figure 5-14 shows the hardening exponent, n, versus the maximum applied Hertzian stress. This exponent was determined by fitting a power-law curve to the plastic portion of the stress-strain curve from 5-7% true strain. The hardening exponent for the unprocessed RCF affected balls is seen to be slightly higher than for the virgin material taken from these same balls. This higher value appears to be nearly constant for the RCF affected unprocessed specimens as it remains within the 95% confidence interval. There is significantly more scatter in the hardening response of the MP balls.

This is likely due to the imprecise nature of mechanical processing not equally affecting every point of the ball. The hardening exponent of the MP balls is higher than for the unprocessed, but this could be simply due being from a different batch of material. More importantly, all of the specimens tested show a positive hardening exponent. This represents the materials ability to continue to harden. A negative hardening exponent represents material softening, which is detrimental for ball bearings because it implies the loss of load bearing ability of the material.

Relationship with Indentation

Micro-indentation is simpler, quicker, cheaper, and requires less material than miniature compression testing, but the miniature compression test gives more mechanistic data including the material constitutive response i.e. yield strength and work hardening characteristics. Hardness and yield strength are related through a constraint factor, C, via the Tabor relationship, $H=C\sigma_y$. Here, the data generated thus far is used to find C so that the need for more complex compression experiments can be eliminated and only the simpler indentation can be used to estimate the local yield strength of the material. The plot of hardness versus yield strength for the balls tested is given in Fig. 5-15. The slope of this curve was found to be 2.7, which is the constraint factor for the material. This value is in line with the value reported by Klecka et al. for virgin M50 [45]. Thus, the local yield strength of the material can be determined from indentation measurements using the above Tabor relationship.

Summary

A new test protocol to extract and prepare miniature specimens from the small RCF affected volume of ball bearings and perform valid compression tests is presented. The influence of specimen geometry on the stress-strain response was systematically

analyzed and the tolerances for these features were established. The method was verified using specimens extracted from virgin regions of M50 steel ball bearings. The yield strengths and elastic moduli of these specimens were consistent with literature values.

The method was then used to determine the stress-strain response of RCF affected material from several M50 balls subjected to different rolling contact fatigue conditions. The results indicate that an increase in Hertzian stress in the ball is directly related to an increase in yield strength of the RCF affected material. Interestingly, the work hardening exponent increases from the virgin response to the RCF response, but then the work hardening exponent for all of the RCF affected specimens are similar. The results revealed that the number of RCF cycles had a relatively minor effect on the yield strength compared to the Hertzian stress. It was also shown that the initial residual stresses, induced through mechanical processing, significantly slow the material's hardening due to RCF. None of the MP balls experienced significant hardening at 95% confidence, while the unprocessed balls showed an over 13% increase in yield strength. More scatter is seen between specimens extracted from the MP balls, which is likely due to the mechanical processing. Finally, a constraint factor was found that can be used to estimate the yield strength from indentation tests. This value is in line with the constraint factor for virgin M50 previously found in literature.

In the following chapter, the microstructural evolution due to RCF is discussed. Although, the primary focus of this thesis is the evolution of mechanical properties, this is directly related to changes in the microstructure. Also, the experimental method to observe changes in the microstructure is both faster and simpler than methods to

determine the changes in mechanical properties. Unfortunately, the observations of the material changes are qualitative. Therefore, it would be advantageous to find a link between the evolution of the mechanical properties and the evolution of the material microstructure.

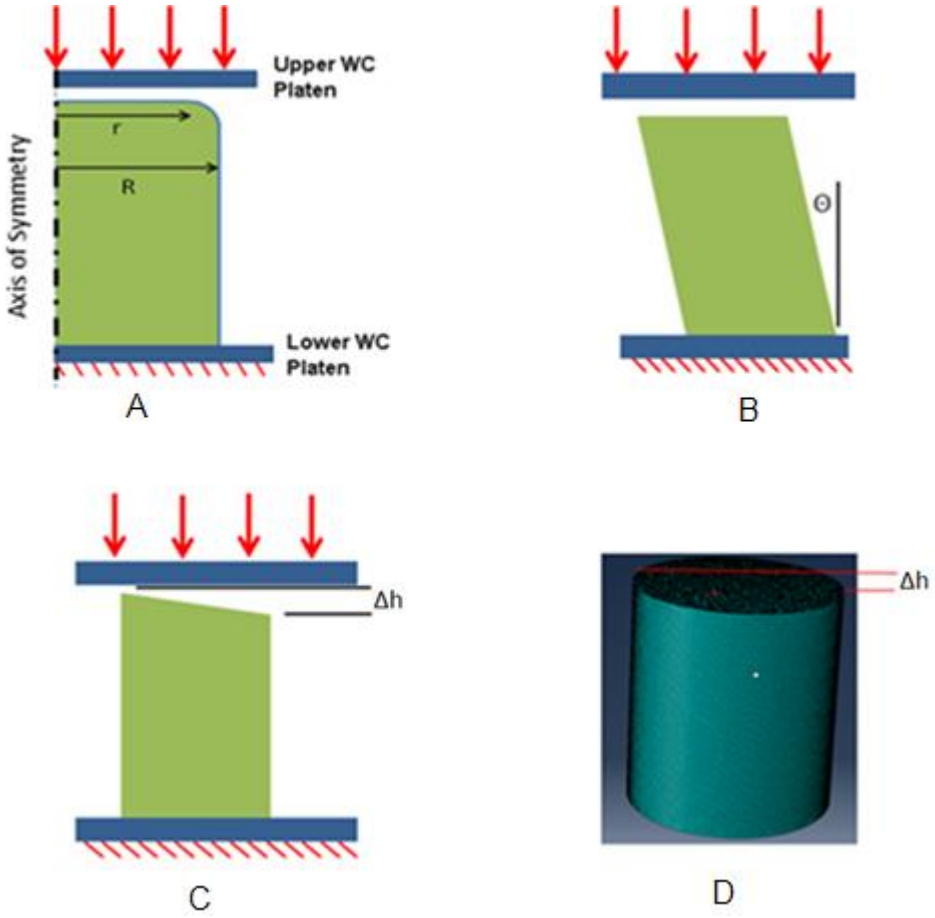

Figure 5-1. Schematics of the geometric imperfections modeled to define allowable limits for: A) edge retention (ratio *r/R*), B) perpendicularity (angle *Θ*), and C) parallelism (height difference, *Δh*). D) 3-D FE model containing all three imperfections.

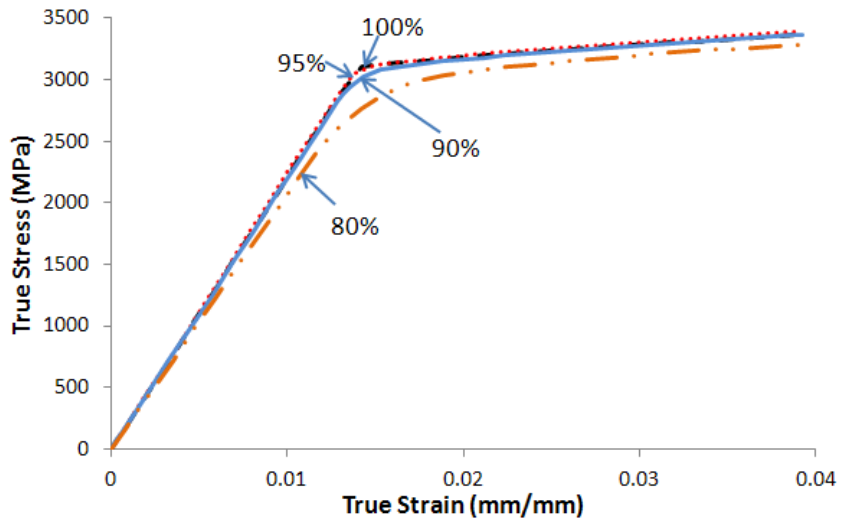

Figure 5-2. Stress-strain response with varying fractions of edge retention. Note that the curves are nearly identical even when only 90% of the radius (or 81% of the top surface) is in-plane.

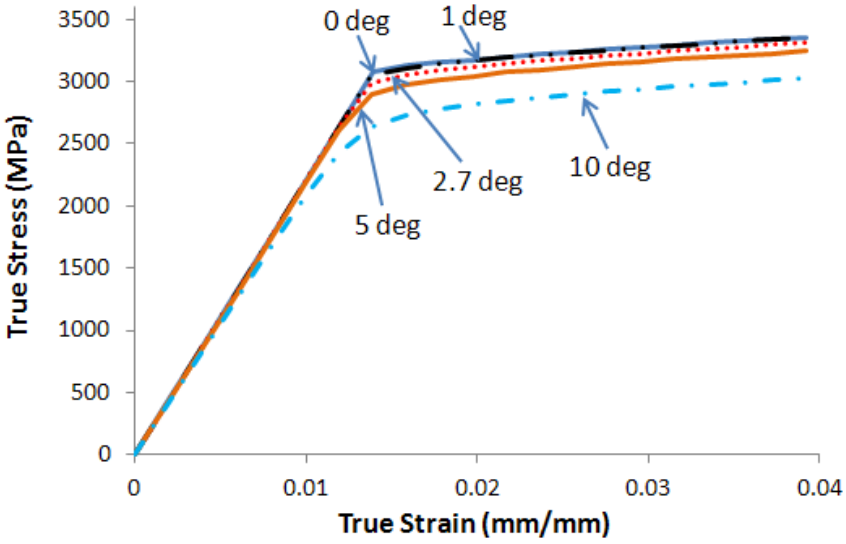

Figure 5-3. Flow curves with varying degrees of perpendicularity. One-degree deviation from perpendicular has negligible effect, while 2.7 degrees causes a decrease in modulus and yield strength by less than 1%.

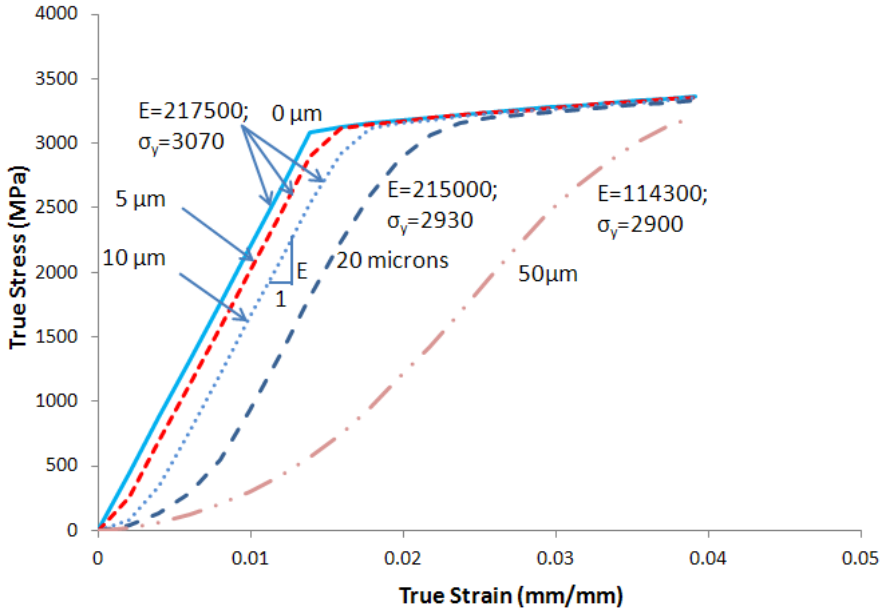

Figure 5-4. Flow curves with varying levels of parallelism. The numbers next to each curve are the elastic modulus and yield strength in MPa. A height difference (Δh) of up to 10 microns has no effect on the flow curve (other than a slight heel at the beginning). The elastic modulus is measured midway in the elastic range.

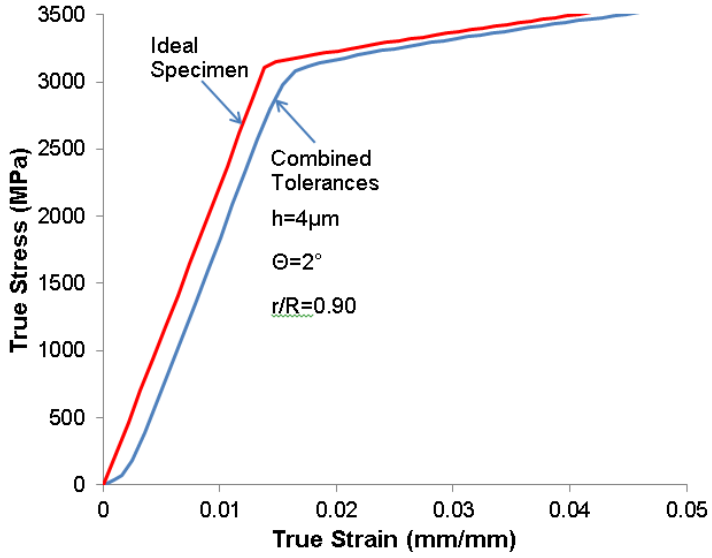

Figure 5-5. Constitutive response of a specimen with the limiting acceptable tolerances for parallelism, perpendicularity, and flatness compared to an ideal specimen. The imperfect specimen has a small heel at the beginning of the curve, but after this is accounted for, the curves are nearly identical.

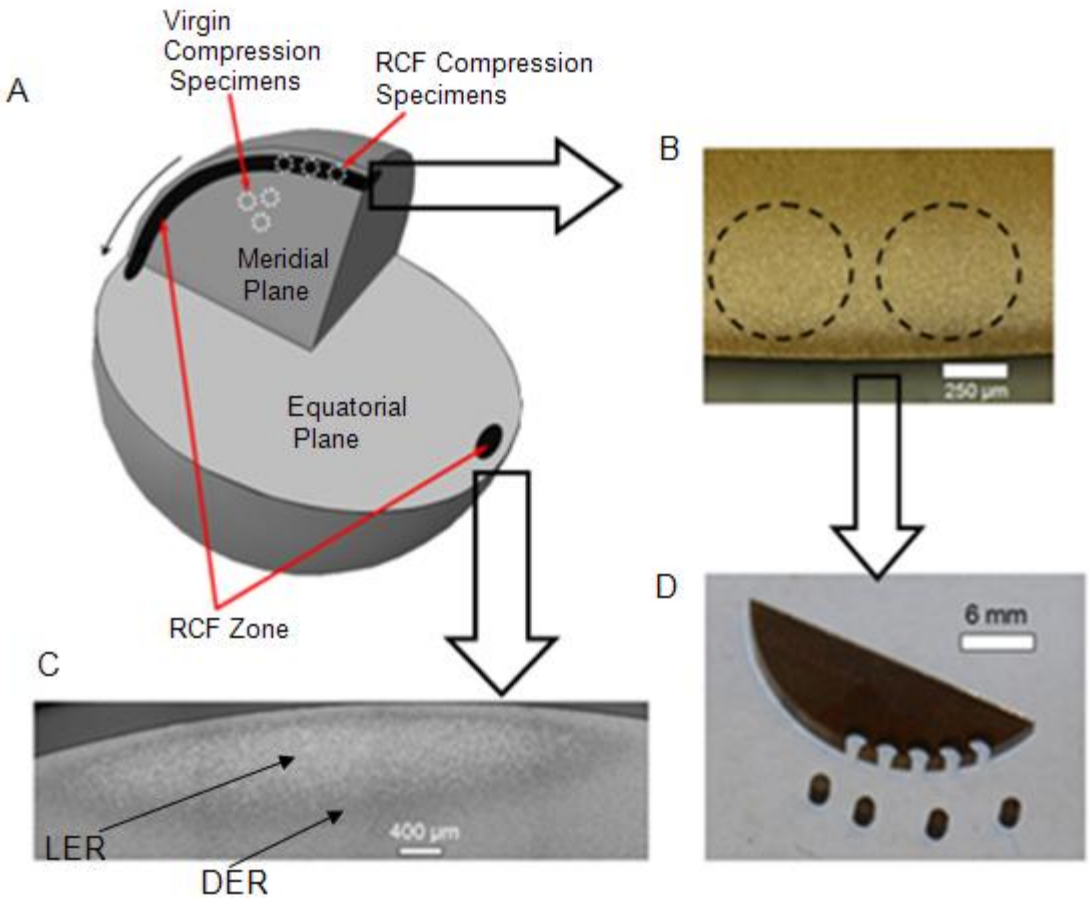

Figure 5-6. Locations from which miniature compression specimens were extracted. A) Schematic showing the plane definitions and RCF affected regions in a ball. B) Micrograph of the RCF affected region in meridial section after etching. C) Micrograph of the RCF affected region in equatorial section after etching. D) Miniature compression specimens extracted from the RCF affected zone of meridial section.

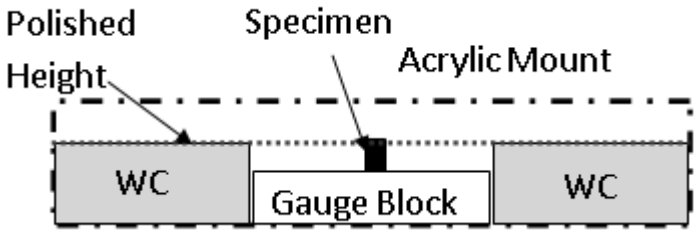

Figure 5-7. Schematic of the layout for polishing the compression specimens to achieve the required parallelism and flatness tolerances.

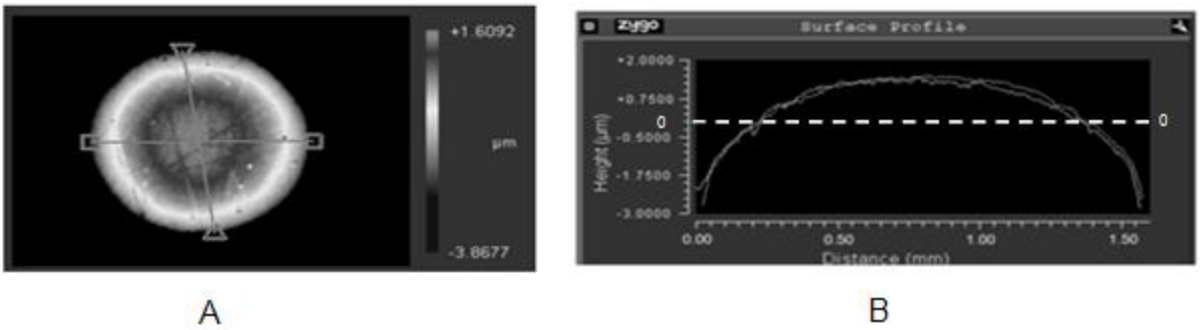

Figure 5-8. Flatness data of the top surface recorded by the profilometer: A) scan of the entire area. B) line scans along the two diagonals used to highlight the flatness of the surface which varies by less than 4 µm over 1.5 mm.

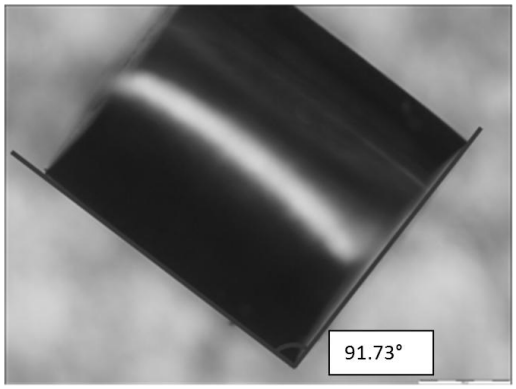

Figure 5-9. Image of the specimen captured by the profilometer for measurement of the perpendicularity of the specimen.

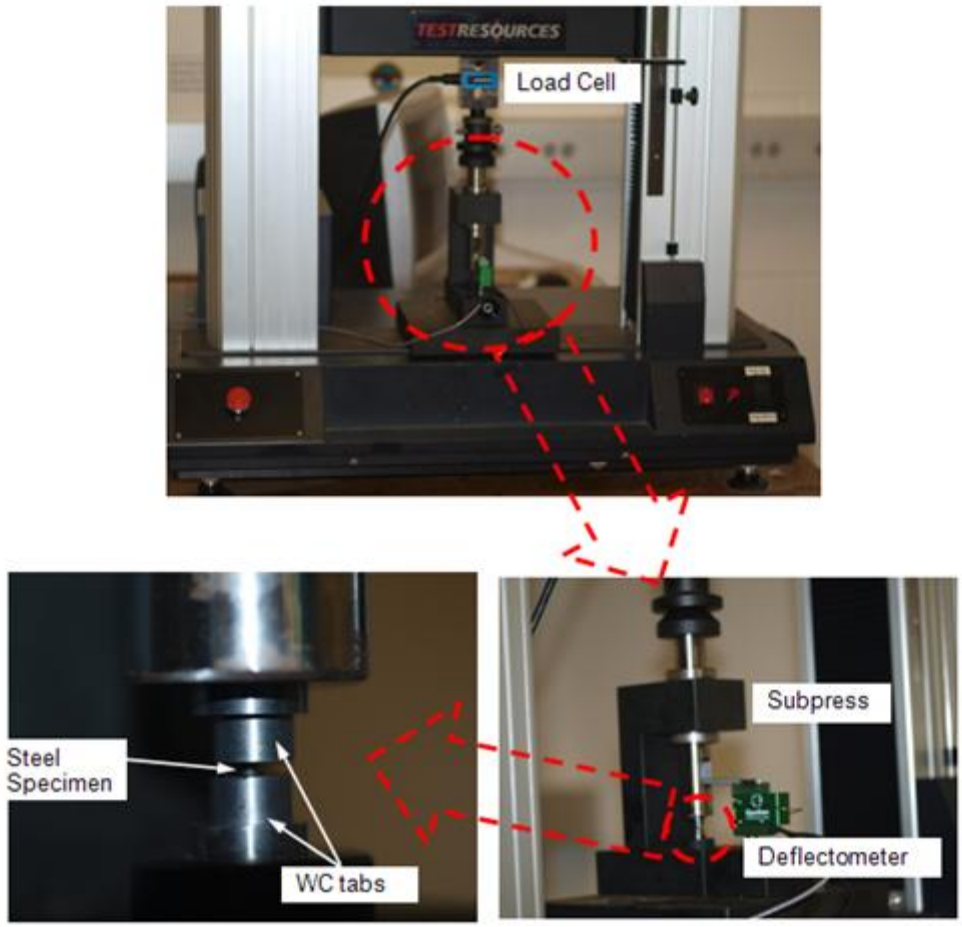

Figure 5-10. Machine setup used to perform compression tests. A deflectometer and a load cell were used to record the test data. (Photos courtesy of Bryan Allison)

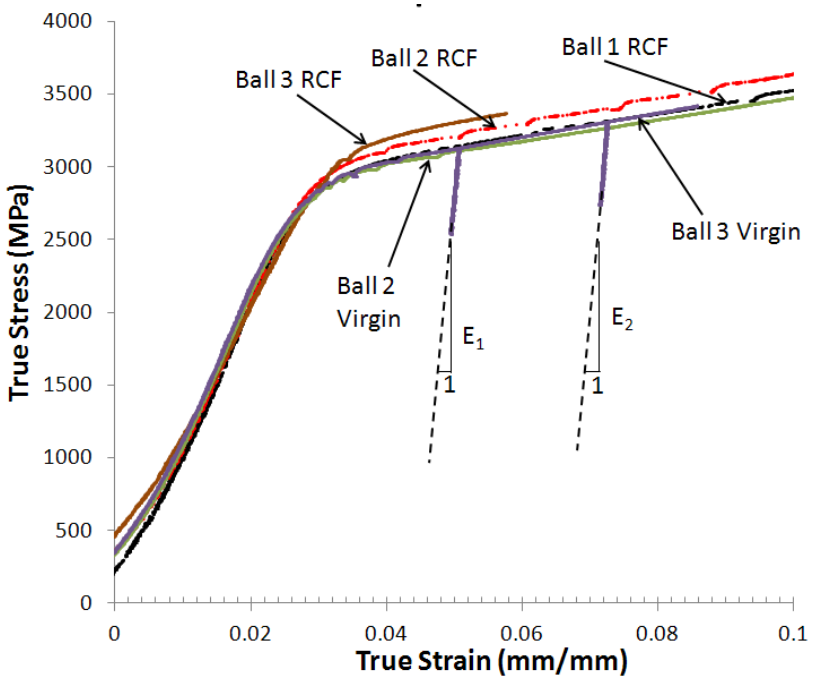

Figure 5-11. Representative flow curves for specimens tested. The unloading is shown for only one of the curves for clarity.

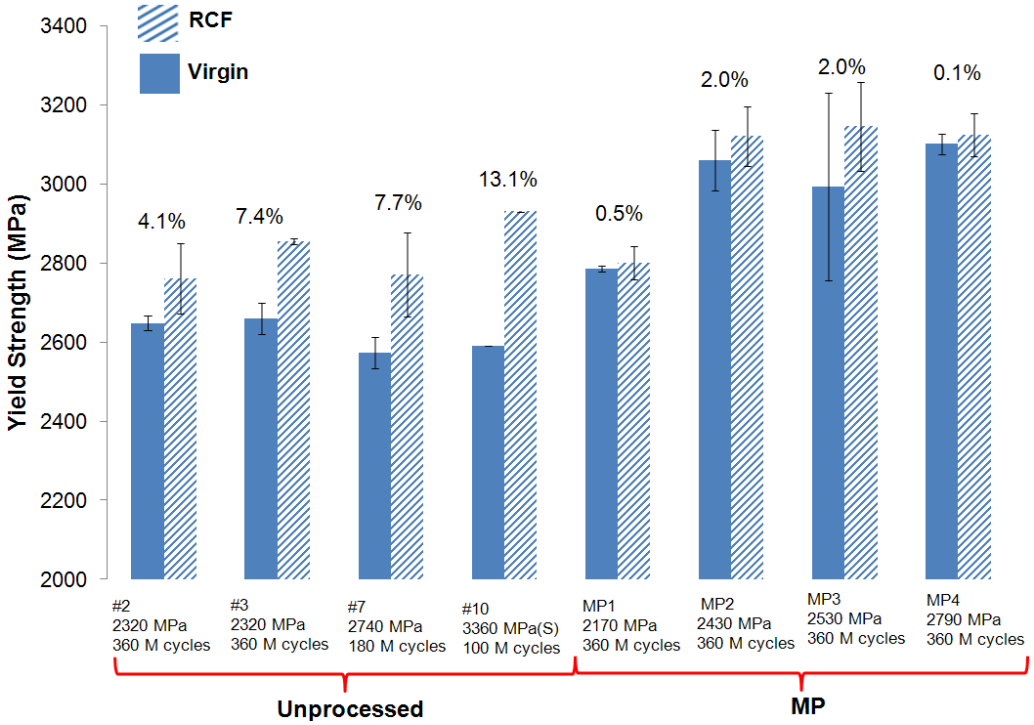

Figure 5-12. Comparison of the yield strength of the virgin material and the RCF material MP and unprocessed balls.

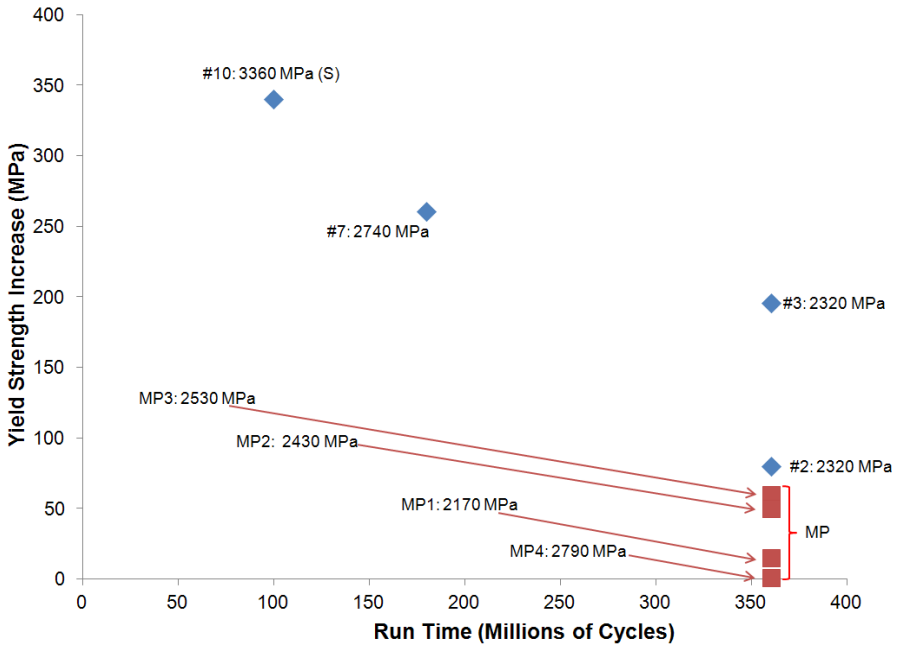

Figure 5-13. Data on yield strength increase (RCF yield minus virgin yield) vs. number of RCF cycles. It is seen that the increase in yield strength is greater for unprocessed balls compared to MP balls. Also, an increase in Hertzian stress leads to a greater increase in yield strength.

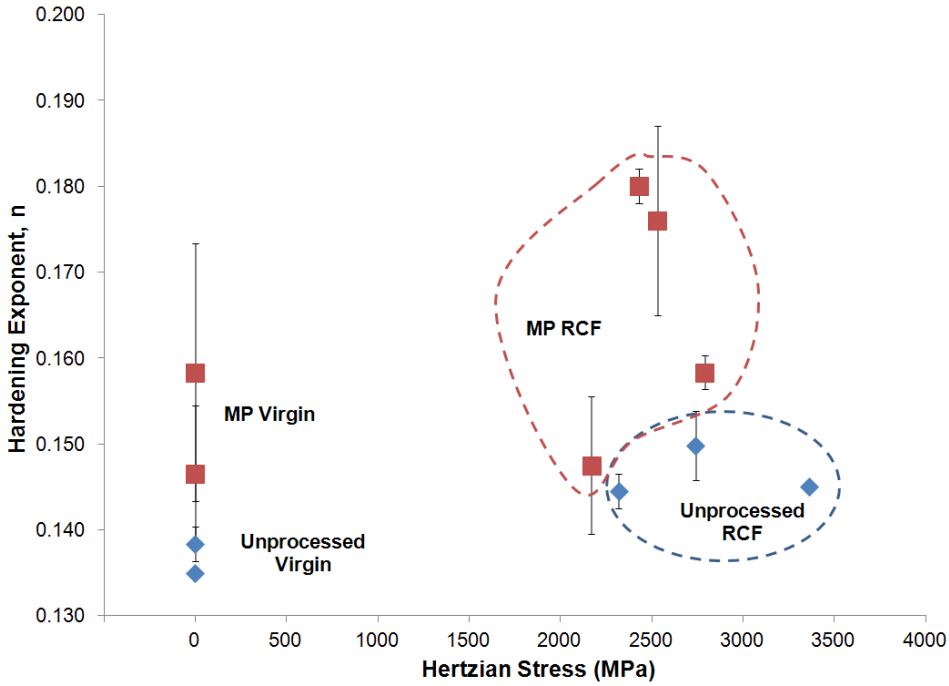

Figure 5-14. Work hardening rate vs. Hertzian stress for all of the samples tested. The hardening exponent is higher in the MP balls than in the unprocessed balls. The hardening exponent increases from virgin to RCF specimens for unprocessed balls.

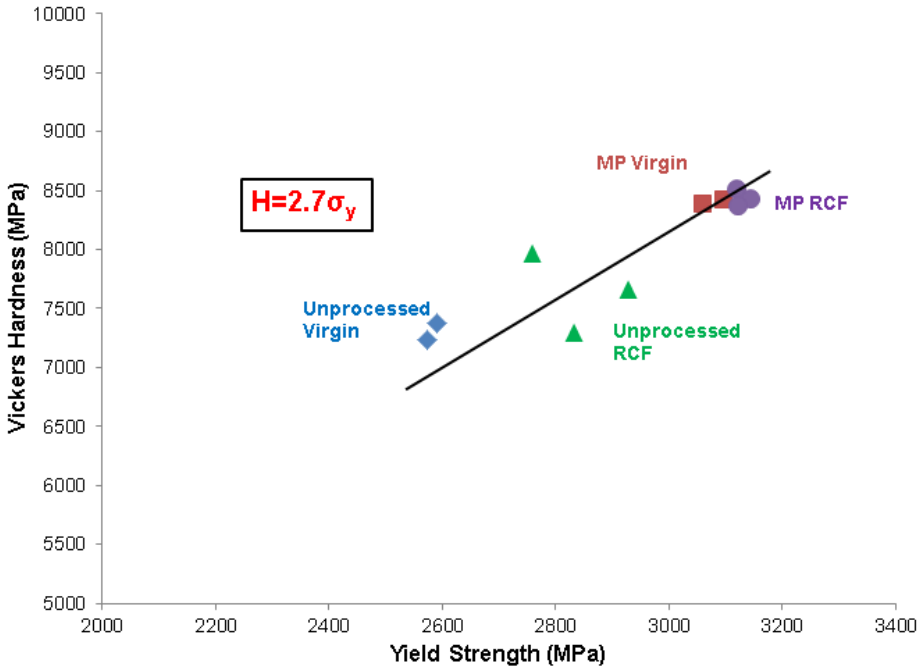

Figure 5-15. Hardness versus yield strength relationship for virgin and RCF affected materials. The slope of this curve can be used for estimating the local yield strength from simple microhardness measurements.

Table 5-1. Summary of miniature compression results for various balls.

Ball ID #	Test conditions	Yield strength (MPa)	Hardening Coefficient, K (MPa)	Hardening exponent, n
7 Virgin	N/A	2575±40	4750±95	0.138±0.002
10 Virgin	N/A	2590	4680	0.135
MP1 Virgin	N/A	2785±10	5145±20	0.147±0.002
MP2 Virgin	N/A	3060±75	5755±180	0.166±0.011
MP3 Virgin	N/A	3095±280	5690±385	0.158±0.001
2	2320 MPa 360 M cycles	2760±90	4970±165	0.145±0.002
3	2320 MPa 360 M cycles	2855±10	4975±165	0.139±0.002
7	2740 MPa 180 M cyles	2835±105	5145±150	0.150±0.004
10	3360 MPa 100 M cycles (S)	2930	5090	0.145
MP1	2170 MPa 360 M cycles	2800±40	4905±30	0.148±0.008
MP2	2430 MPa 360 M cycles	3120±75	6150±150	0.180±0.015
MP3	2530 MPa 360 M cycles	3145±110	6305±175	0.176±0.0023
MP4	2790 MPa 360 M cycles	3125±55	5775±105	0.158±0.008

CHAPTER 6
MICROSTRUCTURAL EVOLUTION

Background

Significant research been performed on the evolution of the microstructure within the RCF affected region of 52100 steel bearings [56,75,76,77,95,96]. Previous investigations have revealed the formation of a dark etching region (DER) followed by a light etching region (LER) and simultaneous accumulation of fatigue damage leading to failure due to spall [56,74,75,77,91]. These studies primarily used metallurgical sectioning, polishing, etching, and optical microscopy to examine a dark etching region (DER) occurring in the subsurface region of 52100 bearings. Larger DER formation has been found to relate to higher stress, but it is yet unclear, which stress components contribute [95,96,97]. Several possible causes for the formation of the DER have been suggested including steel tempering due to the cycling creating heat [98], plastic flow [95,99], and carbon migration [75]. There are also several proposed explanations as to why the DER appears dark compared to the rest of the material [96,100]. The LER is actually formed by small bands, which form at 30° and later 80° to the rolling direction [75,95,96,98]. The bands themselves are believed to be ferrite [96], and are often surrounded by lenticular carbides [95,96,101]. A minimum pressure for which no transformation will occur is observed for both DER and LER [101]. Local white etching areas have also been found to form near non-metallic inclusions form independent of the DER and LER [11,102].

Though there are numerous papers on microstructural alterations with 52100 bearings, there is very little on these phenomena with M50. Braza, et al. [102] investigated the microstructure of M50, M50 NiL, and 52100 bearings after high load

testing. They noted that the alteration in the microstructure is a long-life, high-stress event, seldom observed in service. Formation of localized white etching areas and work hardening, but no appreciable loss of hardness was reported for M50. The reduction in damage in M50 relative to 52100 was attributed to higher alloy content and secondary hardening that helps stabilize the microstructure. Forster et al. [11] performed a similar set of experiments and came to the same conclusions, although they proposed that the reduction in damage may also be due, at least in part, to the difference in density between 52100 and M50.

Although research has been performed on the evolution of the microstructure during RCF, an in-depth understanding of the link between these microstructural features and the changes in the mechanical properties of the material is still lacking. For instance, there is disagreement as to whether the microstructural changes lead to material hardening [11], softening [95], or initial hardening followed by softening [96]. Such an understanding would be helpful for the bearing industry to estimate the residual life of a bearing element. This link may prove especially useful since the experimental methods required to view the microstructural changes are much quicker and simpler than the methods to experimentally determine the changes in mechanical properties. In this chapter, the microstructural changes within the RCF affected region is studied and compared with the changes in mechanical properties discussed in previous chapters. The cause of such microstructural changes and what they entail is not discussed herein, but rather the size and location of the DER and/or LER were measured.

Experimental Methods

After the RCF test, the balls were sectioned perpendicular to the rolling plane to reveal the equatorial section. This section has an elliptical region of RCF affected

material at either end as shown in Fig. 5-6A. The section was polished according to standard metallurgical practices. The final polishing involved chemical-mechanical polishing (CMP) with a mixture of 0.05 micron colloidal silica and alumina with a pH of 8.5. This procedure slowly removes the steel matrix and exposes the hard carbide phase. To further enhance the contrast under an optical microscope, the ball surfaces were etched with a 3% nital solution. Light microscopy was then used to observe the surface. In particular, the RCF affected region can be identified by the contrast with the rest of the surface as the microstructural transformation occurs, see Fig. 6-1. The size of this region varies depending on the RCF conditions. Initially, no DER is visible (Fig. 6-1A), then a small DER forms (Fig. 6-1B) followed by a larger DER and formation of a small LER which is concentric with the DER (Fig. 6-1C), and finally both the DER and LER continue to grow until failure due to fatigue spall (Fig. 6-1D). The size and location of the DER and LER were measured and recorded for each of the balls tested. While these RCF zones appear as dark and bright regions in the subsurface of the ball, the influence of mechanical processing (to induce residual stress) appears as a slightly brighter region starting at the surface of the ball and continuing to a depth of approximately 600 μm, see Fig. 6-2A. When RCF is performed on MP balls, the DER becomes superimposed over the MP region as shown in Fig. 6-2B.

Results and Discussion

The relationship between the microstructural changes (i.e. evolution of DER and LER) and the evolution of mechanical properties are of key interest because they can assist in residual life modeling of a bearing ball. Table 6-1 summarizes the area of the DER and LER along with the maximum measured values for the residual stresses, hardness increase, and yield strength increase for each of the balls. It is clear that an

LER forms in only the highest stressed unprocessed balls, with the exception of #7, which was tested with a moderate stress for a much higher number of cycles. The DER grows in size with increased RCF cycles. The residual stress continues to increase with both increased Hertzian stress and number of RCF cycles (refer to Table 6-1). Similarly, the hardness and yield strength of the material continue to increase with increasing number of RCF cycles, and Hertzian stress, independent of the formation of DER or LER. This is in contrast to the general perception that formation of LER is an indication of material weakening during RCF [56,57,75,76,77]. However, half of the balls (#9, #10, #12) that formed an LER spalled before the preset number of RCF cycles (in as few as 52 M cycles), but when an LER did not form neither did a spall. This observation implies that the formation of an LER is an indication of material deterioration, although yield strength and hardness do not capture this deterioration. Therefore, some other properties that are not measured here need to be identified, to capture the degradation mechanism. The size of the DER within the MP balls remains fairly consistent, but all of them were run for the same number of cycles with fairly constant Hertzian stress. A plot of the DER area as a function of peak Hertzian stress is given in Fig. 6-3. A linear relationship between these two variables fits the unprocessed ball data well; while the size of the DER within the MP balls is seen to be relatively constant. This is similar to the relationship between the residual stress and applied Hertzian stress found previously in Fig. 3-3.

Conclusion

The evolution of microstructure of M50 steel balls due to RCF was studied. After RCF testing, the balls were sectioned, polished, chemically etched with a 3% Nital solution, and then observed under a light microscope. For unprocessed balls, a linear

relationship was found between the size of the DER and the applied Hertzian stress independent of run time. An LER was found for all of the balls tested at the highest stress and one of the balls tested at a moderate stress for a longer time. The material continued to harden through the formation of both a DER and later an LER. The formation of an LER, however, was associated with failure due to spall indicating that it is related to a loss of material integrity which indentation hardness and yield strength are not able to capture. Only a small DER and no LER was formed within the MP balls tested even after 360 million cycles at high Hertzian stress. The additional residual stress in the MP balls clearly slows the microstructural transformation due to RCF.

Single ball testing subjects a ball to similar conditions to those experienced in the field, but they are resource intensive, and the material may change between each test obfuscating conclusions about its evolution. Therefore, testing was continued with a ball-rod fatigue method, which is the subject of the following chapter. This method allows for significantly more test conditions to be studied as well as allowing multiple tests to be performed on one rod specimen, thereby minimizing initial material differences.

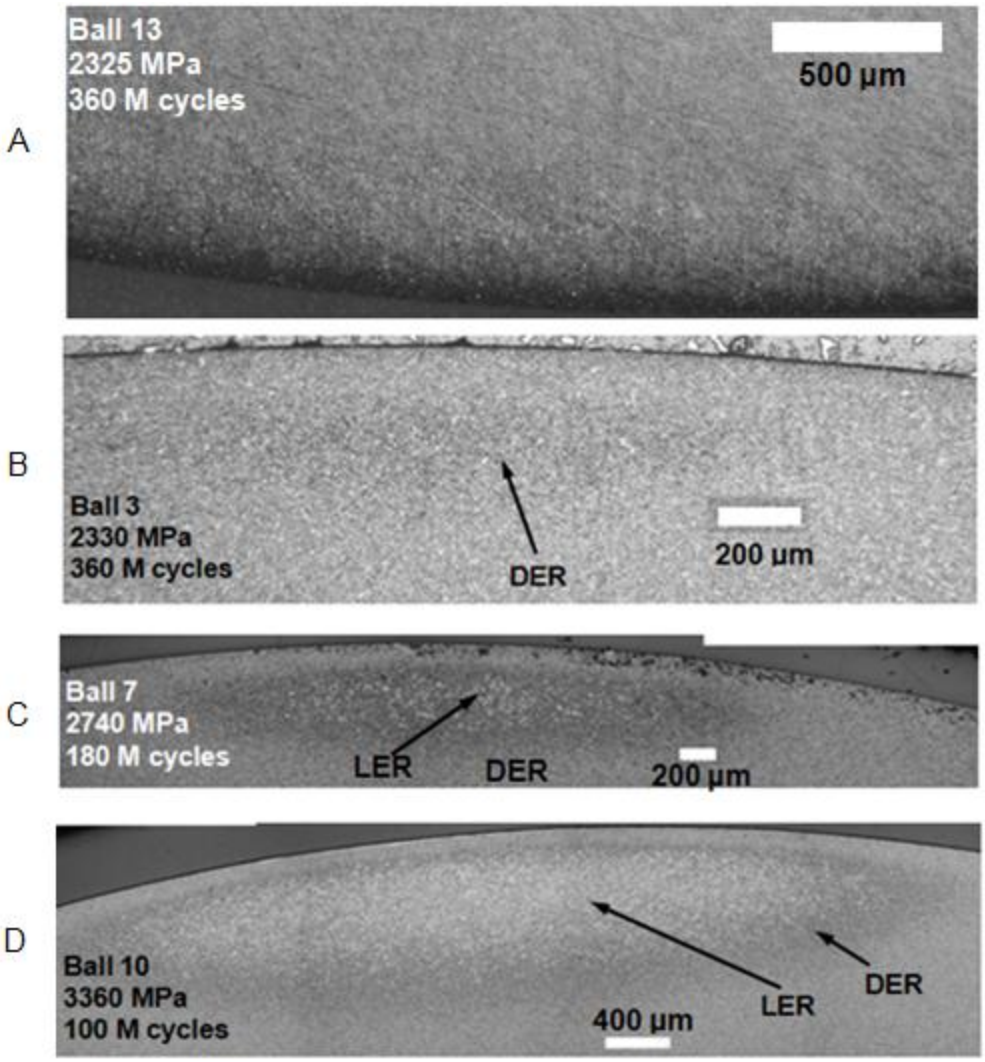

Figure 6-1. Micrographs of the equatorial section of unprocessed balls after polishing and chemical etching. It is evident that an LER forms due to high stress, not necessarily increased cycles.

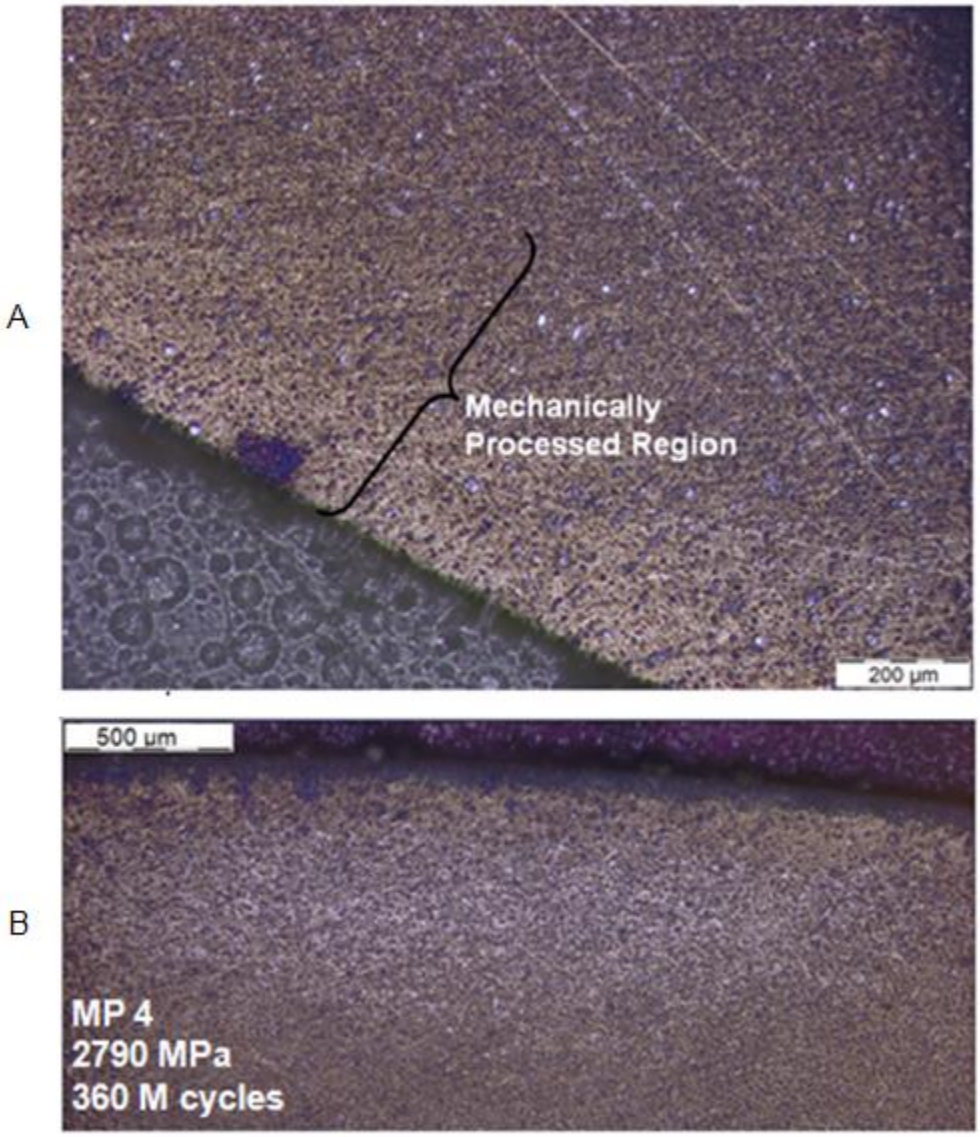

Figure 6-2. Micrographs of the equatorial section of an MP ball after polishing and chemical etching: A) mechanically processed region and B) MP + RCF affected region.

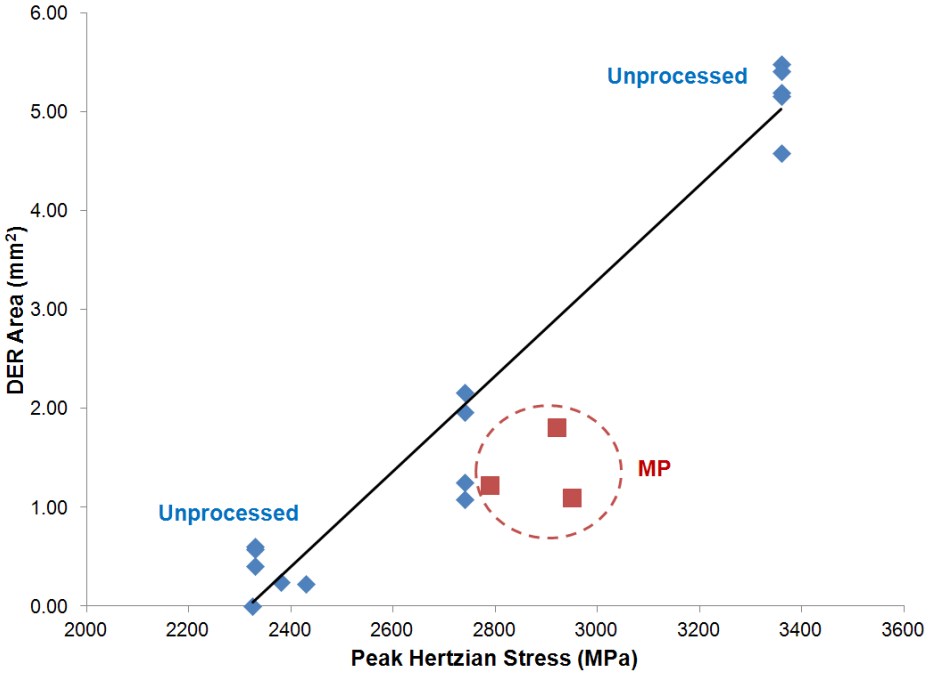

Figure 6-3. Plot of DER area as a function of peak Hertzian stress revealing a linear relationship between the two for the unprocessed balls.

Table 6-1. Summary of the test parameters, mechanical property changes, and microstructural changes for the balls tested.

Ball ID #	Peak Hertzian Stress (MPa)	Run Time (M of cycles)	Residual Stress (MPa)	DER Area (mm^2)	LER Area (mm^2)	Hardness Increase (MPa)	Yield Stress Increase (MPa)
1	2330	36	168	0.40	0.00	200	--
2	2330	360	197	0.60	0.00	--	80
3	2330	360	218	0.57	0.00	170	--
4	2740	36	305	1.08	0.00	110	--
5	2740	108	--	1.25	0.00	170	--
6	2740	180	--	2.16	0.00	220	--
7	2740	180	450	1.96	0.69	60	261
8	3360	36	793	5.19	2.15	490	--
9	3360	(S)52	--	5.48	2.87	450	--
10	3360	(S)103	--	5.41	2.20	660	340
11	3360	108	--	4.58	2.53	550	--
12	3360	(S)123	957	5.16	2.71	650	--
13	2325	360	--	0.00	0.00	230	--
14	2380	360	--	0.24	0.00	210	--
15	2430	360	--	0.22	0.00	200	--
MP1	2170	360	496	--	--	--	15
MP2	2430	360	--	1.09	0.00	120	60
MP3	2535	360	--	0.00	0.00	-10	50
MP4	2790	360	--	1.23	0.00	-10	1
MP5	2920	360	--	1.81	0.00	30	--
MP6	2950	360	303	1.10	0.00	30	--

CHAPTER 7
ROD TESTING

Background

The ball-rod RCF test method is a common way to test the behavior of materials undergoing RCF [64,67,103,104,105,106,107,108]. This method is simpler and less expensive than single ball testing and reduces the variability between initial material conditions since as many as twenty tests can be performed on a single specimen. These factors make it ideal for laboratory studies on the relative effectiveness of different ball materials, lubricants, etc. Further, the high stress, high speed, low cost, and small floor area required means that more combinations of RCF parameters (number of cycles, stresses, and temperatures) can be studied. However, it can be difficult to interpret the results of these experiments. The stress distribution experienced by the rod is different from that experienced by a ball within a bearing and higher stresses are used to accelerate testing. The higher stresses used for ball-rod tests may also lead to changes in failure mechanisms and thus life prediction [109,110].

Hybrid bearings using silicon nitride balls and steel raceways have been an area of interest for the past several decades [12,13,17,64,67,103,104,106,111,112,113,114,115,116,117,118]. Silicon nitride has a lower density, higher corrosion resistance, higher hardness, higher elastic modulus, and lower friction coefficient than steel [12,13,14]. The main advantage of using silicon nitride balls is the reduction of centrifugal forces on the outer raceway due to the balls' lower density [12,13]. Research has found increased fatigue life for hybrid bearings compared to all steel bearings with the fatigue life of the steel raceway being the limiting factor [16,17,18]. However, the higher elastic modulus of silicon nitride balls leads to

the raceway experiencing higher contact stresses when the same load is applied, which may in turn lead to shorter bearing fatigue life than all steel bearings [14,119].

In this chapter, a ball-rod RCF tester is used to continue the study of the evolution of mechanical properties of M50 bearing steel due to RCF. The number of cycles and the applied stress were varied to study the relative effect of these in a similar fashion to the ball tests. The rods used were all M50, while M50, 52100 steel, and silicon nitride balls were used. These materials were chosen because 52100 is currently the most common material for industrial bearings, M50 is commonly used in high performance applications such as aerospace, and silicon nitride is being introduced due to the reasons discussed above. The purpose of this is to develop insight into the difference in mechanical property evolution between hybrid and steel bearings. After RCF testing, the rods were sectioned and tested in a similar manner to the balls. XRD was used to measure the residual stresses at the surface of one of the rods tested, micro-indentation was performed within the subsurface of each RCF track, and chemical etching was used to observe the RCF zone. Miniature compression testing was not performed on the rods, since the RCF affected zone within the rods is too small for compression specimens to be reliably extracted using the current method.

Experimental Methods

A 9.75 mm M50 steel rod was subjected to RCF testing at a rate of 8600 cycles/min as described in Chapter 2. Three different ball materials were used for testing: silicon nitride, M50 steel, and 52100 steel. For each ball material, a series of RCF tests were performed with a peak Hertzian stress of 7240 MPa, while the number of RCF cycles was varied. Silicon nitride balls were also used to test rods with peak Hertzian stresses of 6200 and 8270 MPa. The number of RCF cycles was varied from

10^3 cycles up to $70x10^6$ cycles, so that the evolution of the hardness and microstructure as a function of number of cycles could be observed. All of the tests were performed at a single temperature. This matrix of tests means that the effect of material properties, applied Hertzian stress, and number of cycles on RCF may be distinguished.

Residual Stress Measurement

The residual stresses were measured for one of the rods tested in a similar fashion to the one described above for the balls by the Air Force Research Lab in Dayton, OH (Table 1-3). First, a number of RCF tests were performed on the rod. M50 balls were used for all of the RCF tests on this rod and the number of cycles was varied from $2.6x10^6$ to $23.2x10^6$ in increments of $2.6 x10^6$. XRD was then used to measure the residual stresses parallel to the rolling direction for each RCF track. The residual stresses were only measured at the surface of the rod, rather than as a function of depth as was done for the balls.

Sectioning and Specimen Preparation

After RCF testing, each rod was sectioned to reveal the subsurface RCF affected region from each RCF track formed. Immediately after RCF testing, the rod has multiple tracks along its length, as shown in Fig. 7-1A. The rod was then cut in half lengthwise to reveal the subsurface region as shown in Fig. 7-1B. This section was then cut perpendicular to its length (along the dotted lines) to create specimens which contained a pair of RCF zones from a given wear track, see Fig. 7-1C. This section is equivalent to the equatorial section in the balls. There are two elliptical RCF affected regions; one at either end of the cross-section. The specimens were intentionally cut wider than the wear track in each instance, to prevent additional damage to the RCF

affected region due to the cutting and polishing. The specimens were then mounted in acrylic and polished according to standard metallurgical practices.

Chemical etching was used to reveal the microstructural affected region, so that indentation may be performed in the proper position. After polishing, one half of the cross section was chemically etched using a 3% Nital solution to reveal the RCF affected zone, see Fig. 7-2A. The size of this region will vary based on the RCF conditions, and was not considered for this study. The axial location of the RCF affected zone was noted and then used to identify the proper region for micro-indentation of the opposite end of the cross-section.

Micro-Indentation

Micro-indentation was performed on the opposite side of the polished cross-sections using a Wilson Tukon 2100B tabletop indentation tester. A 200 gram load was selected because it is the smallest indent which can be reliably measured with an optical microscope. This resulted in an average indentation diagonal of approximately 20 microns. Indents were placed 75 microns apart as well as from the edge as per ASTM E384 [120]. Three parallel rows of indents were made within the RCF affected zone to determine an average hardness as a function of depth, see Fig. 7-2B. The hardness of each of these indents was recorded as a function of depth. Indentation was performed to a depth of at least 800 μm, which is more than sufficient to map the RCF affected zone which extends to a depth of approximately 250 μm. Finally, several indents were made in the center of the cross-section (e.g. far away from the RCF affected zone) to determine the virgin hardness of that specific cross-section. This same process was also repeated for a cross-section that had not been subjected to RCF testing to verify that the virgin hardness was not a function of depth.

Results and Discussion

Micro-indentation was performed on M50 rods that had been subjected to RCF testing with varying number of RCF cycles, Hertzian stress, and interacting ball material. A summary of results is given Table 6-1. A plot of the hardness as a function of depth for one of a representative track (#32) is shown in Fig. 7-3. The highest hardness is observed for the indent closest to the surface at a depth of 75 μm. The maximum Hertzian stress is calculated to occur at a depth of approximately 65 μm below the surface. Therefore, the first indent within the subsurface is near the maximum value, but already below the depth at which the maximum hardness is expected. If smaller indents were made, then it is expected that the hardness distribution within the rods would follow a similar distribution to that seen within the balls meaning that the hardness is equal to the core hardness at the surface and then increases to a maximum value within the subsurface before reducing the core hardness. The hardness increase (difference between maximum hardness and the core hardness) was used for comparison purposes due to the variation in virgin hardness and to keep consistent with the ball results.

Indentation was performed on rods that were subjected to RCF with silicon nitride balls at three different stress levels e.g. 6200, 7240, and 8270 MPa. The number of RCF cycles was varied from $10x10^3$ (#6) to $100x10^6$ (#5) cycles. The hardness increase as a function of time is given in Fig. 7-4. Several RCF tests (#6 -- #13) were performed with silicon nitride balls and a moderate stress (7240 MPa) for a low number of cycles ($<10^6$). It was observed that the hardness increases very quickly over the first one million RCF cycles (#6 -- #10), as shown in Fig. 7-4A. The rod continues to harden due to additional RCF cycles beyond this point, but the rate of hardening is much lower.

This is consistent with the idea discussed previously of the material undergoing large amounts of work hardening during a relatively short shakedown period, although one million cycles is longer than this is traditionally considered to be. The plot shown in Fig. 7-4B shows the hardness increase as a function of the log of the number of cycles. Lines are used to represent the rate of hardening for each of the three stress levels. There is a large amount of experimental scatter, but it is clear that an increase in the applied Hertzian stress contributes to a faster rate of hardening. The rates of hardening for the two higher stresses are similar and much higher than the rate of hardening for the lower stress level even though the change between the low stress (6200 MPa) and the medium stress (7240 MPa) is equivalent to the increase in stress from the medium stress (7240 MPa) to the high stress (8270 MPa).

The hardness increase as a function of number of RCF cycles for each of the tests performed at 7240 MPa is shown in Fig. 7-5. The rods tested with 52100 balls appear to be cyclically softening after only 1 million cycles (#18 -- #21) and fail after less than 10 million cycles (#20 and #21). This is consistent with previous literature that reported 52100 steel softening due to RCF prior to failure [65]. The rate of hardening for the rods tested with M50 balls is seen to be higher than with silicon nitride balls, which implies that they will fail earlier similar to applying a higher stress. This is consistent with literature that shows that hybrid bearings last longer than traditional steel bearings [16,17,18]. In fact, the rate of hardness increase for the rods tested with M50 balls is significantly higher than for the rods tested with silicon nitride balls with a 14% higher applied Hertzian stress (8270 MPa versus 7240 MPa). This is especially

poignant, since hybrid bearings will induce a higher stress in the raceway during RCF due to the high stiffness of the silicon nitride balls.

The residual stresses at the surface of the specimen were measured after RCF testing for one of the rods using XRD, see Table 6-1. The surface residual stress and the maximum subsurface hardness increase versus the number of RCF cycles are given below in Fig. 7-6. The residual stress is seen to increase quickly to a value of approximately 250 MPa over the first 4 million cycles, and then continues to increase slowly over the entire time for which testing was performed. The hardness increase is shown to follow a similar trend. This relationship might prove useful in the future, since the measurement of residual stresses at the surface is non-destructive and is a common procedure. This relationship could be used to estimate the remaining life in a rolling element.

Summary

A series of three ball-rod RCF experiments were performed to expand upon the experimental results that were found from the single ball experiments discussed in previous chapters. Three different stress levels were used with silicon nitride balls on M50 steel rods and then three different ball materials (52100 steel, M50 steel, and silicon nitride) were used at the median applied Hertzian stress (7240 MPa). The temperature was kept constant for all of these tests, while the number of RCF cycles was varied. It was found that the applied Hertzian stress has a direct and significant effect on the rate of hardness increase as was previously seen for the single ball tests. It was also demonstrated that an increase in ball stiffness and hardness (52100→M50→Si_3N_4) decreases the rate of hardness increase and therefore presumably increasing life. Also, it was found that most of the hardness increase

occurs over a relatively short number of cycles ($<10^6$). Finally, it was shown that the residual stress at the surface of the material follows a similar trend to the hardness increase as a function of number of cycles. In the following chapter, these results are combined with the results from the previous single ball test results to derive a model to predict the evolution of the constitutive response of M50 bearing steel due to RCF.

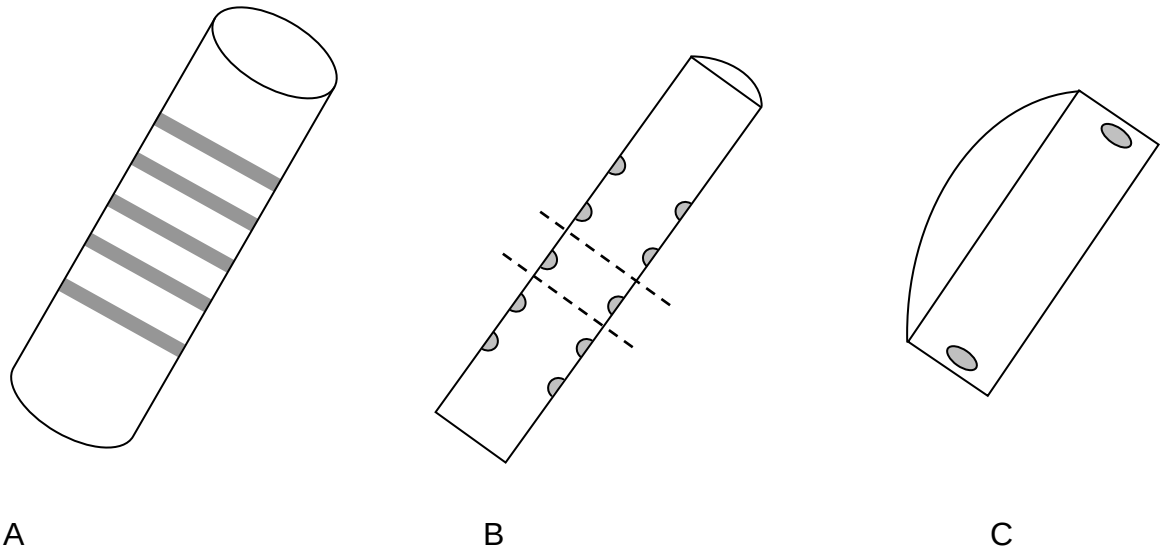

Figure 7-1. Schematic of the sectioning of the rod. A) Initial rod with several wear tracks. B) Rod after being cut along the length; dotted lines represent the horizontal cuts made next. C) Final sample with two transformed zones, each from the same wear track.

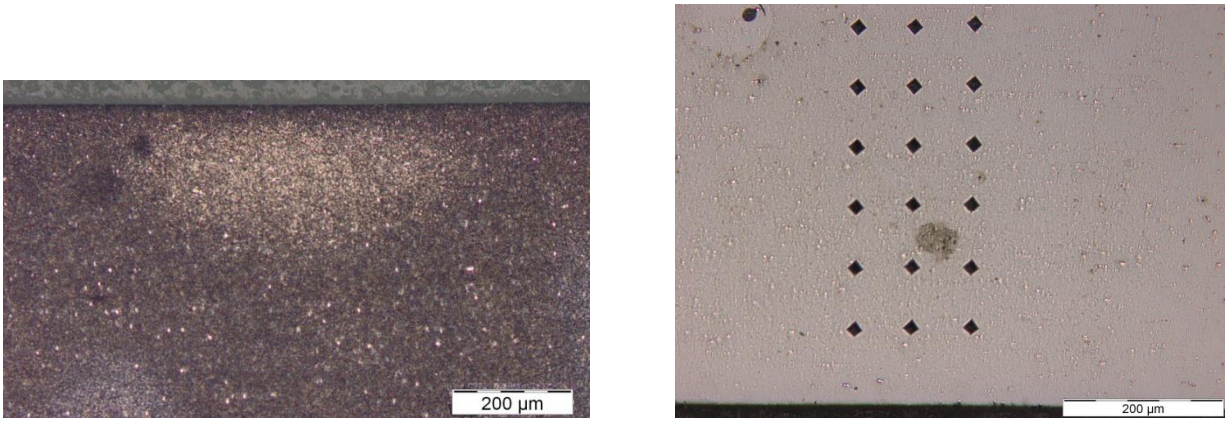

Figure 7-2. Micrographs of the RCF affect zones in the rod. One side is etched and the other indented. A) Section below the wear track after being chemically etched. The light spot in the center has been plastically deformed and the microstructure changed due to these stresses. B) Indents through the RCF-affected zone. Three parallel rows are made within this zone beginning at a depth of 75 µm.

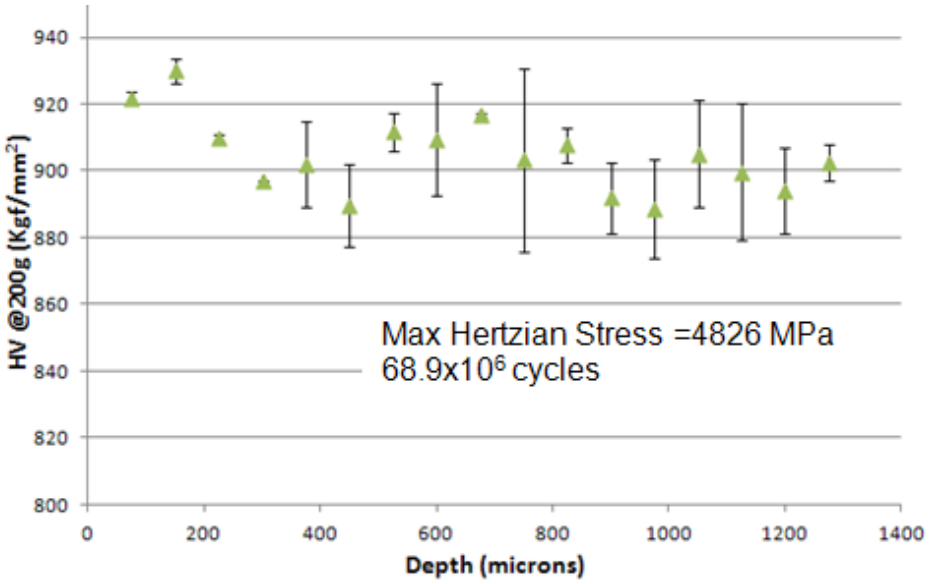

Figure 7-3. Maximum Vickers hardness in the RCF affected zone as a function of depth for a representative rod track (#12).

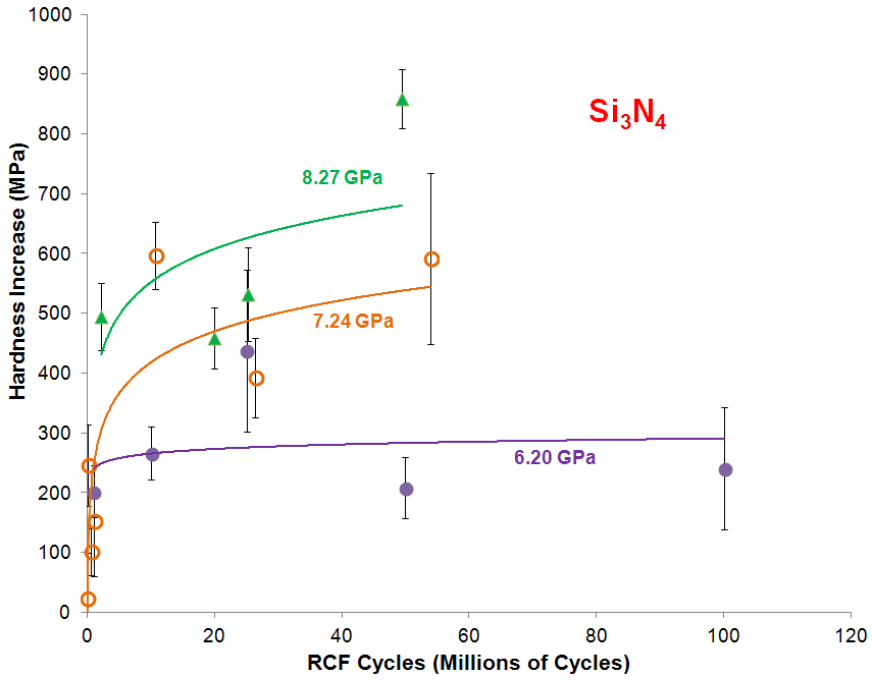

A

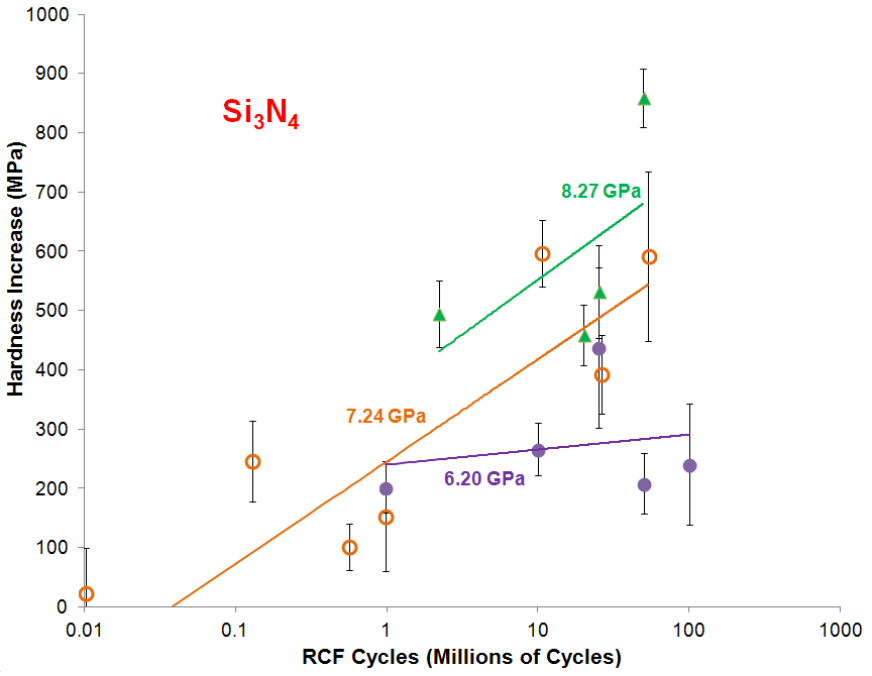

B

Figure 7-4. Hardness increase as a function of RCF cycles for the rods tested with silicon nitride balls. A) linear scale B) log scale.

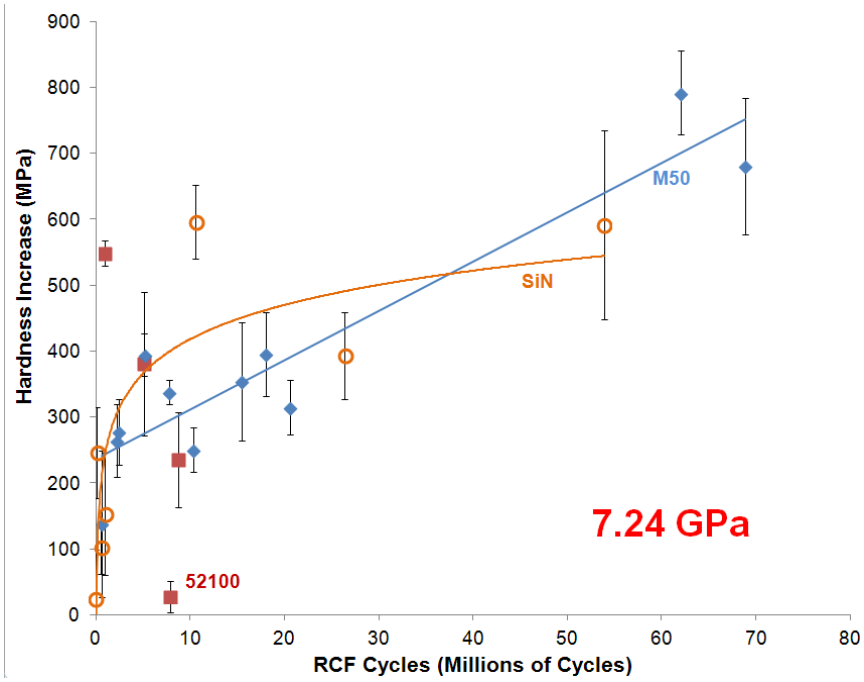

A

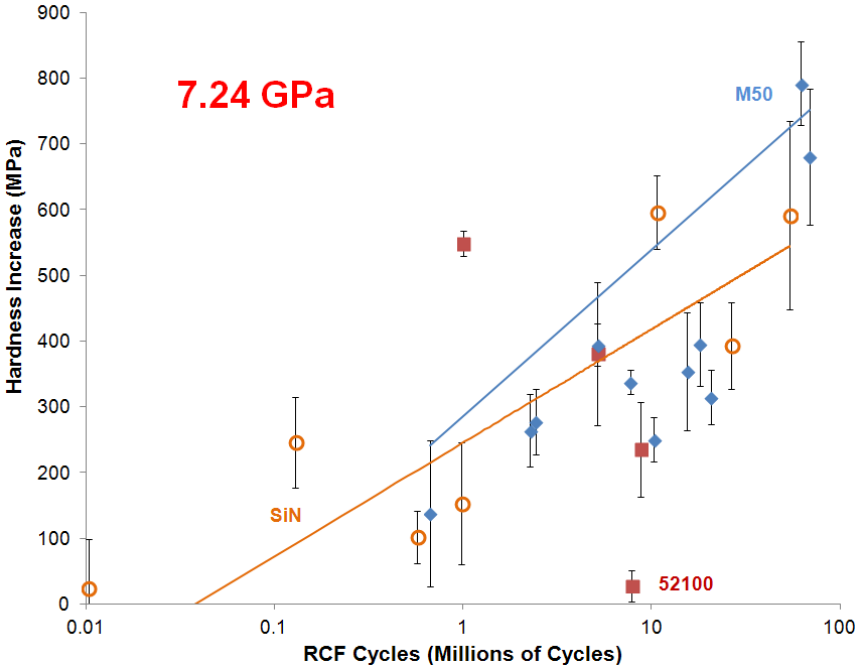

B

Figure 7-5. Hardness increase as a function of RCF cycles for the rods tested at 7240 MPa max Hertzian stress. A) linear scale B) log scale.

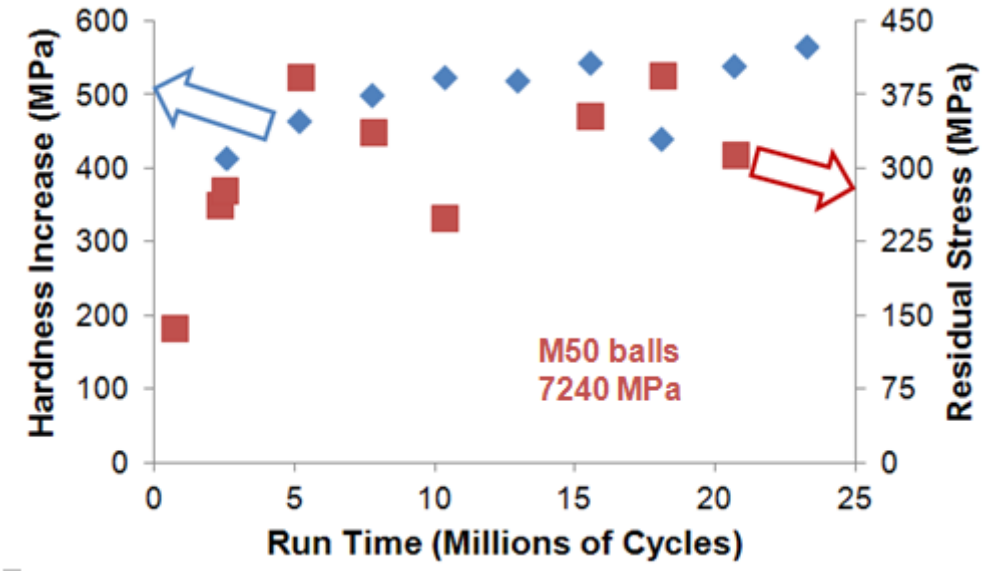

Figure 7-6. Hardness increase and residual stresses as a function of number of RCF cycles for the rods tested with M50 balls.

Table 7-1. Summary of the test parameters and results for the rod tests performed.

Track ID #	Ball material	Max hertzian stress (MPa)	Run time (M of cycles)	Virgin hardness (MPa)	Max hardness (MPa)	Hardness increase (MPa)	% Hardness increase (MPa)	Residual stress (MPa)
1	Si_3N_4	6200	0.98	7904±130	8106±57.7	200±43	2.5±0.55	--
2	Si_3N_4	6200	9.98	7490±157	7757±0.0	270±44	3.6±0.59	--
3	Si_3N_4	6200	25.00	8087±130	8524±280	440±140	5.4±1.7	--
4	Si_3N_4	6200	49.95	8143±100	8350±76	210±51	2.6±0.63	--
5	Si_3N_4	6200	100.10	7948±100	8189±200	240±100	3±1.26	--
6	Si_3N_4	7240	0.01	8083±168	8106±110	23±76	0.3±0.94	--
7	Si_3N_4	7240	0.08	7490±157	7757±0.0	154±120	2.1±1.6	--
8	Si_3N_4	7240	0.13	8087±130	8524±280	246±69	3±0.85	--
9	Si_3N_4	7240	0.57	8143±100	8350±76	101±40	1.2±0.49	--
10	Si_3N_4	7240	0.98	7948±100	8189±200	153±92	1.9±1.2	--
11	Si_3N_4	7240	10.60	8072±110	8668±52	596±56	7.4±0.70	--
12	Si_3N_4	7240	26.4(S)	8401±120	8794±110	392±66	4.7±0.79	--
13	Si_3N_4	7240	53.87(S)	7869±150	8460±270	592±140	7.5±1.8	--
14	Si_3N_4	8270	2.21(S)	8036±130	8530±90	494±56	6.1±0.70	--
15	Si_3N_4	8270	19.92(S)	7793±170	8252±70	459±51	5.9±0.67	--
16	Si_3N_4	8270	25.18(S)	7895±180	8427±120	532±78	6.7±1.0	--
17	Si_3N_4	8270	49.4(S)	7894±160	8752±67	858±50	10.9±0.67	--
18	52100	7240	1.00	7875±33	8424±21	549±19	7±0.24	--
19	52100	7240	5.16	8027±91	8412±200	380±110	4.7±1.37	--
20	52100	7240	7.84(S)	7950±130	7978±70	27.5±23	0.3±0.29	--
21	52100	7240	8.75(S)	7930±77	8165±72	235±72	3±0.91	--
22	M50	7240	0.67	8492±170	8630±190	138±110	1.6±1.3	--
23	M50	7240	2.27	8418±130	8682±90	263±55	3.1±0.66	--
24	M50	7240	2.43	8418±130	8682±90	277±50	3.3±0.60	--
25	M50	7240	5.16	8334±70	8730±110	394±32	4.7±0.39	465
26	M50	7240	7.74	8334±70	8730±110	337±18	4±0.22	500
27	M50	7240	10.30	8135±90	8473±0.0	250±33	3.1±0.41	525
28	M50	7240	15.48	8516±160	8869±140	353±89	4.1±1.0	545
29	M50	7240	18.06	8381±140	8777±100	395±64	4.7±0.77	440
30	M50	7240	20.64	8806±140	9120±35	314±41	3.6±0.47	540
31	M50	7240	62.07	9106±200	9898±83	792±64	8.7±0.73	--
32	M50	7240	68.90	8927±230	9607±160	680±100	7.6±1.1	--

CHAPTER 8
CONSTITUTIVE RESPONSE MODELING

Background

Accumulation of plastic strain and microstructural evolution are known to occur during RCF, thus the constitutive response of the material will necessarily evolve as well. Therefore, the stress-strain response of the material within the RCF affected zone is not only a function of the initial material, but also the RCF conditions. Since finite element modeling is becoming an ever more common technique within the engineering community, and the stress-strain response of the material is a required input for this method, the evolution of the constitutive response of bearing steel due to RCF is a key component to developing a new mechanistic bearing fatigue life model. Unfortunately, there is currently very limited literature about the evolution of the constitutive response of bearing steel due to RCF. Klecka et al. [45] used nano-indentation to find the mechanical properties of the inclusions. Vincent et al. [121] used a similar method within the matrix Bhattacharyya et al. [67] performed micro-indentation within the RCF affected zone to estimate the change in local yields strength. Allison et al. [78,122] extracted compression specimens from within the RCF affected zone of balls, which had been subjected to RCF. Alley et al. [123,124,125] used FEA and crystal plasticity to model the RCF process and allowed the matrix grains to accumulate strain and transform between microstructures. By this method, the resulting constitutive response after RCF of a specific initial microstructure can be determined. While this is certainly an interesting result, the variability in bearing microstructure makes it impractical for regular application. Similarly, performing experiments and/or developing models for every possible set of RCF parameters is not possible. Therefore, it becomes necessary

to develop a model, which can estimate the evolution of the constitutive response over a range of conditions. In this chapter, the results of the preceding chapters are combined to develop an empirical model for the evolution of the local constitutive response of M50 steel due to RCF.

Method

An empirical model for the evolution of the constitutive response of M50 steel, as a function of the RCF test conditions (peak Hertzian stress and number of RCF cycles), was developed by combining the results presented in the previous chapters. Only unprocessed balls were considered for this model, since all of the MP balls were tested for the same number of cycles and showed considerably less hardening than the unprocessed balls even with higher applied Hertzian stress. Three main components are required to define the constitutive response: the elastic modulus, the yield strength, and the plastic response. The plastic response and elastic modulus were determined for virgin and RCF affected material during the miniature compression testing presented in Chapter 5. It was found that the elastic modulus does not change from virgin to RCF affected material. On the other hand, the plastic response does change from the virgin to RCF affected material, but it does not change significantly between the various RCF conditions. Finally, an empirical model to predict the maximum increase in indentation hardness within the RCF affected region as a function of the number of RCF conditions and peak Hertzian stress was developed. This model was then combined with the constraint factor (Fig. 5-15) and the observation that the hardness follows a distribution with depth to the Hertzian stress (Fig. 4-4). The result is a model for the constitutive response as a function of number of RCF cycles, Hertzian stress, and depth.

Results and Discussion

The elastic modulus and the plastic hardening rate were each determined during miniature compression testing in Chapter 5. The elastic modulus for virgin M50 steel is 203 GPa, and it was found to not change significantly due to RCF. The plastic hardening responses of the compression specimens tested were modeled with a power-law fit ($\sigma=K\varepsilon^n$) and the results are summarized in Table 5-1. It was observed that both K and n increase from the virgin specimens to the RCF specimens, but the values for the unprocessed RCF tested specimens are within experimental scatter of the average values of 5045 MPa and 0.148, respectively. The majority of the microstructural and mechanical evolution occurs during the initial shakedown period as discussed in Chapter 7 and literature [56,74,75,76,77]. Hence, it is reasonable to assume that both K and n will be constant across the range of parameters considered. The model for the hardness increase was combined with the known values for the elastic modulus and the plastic response to determine the constitutive response of the material.

Next, an empirical model for the evolution of the maximum yield strength within the RCF affected region was developed. The empirical model, $\Delta H=(7.5E\text{-}5)\sigma^2+(4E\text{-}7)N-375.7$ [MPa], where ΔH is the maximum increase in hardness within the RCF affected zone (in MPa), σ is the peak Hertzian stress (in MPa), and N is the number of RCF cycles, was found to fit the increase in hardness for all of the balls indented, as shown in Fig. 8-1. The coefficient of determination for this model is 0.85, which implies a strong correlation considering the variability in bearing microstructure. The constraint factor is then used to convert the hardness increase into yield strength increase, resulting in the equation $\Delta\sigma_y=(2.8E\text{-}5)\ \sigma^2+(1.5E\text{-}7)N-139.1$ [MPa], where $\Delta\sigma_y$ is the

increase in the maximum yield strength (in MPa), σ is the peak Hertzian stress (in MPa), and N is the number of RCF cycles. The yield strength increase can be added to the virgin yield strength to determine the maximum increase within the RCF affected material. This is combined with the observation that the hardness increase follows a similar trend with depth to the Hertzian stress (Fig. 4-4), which is readily calculated as a function of the materials, geometry, and applied load. This is manipulated by taking using the ratio, $(\tau_z - \tau_0)/(\tau_P - \tau_0)$, where τ_z is the calculated shear stress at the depth being considered, τ_0 is the calculated shear stress at the surface of the ball, and τ_P is the peak shear stress within the RCF affected region. This ratio is then multiplied with the maximum yield strength increase to give the yield strength increase at the depth being considered. A comparison of the predicted yield strength and the estimated yield strength from micro-indentation measurements as a function of the depth into the ball for one of the balls tested (#8) are provided in Fig. 8-2. It can be seen that the two of these are quite similar meaning that it is now possible to estimate the yield strength as a function of depth given only the test conditions and the initial yield strength.

Now with the elastic modulus, yield strength, and plastic response all defined, the entire stress-strain response has be determined. The stress-strain response is expected to follow the equation $\sigma=E\varepsilon$ up to the yield strength and then $\sigma=K\varepsilon^n$ beyond initial yielding until failure. A superposition of the flow curve predicted by the model developed above and the experimental flow curve for one of the balls tested (#10) is given in Fig. 8-3. It can be seen that the elastic modulus and plastic response are nearly identical. The experimental yield strength is 0.4% lower, which is well within experimental error (at 95% confidence). Fig. 8-4 and Table 8-1 show the maximum

yield strength within the RCF affected zone predicted by the current model, estimated from micro-indentation testing, and measured during miniature compression testing. The model is shown to be effective at modeling the maximum yield strength for all of the balls tested. The error bars given on the plot represent one standard deviation. The prediction is within the 95% confidence interval for the indentation results (except for ball #1), and within the 95% confidence interval for all of the compression results (except for #3).

Summary

An empirical model for the evolution of the constitutive response of M50 bearing steel due to RCF was developed. The only input which is required is the virgin stress-strain response of the material and the Hertzian stress and number of RCF cycles to be used. The elastic modulus does not change due to RCF, and thus literature values, or compression specimens from the virgin material, suffice to determine this value. The plastic parameters (K and n) do increase from the virgin to the RCF condition, but do not change significantly after the initial shakedown period, thus once a value for these parameters has been established additional testing for each set of RCF conditions need not be performed. A model for peak increase in yield strength within the RCF affected zone, as a function of RCF conditions (i.e. number of cycles and Hertzian stress), was developed based on the hardness and compression testing. This model clearly shows that the Hertzian stress is a dominant factor in increasing the yield strength of the material compared to the number of cycles, which is consistent with previous observations. The trend of the yield strength as a function of depth was then determined. Since the other parameters should be relatively constant it is possible to determine the full stress-strain response as a function of depth and RCF test conditions.

This model should prove useful for the bearing community as new life prediction models are developed.

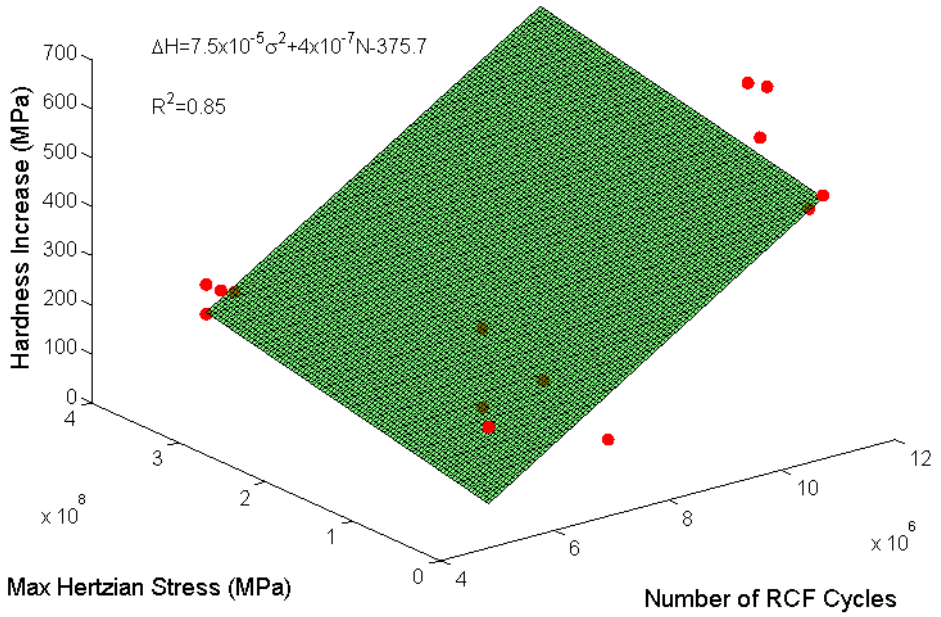

Figure 8-1. Empirical model for the hardness increase as a function of max Hertzian stress and number of cycles.

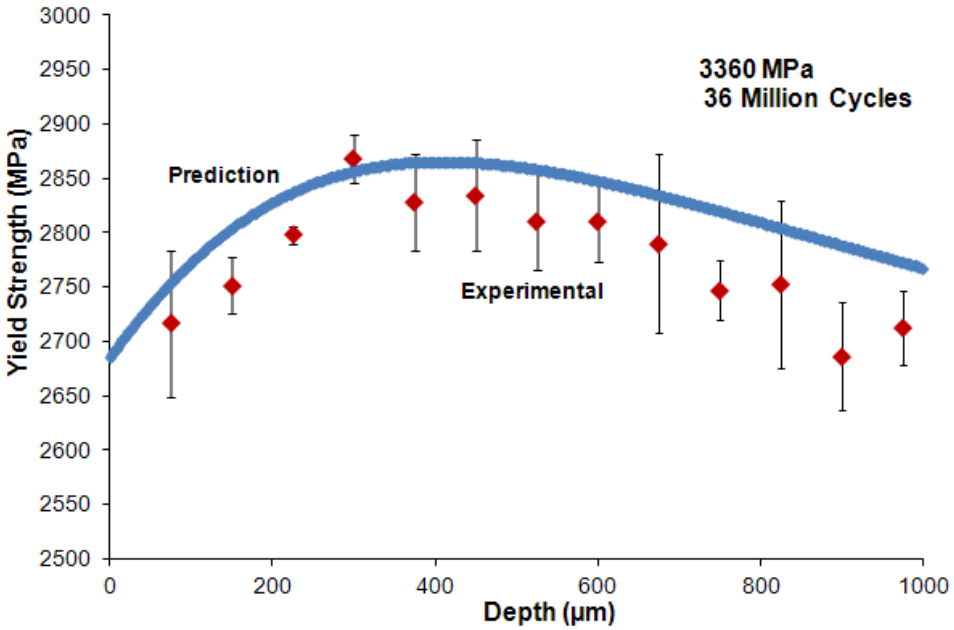

Figure 8-2. Empirical model for the hardness increase versus experimental results for a representative ball (#8).

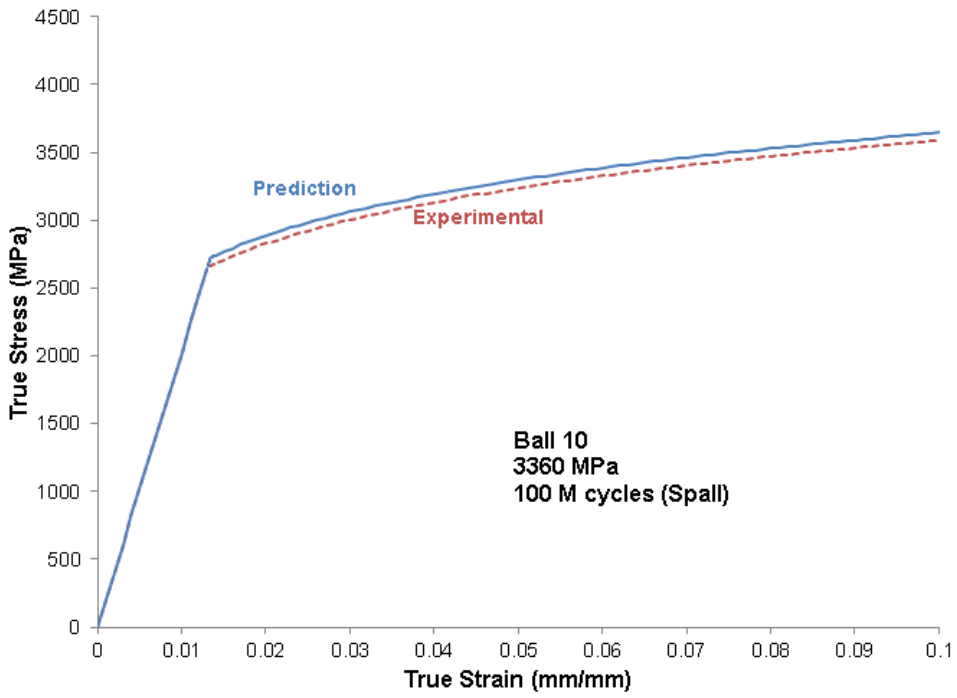

Figure 8-3. Comparison of the flow curve predicted by the current model and the average flow curve found experimentally for a representative ball (#10).

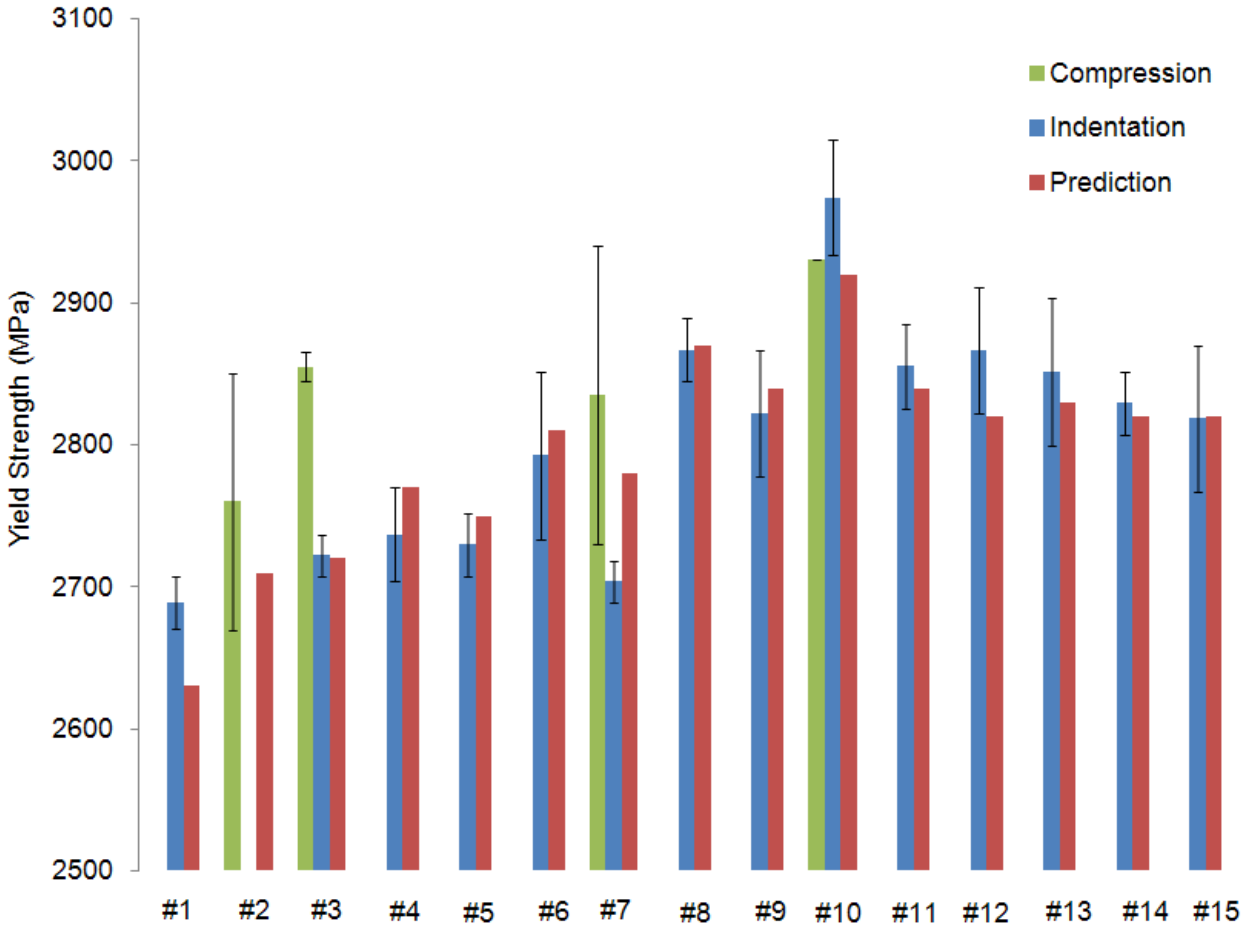

Figure 8-4. Comparison of the yield strength for each untumbled ball determined by various methods.

Table 8-1. Comparison of the yield strength determined by various methods.

Ball ID #	Peak hertzian stress (MPa)	Run time (Millions)	Indentation (MPa)	Compression (MPa)	Equation (MPa)
1	2325	36	2690±20		2630
2	2325	360		2760±90	2710
3	2325	360	2720±15	2855±10	2720
4	2740	36	2740±35		2770
5	2740	110	2730±20		2750
6	2740	180	2790±60		2810
7	2740	180	2700±15	2835±105	2780
8	3360	36	2870±20		2870
9	3360	52	2820±45		2840
10	3360	100	2970±40	2930	2920
11	3360	108	2860±30		2840
12	3360	122	2870±45		2820
13	2325	360	2850±50		2830
14	2380	360	2830±20		2820
15	2430	360	2820±50		2820

CHAPTER 9
CONCLUSIONS

The focus of this thesis was a combined experimental and analytical study of the evolution of the mechanical properties of M50 bearing steel due to RCF. Balls were procured that had previously been subjected to RCF testing with varying RCF parameter (number of RCF cycles and applied stress). Additionally, some of the balls tested had gone through a proprietary mechanical processing to induce compressive residual stresses over the first several hundred microns into the depth of the ball. In addition to the balls, M50 rods were procured and tested in a standard three ball-rod RCF tester with varying conditions (ball material, applied stress, and number of cycles). The series of tests performed include: residual stress measurement via XRD, micro-indentation within the subsurface RCF affected regions, extraction and testing of miniature compression specimens of material from within the RCF affected regions, and chemical etching. An empirical model of the evolution of the constitutive response of the bearing material within the RCF affected region was developed based on the results of these analyses.

Residual Stresses

Subsurface residual stresses are known to evolve do to RCF and affect bearing life. Some of the balls tested were subjected to propriety mechanical processing prior to RCF testing. This method creates high compressive residual stresses near the surface of the ball, which may extend the life of the balls. The highest residual stresses within the MP balls of approximately 280 MPa was found to occur at the surface, and then it decreases to a similar residual stress to the virgin unprocessed balls after approximately 700 μm. It was found that the residual stresses within the RCF affected

zone increase with increased time and Hertzian stress within the unprocessed balls, but the residual stresses within the MP balls do not significantly change due to RCF. A linear relationship was found between the maximum residual stress within the RCF affected zone and the maximum Hertzian stress for unprocessed balls.

Micro-indentation

Micro-indentation was performed within the subsurface RCF affected region balls which had been subjected to various RCF conditions i.e. initial residual stresses, Hertzian stress, and number of cycles. An increase in hardness of over 9% was observed in unprocessed balls. It was shown that the hardness increase follows a similar trend with depth as the Hertzian stress. The Hertzian stress was found to be a much more important factor in the amount of hardening than the number of cycles. Mechanical processing significantly reduced the amount of hardening due to RCF.

Miniature Compression

Miniature compression testing was performed on a selection of the balls tested to determine the full constitutive response within the RCF affected zone. Since the specimens are an order of magnitude smaller than are traditionally used, a finite element analysis was performed to determine the geometric tolerances that would provide acceptable results. A method was then developed to extract specimens from within the RCF affected zone of steel balls, prepare them for miniature compression testing, and then perform the miniature compression testing. Similar to the hardness, the increase in yield strength was found to be more dependent on the increase in the Hertzian stress than the number of RCF cycles. A 13% increase in yield strength was seen in the unprocessed ball tested at the highest Hertzian stress. The yield strength of the MP balls increased, but significantly less so than for the unprocessed balls. All of

the balls had a positive plastic hardening exponent implying that all of the balls retain the ability to continue hardening. Finally, the constraint factor relating the indentation hardness to the yield strength was found. This value can be used along with the micro-indentation results to estimate the local yield strength within the RCF affected region.

Microstructural Evolution

The microstructure within the subsurface RCF affected region is known to evolve over the course of RCF. This evolution can be observed by sectioning, polishing, and chemically etching the cross-section beneath the wear track. The transformed microstructure appears as a different color than the rest of the cross section first forming a DER then as RCF continues an LER forms. The size of the DER is seen to grow with increases in Hertzian stress and number of cycles. An LER only formed in the balls tested for the highest number of cycles and for one of the two balls that were tested at a medium Hertzian stress for nearly twice as many cycles. For unprocessed balls, a linear model was found to relate the size of the DER to the applied Hertzian stress independent of run time, whereas for MP balls, no LER was formed and only a small DER was formed even after 360 million cycles at high Hertzian stress. The formation of a DER and LER did not seem to affect the material's ability to harden.

Effect of Mechanical Processing

The introduction of compressive residual stresses through mechanical processing appears to be highly beneficial for RCF of ball bearings. The residual stress reduces the deleterious effects of RCF and thus is expected to extend life. The residual stresses in the unprocessed balls are seen to increase over the course of RCF testing (Fig. 3-2), while the residual stresses in the MP balls are of the same magnitude as

those in virgin specimens (Fig. 3-1) even after 360 million RCF cycles with a high applied Hertzian stress. Similarly, the hardness and yield strength of the MP balls are seen to increase at a much lower rate during RCF than for unprocessed balls as shown in Figs 4-5 and 5-13, respectively. Finally, the evolution of microstructure through the formation of a DER and LER is slowed due to mechanical processing. Balls #6 and #7 were tested at 2740 MPa for 180 million cycles and only ball #7 formed an LER during this time and the average size of the DER is over 2 mm^2. In contrast, balls MP4 - MP6 were tested at higher stresses for twice as many RCF cycles, but all of them have a smaller DER and no LER formation. This effect is directly attributable to the mechanical processing and the induced residual stress.

Rod Testing

Additional testing was performed using a ball-rod test setup since this arrangement allows for many more tests to be performed. After RCF testing, micro-indentation testing was performed within the subsurface RCF affected region. It was shown that the hardness quickly increases during the initial shakedown regime and then continues to harden at a nearly linear rate. An increase in Hertzian stress was found to relate to a higher rate of hardening and shorter RCF life. At a constant Hertzian stress, testing with balls with a lower yield strength and modulus resulted in a faster rate of hardening and shorter RCF life. The residual stress at the surface of the rod was shown to follow a similar trend to the maximum hardness within the RCF affected region.

Constitutive Response Modeling

An empirical model was developed to estimate the constitutive response of the material within the RCF affected zone of unprocessed balls as a function of the RCF

parameters. A model was developed for the maximum hardness increase within the RCF affected zone as a function of the Hertzian stress and number of RCF cycles. A model using the square of the Hertzian stress superimposed with a linear term of the number of cycles was found to fit the hardening quite well, which is consistent with the previous conclusion that the Hertzian stress is a more important factor than the number of RCF cycles in the rate of hardness increase. This model was combined with the observation that the hardness increase follows a similar trend to the applied shear stress and the constraint factor resulting in a model for the local yield strength as a function of depth after RCF. No similar model was developed for the MP balls due to the fact that there was not enough variation in testing parameters (constant number of cycles) or observed hardness to develop a meaningful model of the evolution of hardness. The miniature compression results showed that the plastic hardening rate evolves from the virgin state to the RCF affected state, but then stays relatively constant, which is consistent with previous research and the results presented herein for the changes in yield strength and microstructural evolution. Finally, it was demonstrated that the elastic modulus does not change due to RCF. The only input required for this model is the stress-strain response of the material. This information should prove useful as input for future finite element analysis of the RCF process to develop advanced life prediction models.

Future Work

Constitutive Response Model Extension

The model developed to predict the constitutive response is a function of the Hertzian stress and the number of RCF cycles. The range of applied Hertzian stress is sufficient for the normal engine operation. However, the highest number of cycles (360

million) is relatively low compared to bearing life. Extrapolation is dangerous as there is no guarantee that the same trend will continue, and thus it is possible that although an output is received this value is in fact meaningless. Therefore, it is suggested that further testing be performed for a higher number of cycles to ensure that the same model is applicable or to determine up to what number of cycles this model is useful. Pratt & Whitney have performed RCF testing on three balls for 3600 million cycles with similar Hertzian stress and temperature to the other balls tested here. Another possible variable is the temperature during RCF testing. Temperature is an important factor in RCF life and thus is likely an important factor in the evolution of the constitutive response due to RCF.

Case hardened Materials

Case hardened steels such as M50 NiL have become popular for use in bearings due to their long RCF life and high hot hardness. The case hardening process produces a decreasing gradient in carbon concentration from the surface, which results in a gradient in yield strength and hardness. This hardness profile can be designed to maximize the RCF life of components by taking advantage of the distribution of the distribution of stress induced by RCF. Ball-rod experiments are currently being performed on M50 NiL and P675 under similar conditions to those used for the M50 rods used herein. A 14% increase in hardness is observed after 246 million cycles with a maximum Hertzian stress of 1200 MPa with Silicon nitride balls as shown in Fig. 9-1, whereas the M50 balls failed after as little as 25 million cycles at this high stress. Further, softening has been observed in the regions adjacent to the hardened region Figs 9-2 and 9-3. It is possible that this softening leads to the initiation of fatigue cracks and eventually spall.

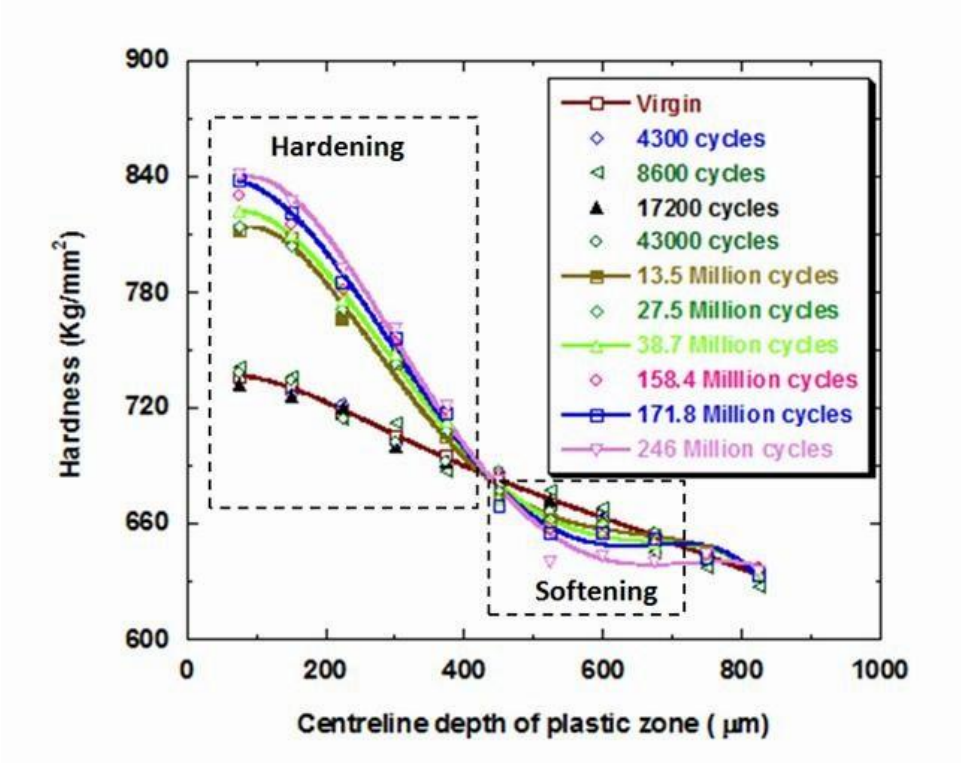

Figure 9-1. Micro-indentation hardness as a function of depth and number of cycles within M50NiL rods. The hardness increase from virgin to 246 M cycles is over 100 kg/mm^2 (~1 GPa).

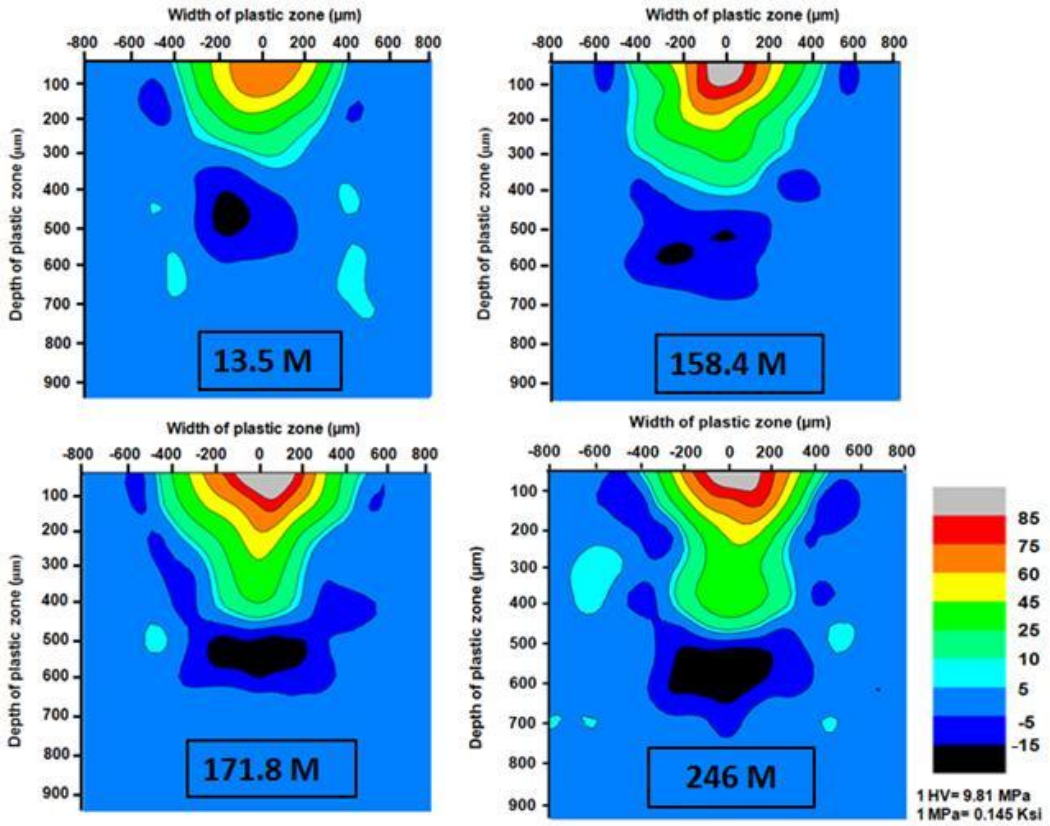

Figure 9-2. Contour plot of the micro-indentation hardness as a function of depth, width, and number of cycles within M50NiL rods. There is a distinct region of softening below the RCF hardened region, which continues to grow with time.

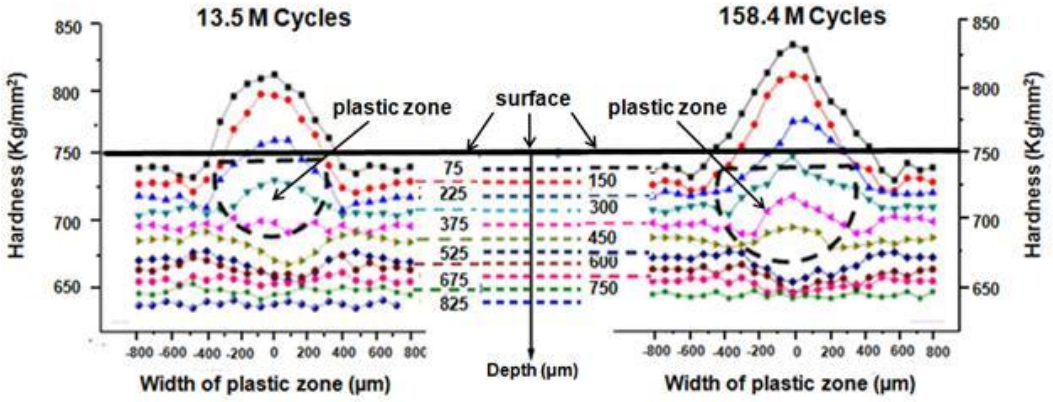

Figure 9-3. Micro-indentation hardness as a function of depth, width, and number of cycles within M50NiL rods. The region of hardening is seen to fit well with the DER (labeled here as the plastic zone). Further, the region of softening is seen to occur immediately below the end of the measured DER.

APPENDIX
ADDITIONAL FIGURES

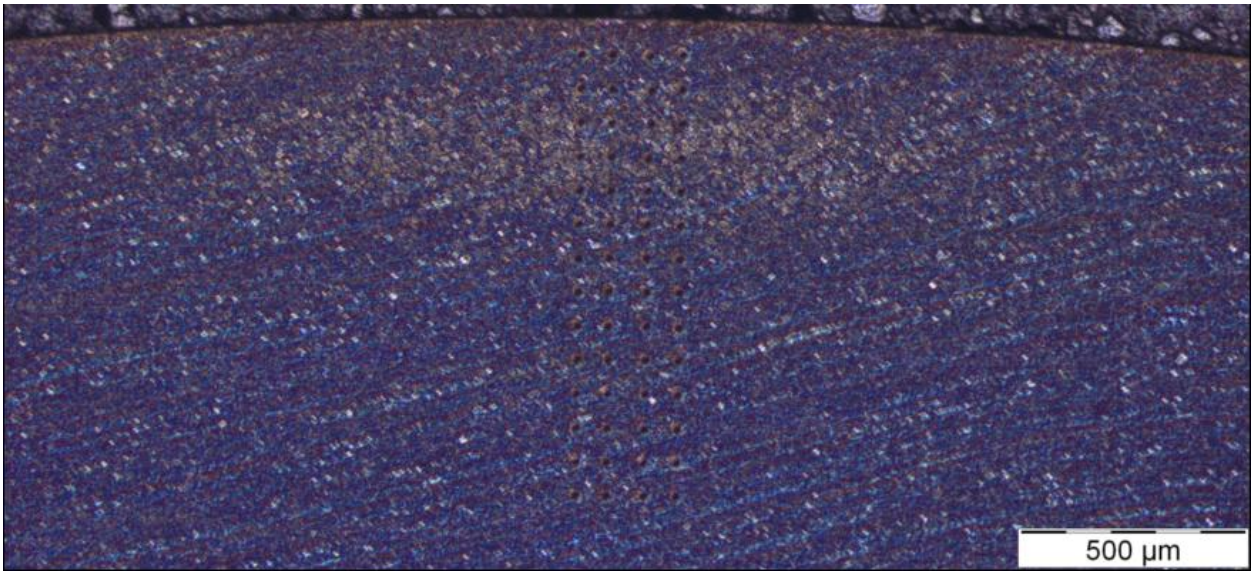

Figure A-1. Micrograph of the RCF affected region of the Ball #3 after chemical etching.

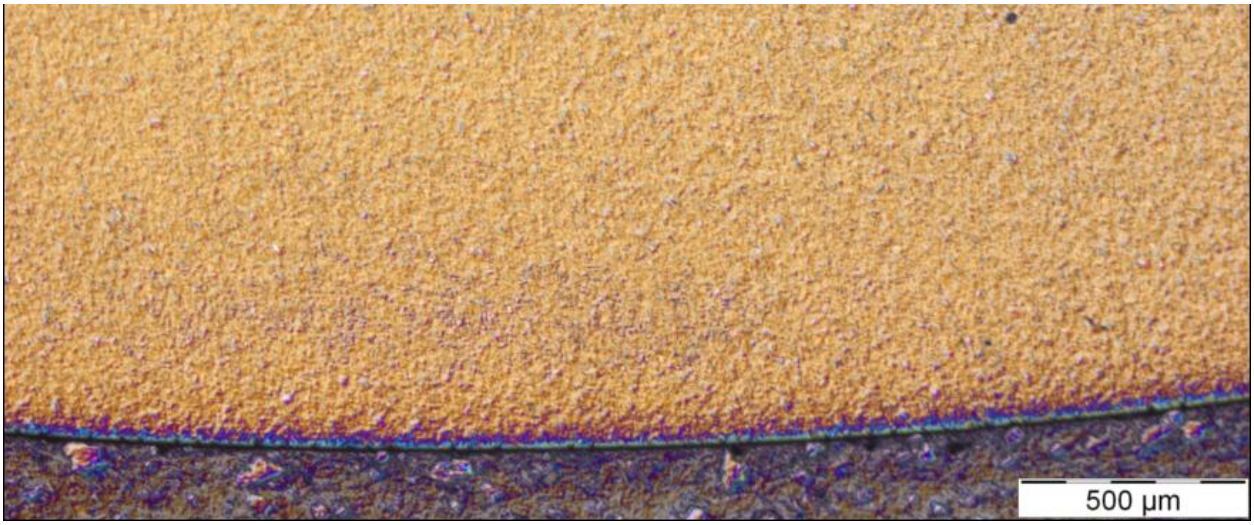

Figure A-2. Micrograph of the RCF affected region of the Ball #13 after chemical etching.

Figure A-3. Micrograph of the RCF affected region of the Ball #14 after chemical etching.

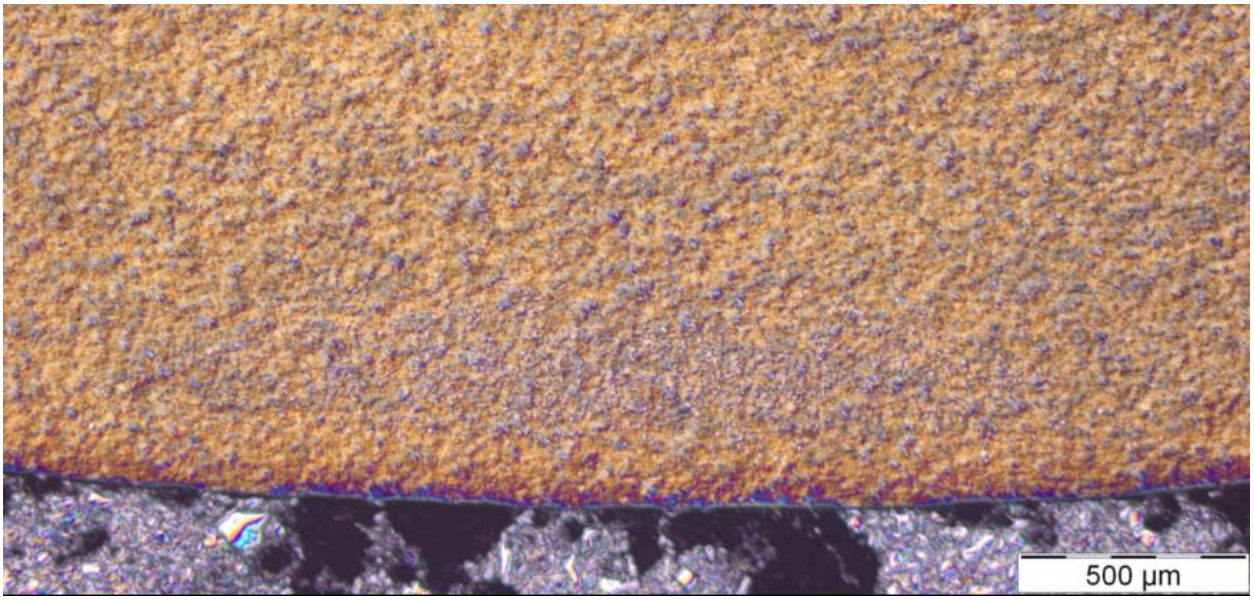

Figure A-4. Micrograph of the RCF affected region of the Ball #15 after chemical etching.

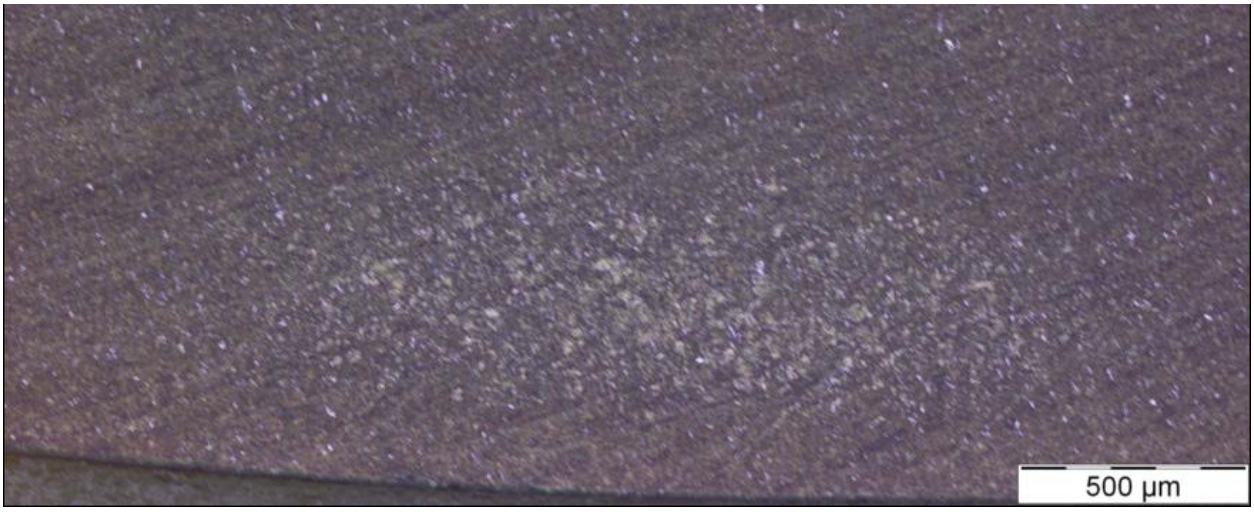

Figure A-5. Micrograph of the RCF affected region of the Ball MP5 after chemical etching.

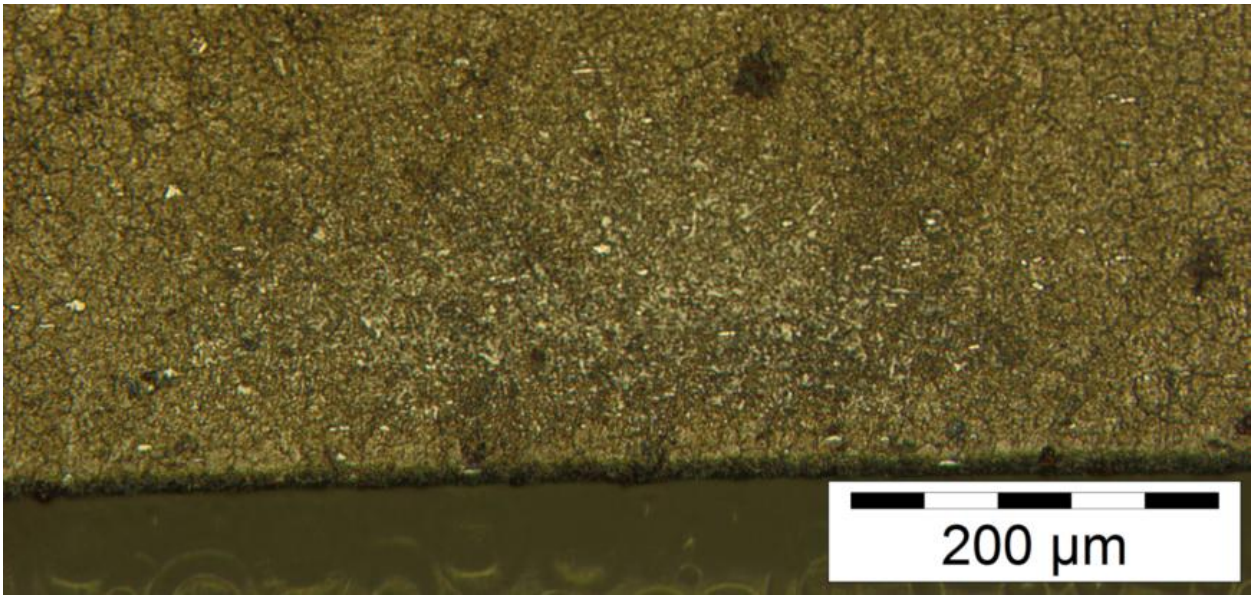

Figure A-6. Micrograph of the RCF affected region of the rod track #3 after chemical etching.

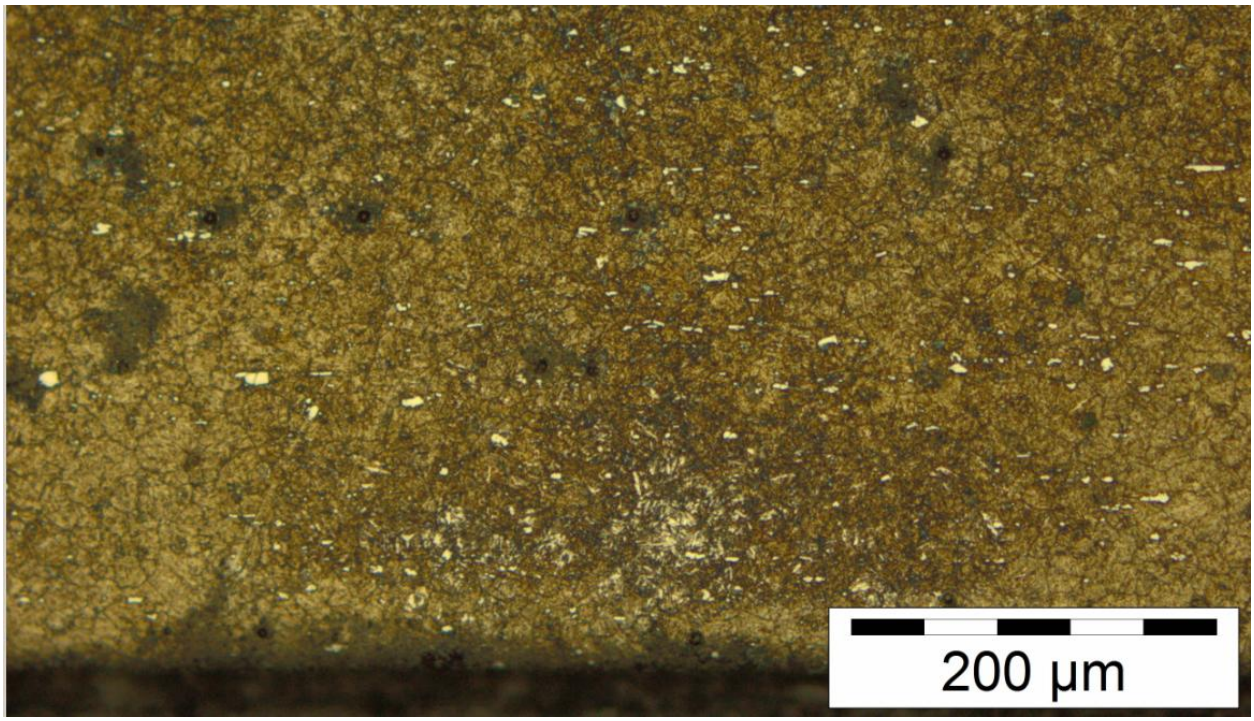

Figure A-7. Micrograph of the RCF affected region of the rod track #11 after chemical etching.

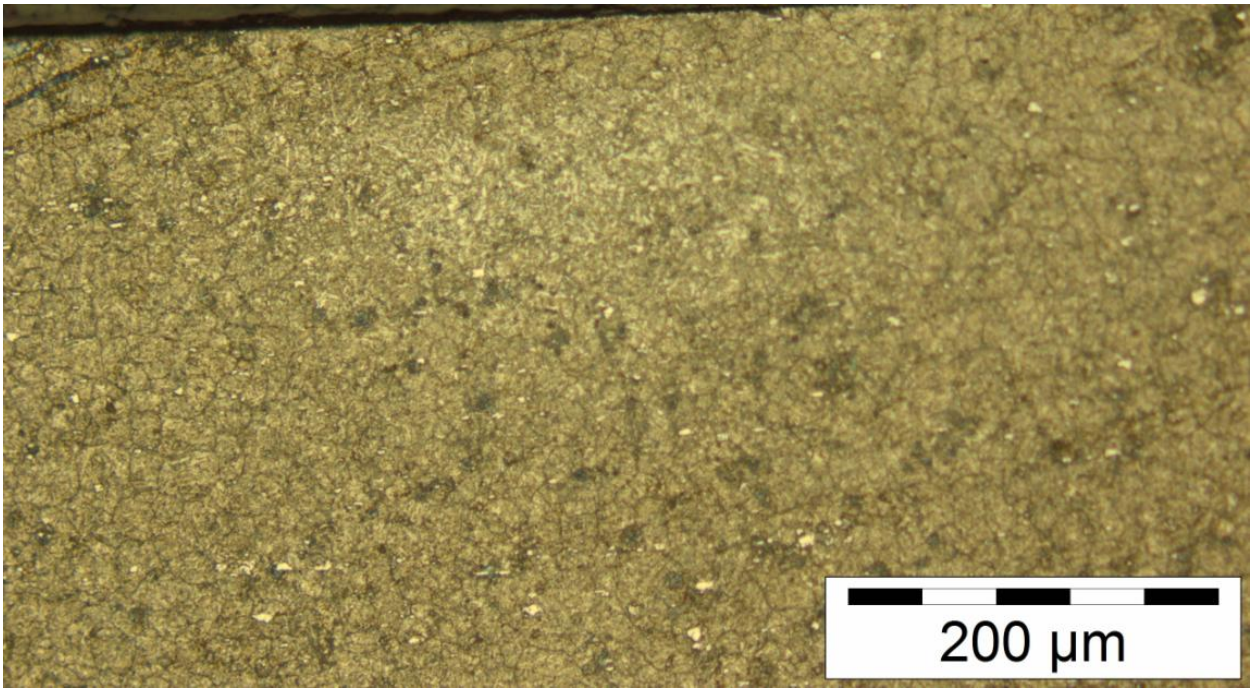

Figure A-8. Micrograph of the RCF affected region of the rod track #12 after chemical etching.

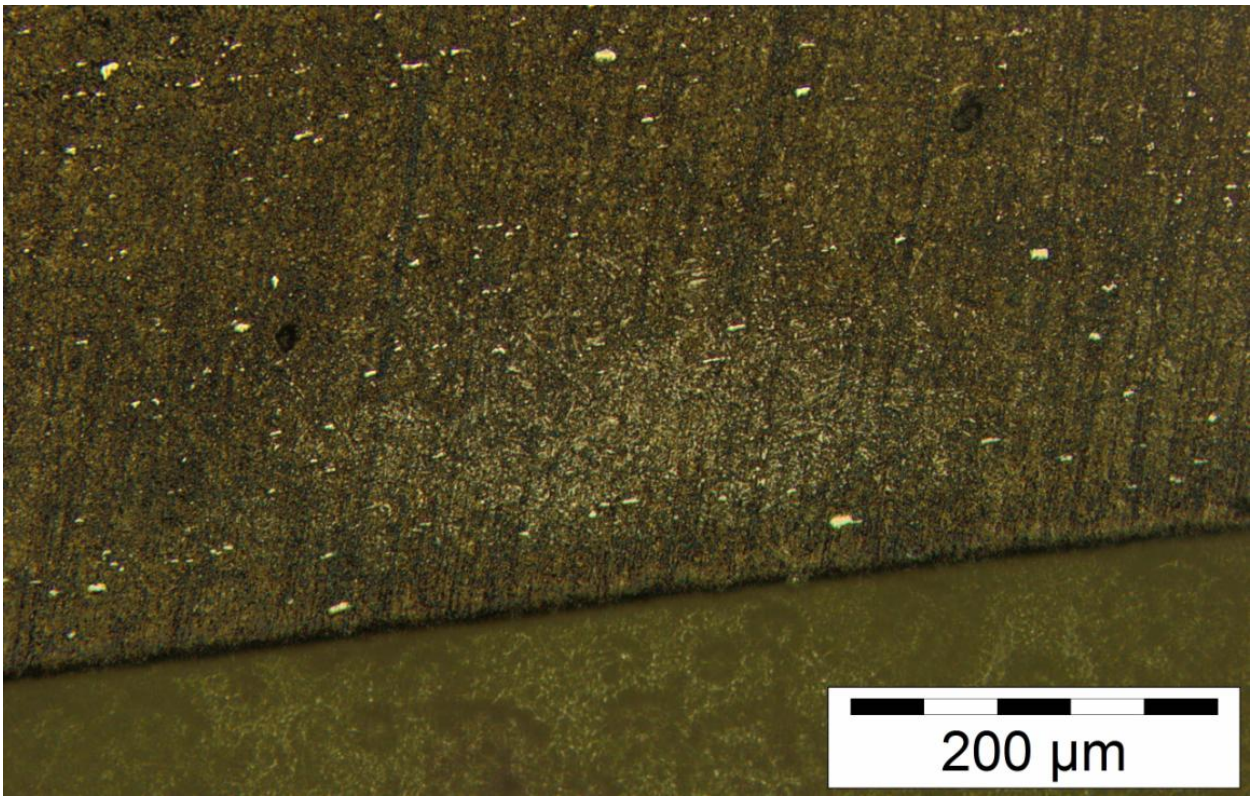

Figure A-9. Micrograph of the RCF affected region of the rod track #13 after chemical etching.

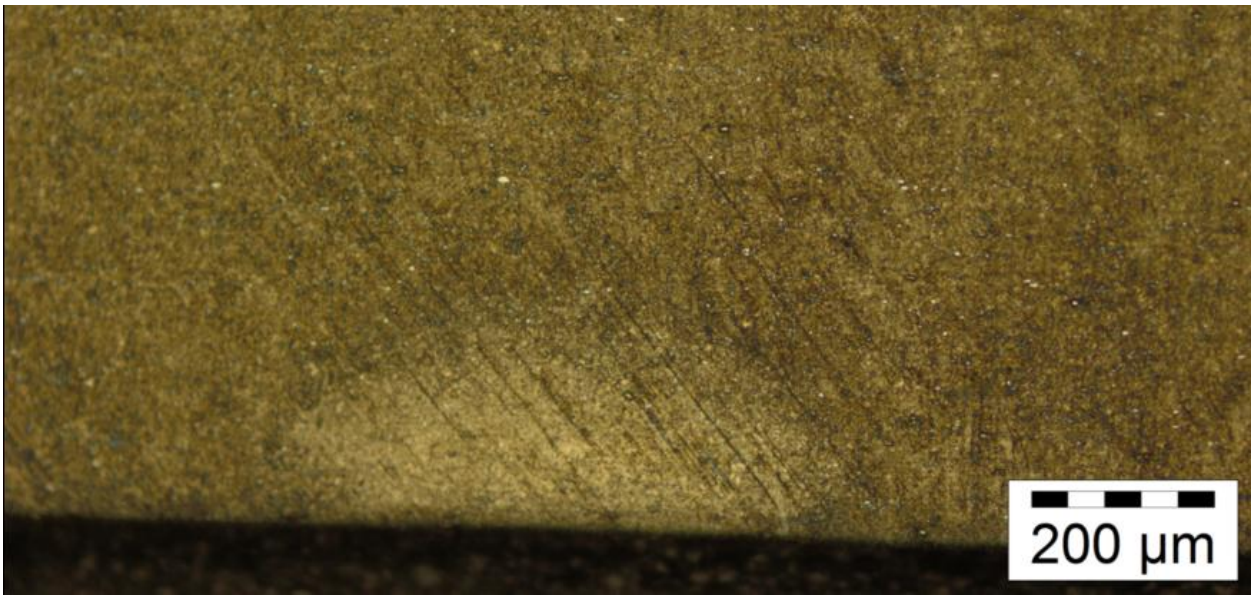

Figure A-10. Micrograph of the RCF affected region of the rod track #14 after chemical etching.

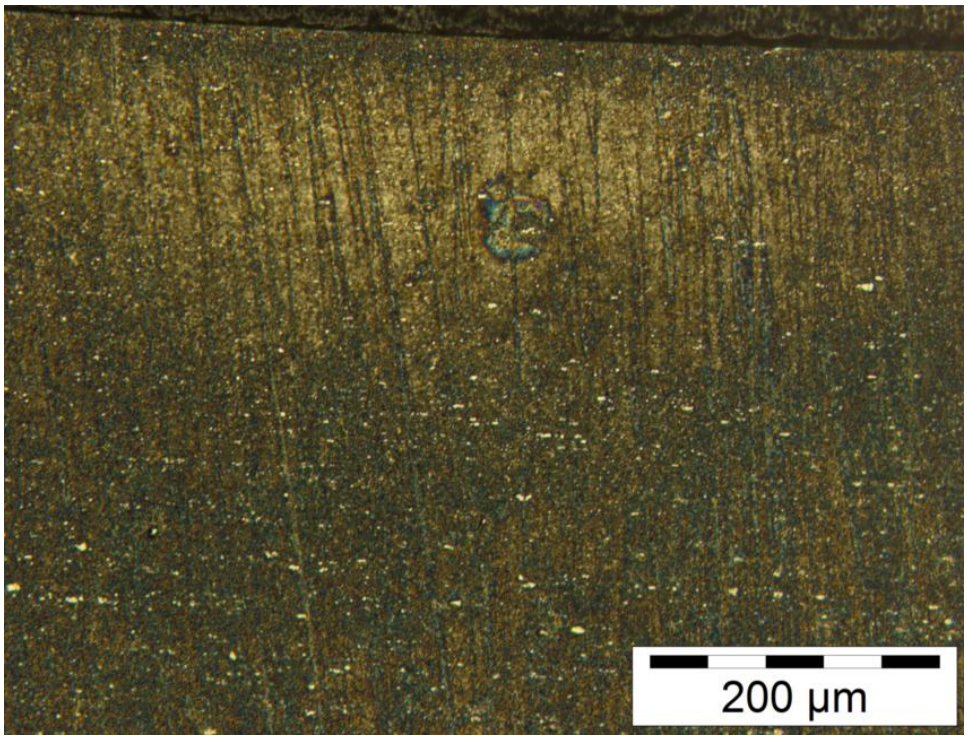

Figure A-11. Micrograph of the RCF affected region of the rod track #15 after chemical etching.

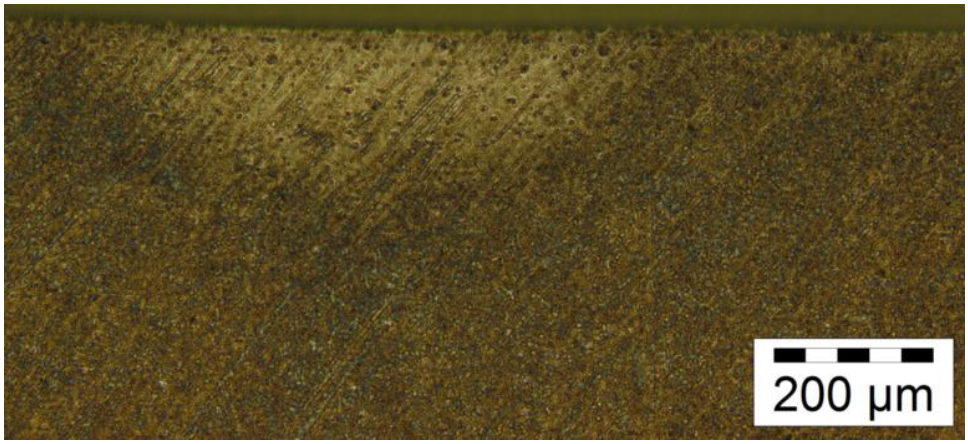

Figure A-12. Micrograph of the RCF affected region of the rod track #17 after chemical etching.

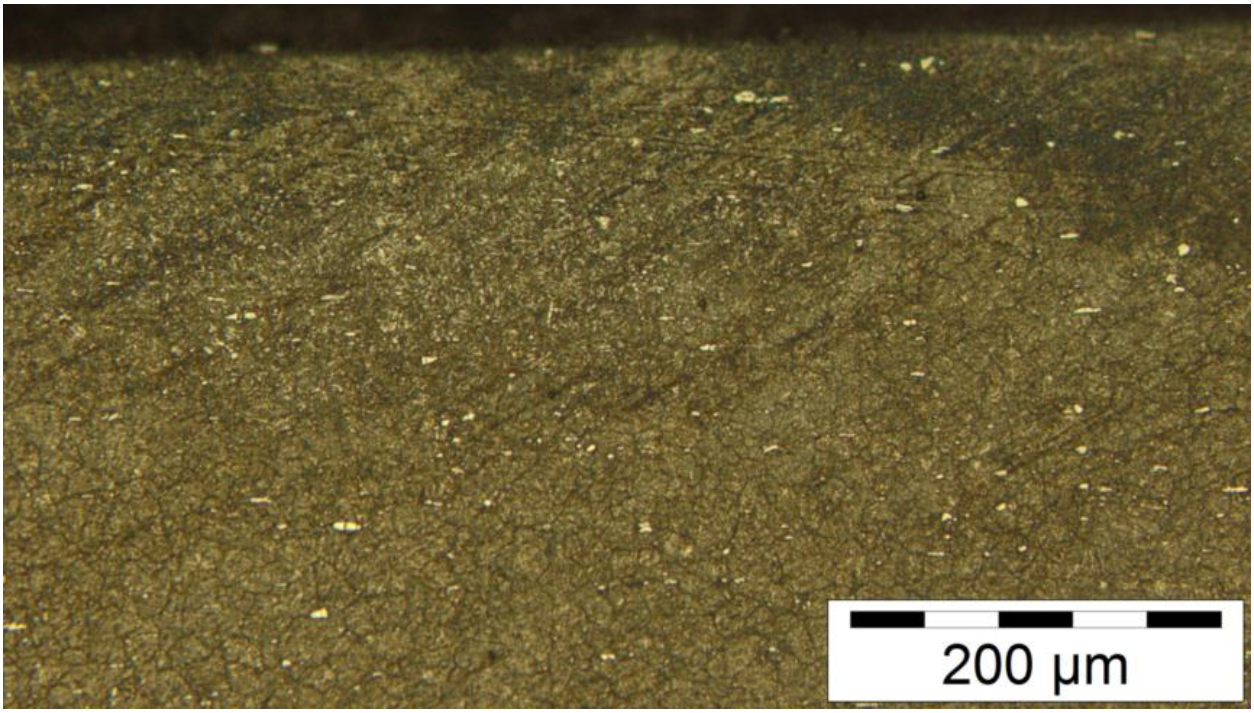

Figure A-13. Micrograph of the RCF affected region of the rod track #18 after chemical etching.

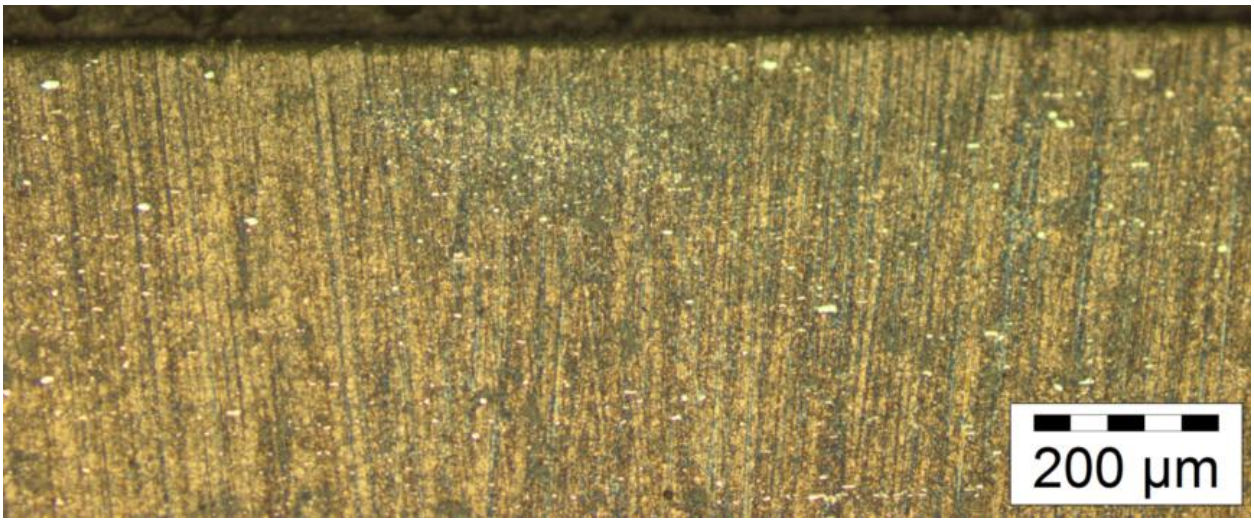

Figure A-14. Micrograph of the RCF affected region of the rod track #20 after chemical etching.

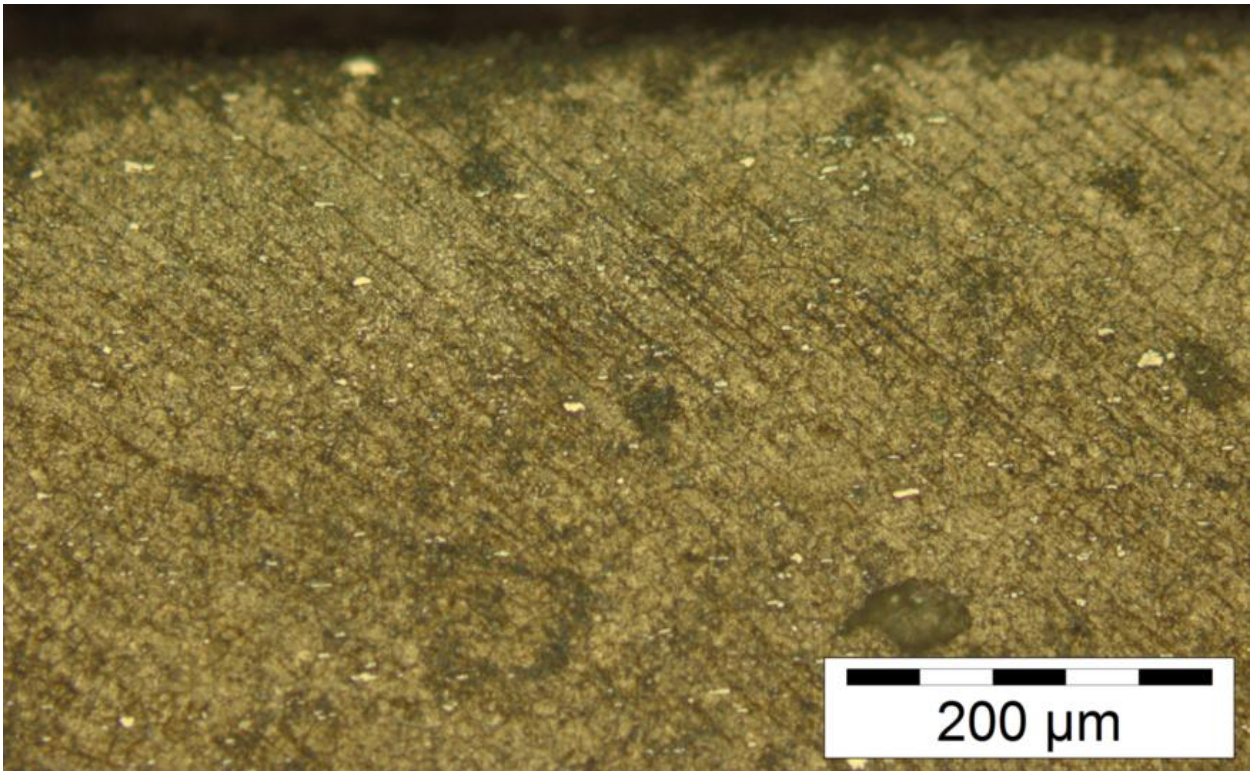

Figure A-15. Micrograph of the RCF affected region of the rod track #21 after chemical etching.

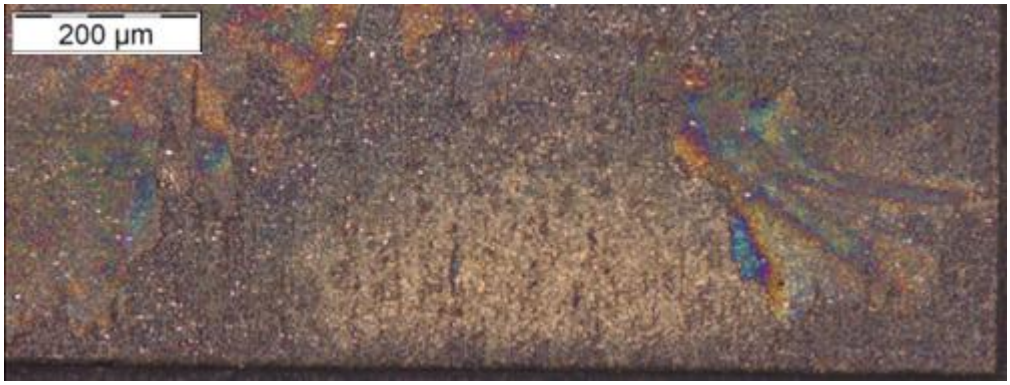

Figure A-16. Micrograph of the RCF affected region of the rod track #22 after chemical etching.

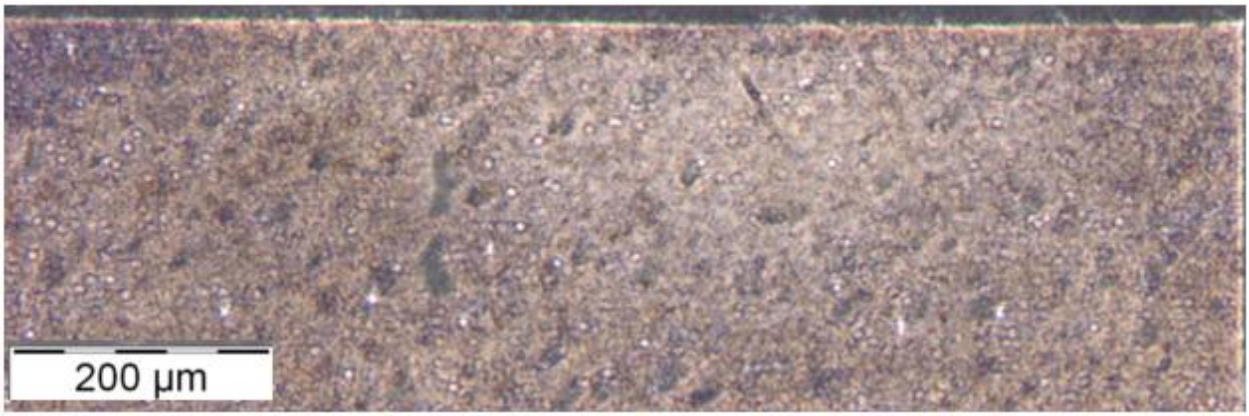

Figure A-17. Micrograph of the RCF affected region of the rod track #26 after chemical etching.

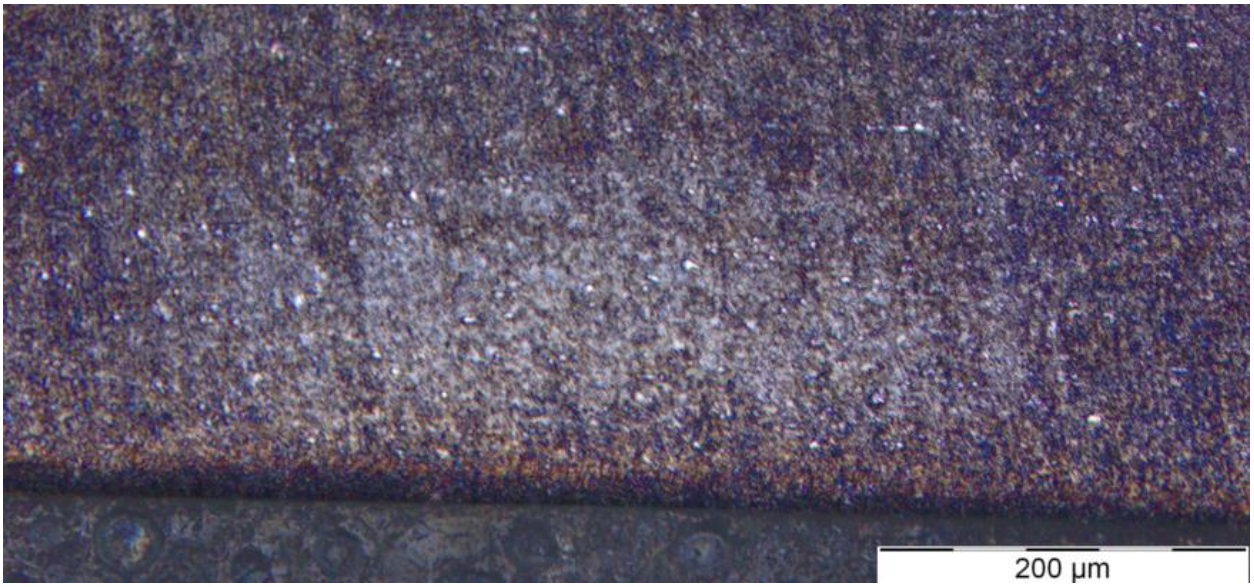

Figure A-18. Micrograph of the RCF affected region of the rod track #27 after chemical etching.

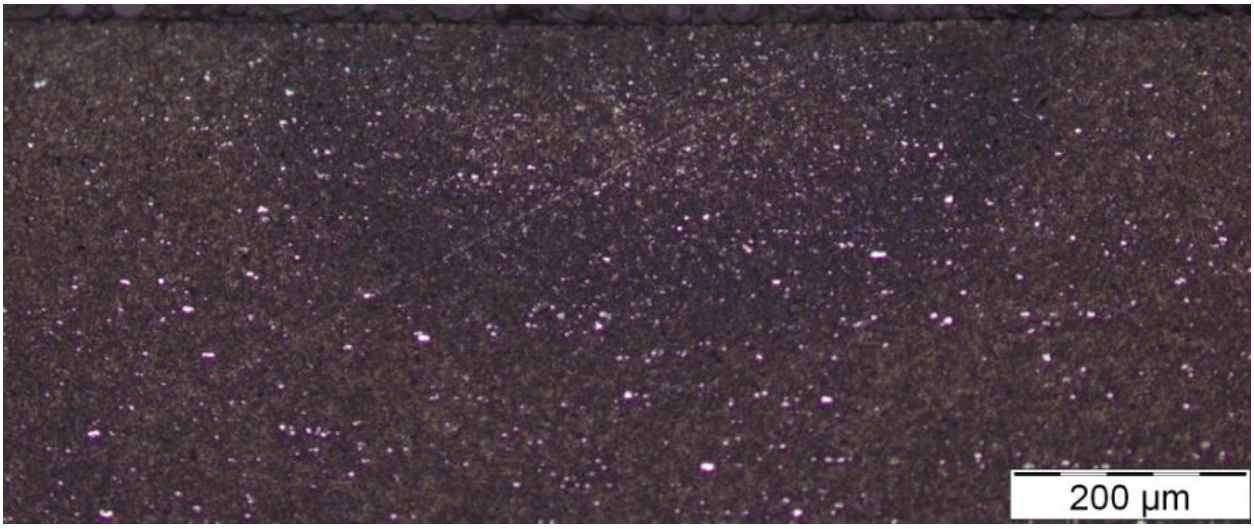

Figure A-19. Micrograph of the RCF affected region of the rod track #31 after chemical etching.

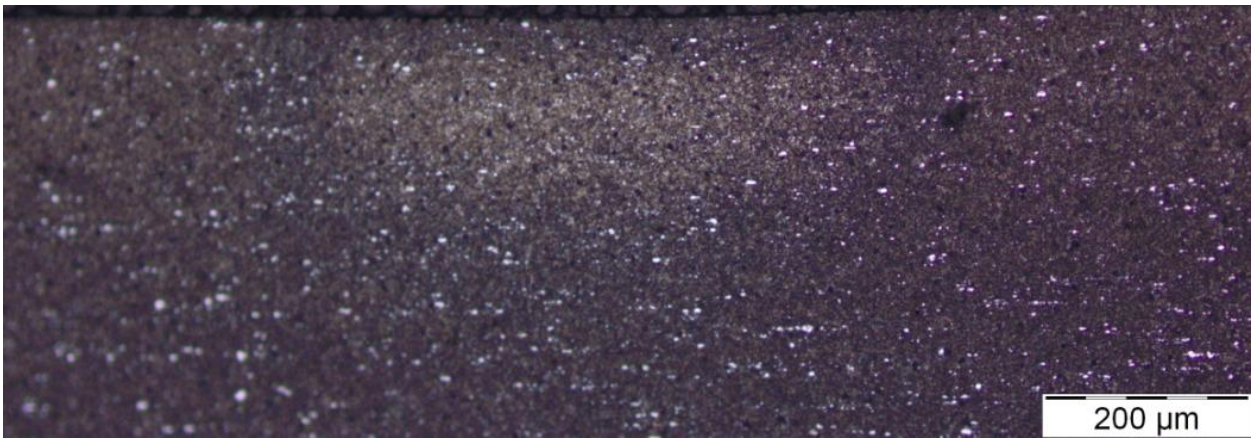

Figure A-20. Micrograph of the RCF affected region of the rod track #32 after chemical etching.

LIST OF REFERENCES

[1] Boresi A, & Schmidt R. Advanced mechanics of materials. 2003.

[2] Harris TA. Rolling bearing analysis. Chichester, West Sussex: Wiley, 1991.

[3] Jabbado M, Maitournam MH. FATIGUE FRACT ENG M 2008;31:67.

[4] Maitournam MH, Krebs C, Galtier A. Int.J.Fatigue 2011;33:232.

[5] Melander A. Int.J.Fatigue 1997;19:13.

[6] McCoy, B. 2013;Aug 27

[7] Hetzner DW, Van Geertruyden W. Mater Charact 2008;59:825.

[8] Hetzner DW. Mater Charact 2001;46:175.

[9] Decaudin B, Djega-Mariadassou C, Cizeron G. J.Alloys Compounds 1995;226:208.

[10] Boyer H. ASM International, 1987, 1987:319.

[11] Forster NH, Rosado L, Ogden WP, Trivedi HK. Tribol.Trans. 2009;53:52.

[12] Wang L, Snidle R, Gu L. Wear 2000;246:159.

[13] Thoma K, Rohr L, Rehmann H, Roos S, Michler J. Tribol.Int. 2004;37:463.

[14] Mosleh M, Bradshaw K, Belk JH, Waldrop JC. Wear 2011;271:2471.

[15] Watari K, Hirao K, Brito ME, Toriyama M, Kanzaki S. J.Mater.Res. 1999;14:1538.

[16] Zaretsky EV, Chiu Y, Tallian T. Journal of materials engineering 1989;11:237.

[17] Zaretsky EV, Vlcek BL, Hendricks RC. Tribol.Trans. 2005;48:425.

[18] Miner J, Dell J, Galbato A, Ragen M. Journal of engineering for gas turbines and power 1996;118:434.

[19] Lundberg G. IVA Handlingar 1947;196:50.

[20] Lundberg G, Palmgren A. Acta Polytech. 1952;2

[21] Jeff Dahl. Jet Engine.SVG**
**Dec 19 2007July 31 2013http://commons.wikimedia.org/wiki/File:Jet_engine.svg

[22] Silberwolf. Spherical-ball-bearing double-row din630-t1.pngMarch 25 2006July 19 2013http://commons.wikimedia.org/wiki/File:Spherical-ball-bearing_double-row_din630-t1.png

[23] Hamrock BJ, & Dowson D. Ball Bearing Lubrication: The Elastohydrodynamics of Elliptical Contacts. Wiley, 1981.

[24] Carter, TL, Zaretsky, EV. 1960;NASA TN D-259

[25] Carter, TL, Zaretsky, EV, Anderson, WJ. 1960;TN D-270

[26] Zaretsky E, & Anderson W. Material Properties and Processing Variables and Their Effect on Rolling-Element Fatigue. National Aeronautics and Space Administration, 1966.

[27] Zaretsky E, Parker R, Anderson W. Rolling Contact Fatigue Testing of Bearing Steels 1982:5.

[28] Parker R, & EV Z. Rolling Element Fatigue Life of AISI M-50 and 18-4-1 Balls. National Aeronautics and Space Administration, 1966.

[29] Zaretsky EV, Anderson WJ. Journal of Basic Engineering 1961;83:603.

[30] Hampshire J, Nash J, Hollox G. Rolling Contact Fatigue Testing of Bearing Steels, ASTM STP 1982;771:46.

[31] Bamberger E, Zaretsky E, Signer H. ATJLT 1976;98:580.

[32] Glover D. ASTM STP 1982;771:107.

[33] Xiao H, Chen Q, Shao E, Wu D, Chen Z, Wang Z. Wear 1991;151:77.

[34] Warhadpande A, Sadeghi F, Evans RD, Kotzalas MN. Tribol.Trans. 2012;55:422.

[35] Choi Y. Int.J.Fatigue 2009;31:1517.

[36] Harris TA, Ragen MA, Spitzer RF. Tribol.Trans. 1992;35:194.

[37] Guo Y, Warren A. Advances in X-Ray Analysis 2008;52:336.

[38] Guo Y, Warren A, Hashimoto F. CIRP-JMST 2010;2:129.

[39] Crețu SS, Popinceanu N. Wear 1985;105:153.

[40] Dommarco R, Kozaczek K, Bastias P, Hahn G, Rubin C. Wear 2004;257:1081.

[41] Bernasconi A, Davoli P, Filippini M, Foletti S. Wear 2005;258:973.

[42] Kobayashi M, Matsui T, Murakami Y. Int.J.Fatigue 1998;20:351.

[43] Matsumoto S, Uehara K. Bulletin of JSME 1976;19:1212.

[44] Kepple RK, Mattson RL. Journal of Lubrication Technology 1970;92:76.

[45] Klecka M, Subhash G, Arakere N. Tribol Trans 2012;accepted

[46] Hetzner DW. Adv Mater Processes 2004;162:37.

[47] Popinceanu N, Diaconescu E, Cretu S. Wear 1981;71:265.

[48] Guo YB, Barkey ME. Int.J.Fatigue 2004;26:605.

[49] AP Voskamp. Subsurface residual stress concentrations during rolling contact fatigue. Materials science forum2000

[50] Rivero IV, Ruud CO. Lubr Eng 2002;58:30.

[51] Ishida M, Abe N. Wear 1996;191:65.

[52] Liu CR, Choi Y. Int.J.Mech.Sci. 2008;50:1572.

[53] Choi Y, Liu CR. Wear 2006;261:485.

[54] Socie D, Kurath P, Koch J. Biaxial and multiaxial fatigue, EGF 1989;3:535.

[55] Ringsberg JW, Loo-Morrey M, Josefson BL, Kapoor A, Beynon JH. Int.J.Fatigue 2000;22:205.

[56] Voskamp A, Osterlund R, Becker P, Vingsbo O. Metals Technology 1980;7:14.

[57] Voskamp A, Nierlich W, Hengerer F. Evolution 1997:25.

[58] Branch NA, Arakere NK, Subhash G, Klecka MA. Int.J.Plast. 2011;27:728.

[59] Branch NA, Subhash G, Arakere NK, Klecka MA. Int.J.Solids Structures 2011;48:584.

[60] Branch NA, Subhash G, Arakere NK, Klecka MA. Acta Materialia 2010;58:6487.

[61] Klecka MA. Microstructure-Property Relationships and Constitutive Response of Plastically Graded Case Hardened Steels. In: University of Florida, 2011. p. 49.

[62] Ahlström J, Karlsson B. Wear 2005;258:1187.

[63] Eden HC, Garnham JE, Davis CL. Materials Science & Technology 2005;21:623.

[64] Arakere N, Subhash G. Mater. Sci. Eng., A 2011;28:34.

[65] Rivero IV, Ruud CO. Mater Charact 2004;53:381.

[66] Reichard DW, Parker RJ, & Zaretsky EV. Residual stress and subsurface hardness changes induced during rolling contact. Springfield, VA: National Aeronautics and Space Administration ;, 1968.

[67] Bhattacharyya A, Subhash G, Arakere NK. Int.J.Fatigue 2013;Submitted

[68] Tabor D. Review of physics in technology 1970;1:145.

[69] Pavlina E, Van Tyne C. Journal of materials engineering and performance 2008;17:888.

[70] ASTM Standard. Standard Test Method for Vickers Hardness of Metallic Materials. In: 1996 Annual Book of ASTM Standards, Easton, MD: ASTM, 1996.

[71] Tsui T, Oliver W, Pharr G. J.Mater.Res. 1996;11:752.

[72] Bolshakov A, Oliver W, Pharr G. J.Mater.Res. 1996;11:760.

[73] Johnson K. Contact Mechanics. New York, NY: Cambridge University Press, 1985.

[74] Österlund R, Vingsbo O. Metallurgical and Materials Transactions A 1980;11:701.

[75] Voskamp A. J.Tribology(Trans.ASME) 1985;107:359.

[76] Voskamp AP. ASTM Spec.Tech.Publ. 1998;1327:152.

[77] Voskamp A, Mittemeijer E. Zeitschrift für Metallkunde 1997;88:310.

[78] Allison B, Subhash G, Arakere N, Chen H, Haluck D, Yamaguchi H. J. Tribol Submitted

[79] ASTM Standard. Standard Test Methods of Compression Testing of Metallic Materials at Room Temperature. In: 1990 Annual Book of ASTM Standards, Easton, MD: ASTM, 1990. p. 98.

[80] Bei H, Shim S, George EP, Miller MK, Herbert EG, Pharr GM. Scr.Mater. 2007;57:397.

[81] Dimiduk DM, Uchic MD, Parthasarathy TA. Acta Mater 2005;53:4065.

[82] Frick CP, Clark BG, Orso S, Schneider AS, Arzt E. Mater. Sci. Eng., A 2008;489:319.

[83] Hosemann P, Swadener JG, Kiener D, Was GS, Maloy SA, Li N. J.Nucl.Mater. 2008;375:135.

[84] Kiener D, Motz C, Dehm G. Mater. Sci. Eng., A 2009;505:79.

[85] Kiener D, Motz C, Schobert T, Jenko M, Dehm G. Adv. Eng. Mater. 2006;8:1119.

[86] Philippe L, Schwaller P, Burki G, Michler J. J.Mater.Res. 2008;23:1383.

[87] Uchic MD, Dimiduk DM, Florando JN, Nix WD. Science 2004;305:986.

[88] Uchic MD, Shade PA, Dimiduk DM. JOM 2009;61:36.

[89] Zhang H, Schuster BE, Wei Q, Ramesh KT. Scr. Mater. 2006;54:181.

[90] Moser B, Wasmer K, Barbieri L, Michler J. J.Mater.Res. 2007;22:1004.

[91] Sadeghi F, Jalalahmadi B, Slack TS, Raje N, Arakere NK. J. Tribol. 2009;131:041403.

[92] Carpenter Steel. Carpenter VIM-VAR M50 Bearing Steel1991July 12 2013http://cartech.ides.com/datasheet.aspx?i=101&c=TechArt&E=164;

[93] Matweb. M50 Tool Steel2012Nov 18 2012http://www.matweb.com/search/DataSheet.aspx?MatGUID=461c9c2ce38842538833a47bccf3c293&ckck=1

[94] Latrobe Steel. Lescalloy M50 VIM-VAR High Performance Bearing Steel Data Sheet2008Sept 7 2012http://www.latrobesteel.com/assets/documents/datasheets/M50.pdf

[95] Bush J, Grube W, Robinson G. ASM Trans 1961;54:390.

[96] Swahn H, Becker P, Vingsbo O. Metallurgical Transactions A 1976;7:1099.

[97] Zwirlein O, Schlicht H. Rolling contact fatigue testing of bearing steels 1982:358.

[98] AB Jones. Metallographic observations of ball bearing fatigue phenomenaProc. ASTM1946

[99] Douglas Scott, B. Loy and GH Mills. Paper 10: Metallurgical Aspects of Rolling Contact FatigueProceedings of the Institution of Mechanical Engineers, Conference Proceedings1966

[100] Schlicht H, Schreiber E, Zwirlein O. Effect of Steel Manufacturing Processes on the Quality of Bearing Steels 1986:81.

[101] Martin J, Borgese S, Eberhardt A. Journal of Basic Engineering 1966;88:555.

[102] Braza J, Pearson P, Hannigan C. SAE TRANSACTIONS 1993;102:437.

[103] Trivedi HK, Saba CS. Tribology Letters 2001;10:171.

[104] Lakshminarayanan R, Chao L, Iyer N, Shetty DK. Wear 1997;210:278.

[105] Dommarco RC, Bastias PC, Hahn GT, Rubin CA. Wear 2002;252:430.

[106] Chao L-, Lakshminarayanan R, Iyer N, Lin G-, Shetty DK. Wear 1998;223:58.

[107] Ueda T, Mitamura N. Tribol.Int. 2008;41:965.

[108] Bouzakis K-, Vidakis N. Wear 1997;206:197.

[109] Dill JF. Journal of engineering for gas turbines and power 1996;118

[110] Hadfield M, Stolarski T. Tribol.Int. 1995;28:377.

[111] Allen DL. Tribol.Trans. 1994;37:410.

[112] Hadfield M. Ceram.Int. 1998;24:379.

[113] Wan GTY, Gabelli A, Ioannides E. Tribol.Trans. 1997;40:701.

[114] Sibley LB. Problems in Bearings and Lubrication 1982

[115] Bhushan B, Sibley LB. ASLE TRANSACTIONS 1982;25:417.

[116] Kalin M, Vižintin J, Novak S, Dražič G. Wear 1997;210:27.

[117] Wang L, Wood R, Harvey T, Morris S, Powrie H, Care I. Wear 2003;255:657.

[118] Scott D, Blackwell J. Wear 1973;24:61.

[119] Poplawski JV, Atwell DR, Lubas MJ, Odessky V. Journal of engineering for gas turbines and power 1996;118

[120] ASTM Standard. 2009;E384

[121] Vincent A, Elghazal H, Lormand G, Hamel A, Girodin D. ASTM Spec.Tech.Publ. 2002;1419:427.

[122] Allison B, Subhash G, Arakere N, Haluck D, Chin H. Tribol Trans Submitted

[123] Alley ES, Neu RW. Int.J.Fatigue 2010;32:841.

[124] Alley ES. Influence of microstructure in rolling contact fatigue of bearing steels with inclusions. ProQuest, 2009.

[125] Alley ES, Sawamiphakdi K, Anderson PI, Neu RW. J ASTM Int 2010;7

BIOGRAPHICAL SKETCH

Bryan Allison completed both his B.S. and M.S. in mechanical engineering from the University of Alabama in Huntsville. He graduated Summa Cum Laude with his BS in 2008 in mechanical engineering. His master's thesis focused on the effect of fiber waviness on the strength of unidirectional S-glass composites. Bryan also worked at the US Army Primary Standards Laboratory (APSL) as a research assistant from 2008 through 2010. During his tenure working at the APSL, Bryan tested and implemented new state of the art equipment, including the addition of an intrinsic calibration standard for several measurements. Using this equipment, the uncertainty values obtained were the lowest known for such dimensional measurements.

Bryan Allison moved to Gainesville, FL in 2010 to pursue a doctoral degree in mechanical engineering at the University of Florida. His research centered on the mechanical characterization and rolling contact fatigue life modeling of advanced aerospace bearing materials. This project was sponsored by the Pratt & Whitney, Air Force Research Labs, and SKF.